EARTHQUAKE RISK TO CIVIL INFRASTRUCTURE SYSTEMS

by

Nafiseh Soleimani

A dissertation submitted to the Faculty of the University of Delaware in partial fulfillment of the requirements for the degree of Doctor of Philosophy in Civil Engineering

Summer 2022

© 2022 Nafiseh Soleimani
All Rights Reserved

EARTHQUAKE RISK TO CIVIL INFRASTRUCTURE SYSTEMS

by

Nafiseh Soleimani

Approved: _____

Jack Puleo, Ph.D.
Chair of the Department of Civil and Environmental Engineering

Approved: _____

Levi T. Thompson, Ph.D.
Dean of the College of Engineering

Approved: _____

Louis F. Rossi, Ph.D.
Vice Provost for Graduate and Professional Education and
Dean of the Graduate College

I certify that I have read this dissertation and that in my opinion it meets the academic and professional standard required by the University as a dissertation for the degree of Doctor of Philosophy.

Signed: _____

Rachel A. Davidson, Ph.D.
Professor in charge of dissertation

I certify that I have read this dissertation and that in my opinion it meets the academic and professional standard required by the University as a dissertation for the degree of Doctor of Philosophy.

Signed: _____

Earl Rusty Lee, Ph.D.
Member of dissertation committee

I certify that I have read this dissertation and that in my opinion it meets the academic and professional standard required by the University as a dissertation for the degree of Doctor of Philosophy.

Signed: _____

James M. Kendra, Ph.D.
Member of dissertation committee

I certify that I have read this dissertation and that in my opinion it meets the academic and professional standard required by the University as a dissertation for the degree of Doctor of Philosophy.

Signed: _____

Shangjia Dong, Ph.D.
Member of dissertation committee

ACKNOWLEDGMENTS

I would like to express my deepest gratitude to my advisor, Professor Rachel A. Davidson, for her extensive help and support throughout this journey. It was an honor for me to have the chance to learn from you. You are genuinely generous about your knowledge and experience. You have been so kind and patient, which helped me go through tough days in my life. Words cannot express my gratitude to you. I will always be thankful for having you as my advisor.

I would like to thank my Ph.D. dissertation committee members, Prof. Rusty Lee, Prof. James Kendra, and Prof. Shangjia Dong, for offering advice and helping me in every step of this dissertation. Special thanks to my friends, professors, and lab mates who extensively helped me during my Ph.D. I would like to thank our research team in the CRISP project, Dr. Craig Davis, Prof. Linda Nozick, Prof. Tom O'Rourke, Prof. Kate Starbird, Prof. Bradley Ewing, and LADWP for their valuable feedback. I would like to thank the National Science Foundation (CMMI-1735483) for the financial support of my research and the Disaster Research Center for their support of this research.

I am extremely grateful to my parents, Mahnaz and Alireza, for their endless love and support. You taught me everything and I could not have been here without you. I know being far away was tough for both of us, but I wish to embrace you soon and celebrate future accomplishments together. I cannot express my feelings in words, I love you both.

TABLE OF CONTENTS

LIST OF TABLES ix
LIST OF FIGURES x
LIST OF NOTATIONS xiii
ABSTRACT xvii

Chapter

1 INTRODUCTION 1

1.1 Introduction 1
1.2 CRISP framework 2
1.3 Objectives 4
1.4 Contributions 5
1.5 Case study 7
1.6 Outline of dissertation 9

2 PROBABILISTIC MULTIHAZARD SCENARIO BASED MODEL FOR SPATIALLY DISTRIBUTED INFRASTRUCTURES 10

2.1 Introduction 10
2.2 Literature review 13

2.2.1 Computationally efficient probabilistic approaches for spatially distributed infrastructure 13
2.2.2 Risk assessment with multiple hazards 14

2.3 Multihazard Optimization-based Probabilistic Scenario (multihazard OPS) method 15

2.3.1 Component hazard models 17
2.3.2 Step-by-step implementation 19

2.3.2.1 Step 1. Generate candidate set of earthquake scenarios 20
2.3.2.2 Step 2. Reduce candidate set of earthquake scenarios based on contribution 21

2.3.2.3 Step 3. Reduce candidate set of earthquake scenarios using optimization 22
2.3.2.4 Step 4. Generate candidate set of multihazard scenarios 25
2.3.2.5 Step 5. Reduce candidate set of multihazard scenarios using optimization 26

2.3.3 Evaluation metrics 27

2.4 Case study 29

2.4.1 Input 29

2.4.1.1 Earthquake sources 29
2.4.1.2 Component hazard models 30
2.4.1.3 "True" hazards 34
2.4.1.4 Pipe damage model 35

2.4.2 Application of multihazard OPS method 36

2.4.2.1 Step 1. Generate candidate set of earthquake scenarios 36
2.4.2.2 Step 2. Reduce candidate set of earthquake scenarios based on contribution 37
2.4.2.3 Step 3. Reduce candidate set of earthquake scenarios using optimization 38
2.4.2.4 Step 4. Generate candidate set of multihazard scenarios 38
2.4.2.5 Step 5. Reduce candidate set of multihazard scenarios using optimization 39

2.4.3 Results 40

2.4.3.1 Final recommended set of probabilistic multihazard scenarios 40
2.4.3.2 Method performance 42

2.4.4 Sensitivity analysis 49

2.5 Conclusion 51

3 SELECTION OF MULTIHAZARD-BASED DAMAGE SCENARIOS FOR THE LOS ANGELES WATER TRANSMISSION NETWORK 53

3.1 Introduction 53
3.2 Damage scenario development method 55
3.2.1 Objective and assumptions 55
3.2.2 Overall framework of the methodology 57
3.2.2.1 Step 1. Generate a set of J multihazard scenarios 57
3.2.2.2 Step 2. Determine Q_j, the number of damage scenarios q for each multihazard scenario j 57
3.2.2.3 Step 3. Generate the set of damage scenarios using the damage scenario optimization 59
3.3 Case study 62
3.3.1 Input 62
3.3.2 Results 64
3.4 Conclusion 69
4 HOUSEHOLD ADAPTATIONS TO AND IMPACTS FROM ELECTRIC POWER AND WATER OUTAGES IN THE TEXAS 2021 WINTER STORM 71
4.1 Introduction 71
4.2 Background 72
4.2.1 Household adaptations to service outages 72
4.2.2 Household impacts from service outages 74
4.3 Research questions 75
4.4 Methodology 76
4.4.1 Data collection 76
4.4.2 Data summary 78
4.4.2.1 Household societal impact, adaptation, and outage duration variables 78
4.4.2.2 Other explanatory variables 82
4.4.3 Imputation 86
4.4.4 Comparison to Los Angeles County data 87
4.5 Analyses and results 88
4.5.1 Adaptation adoption frequency 88

4.5.2 Predictors of adaptation adoption 93
4.5.3 Adaptation groupings 99
4.5.4 Unhappiness 104
4.5.5 Predictors of household unhappiness related to service interruptions 105
4.5.6 Concerns influencing level of unhappiness 109

4.6 Conclusion and future work 110

5 CONCLUSION AND FUTURE WORK 112

5.1 Conclusion 112

5.1.1 Develop probabilistic multihazard scenarios 112
5.1.2 Develop probabilistic damage scenarios 113
5.1.3 Improve understanding of household impact from and adaptation adoption to infrastructure system service outages ... 114

5.2 Future work 115

REFERENCES 117

Appendix

A CITI CERTIFICATES 130
B IRB LETTER 132
C COPYRIGHT PERMISSION FROM AMERICAN SOCIETY OF CIVIL ENGINEERS 133

LIST OF TABLES

Table 2.1. Results of sensitivity analysis for hazard weights 50

Table 3.1. Resistance levels low, moderate, high 63

Table 4.1. Number of responses for each adaptation 80

Table 4.2. Number of respondents associated with each level of categorical variables 84

Table 4.3. Descriptive statistics for continuous variables for Texas and LA 85

Table 4.4. Key differences between Texas and Los Angeles County datasets 88

Table 4.5. (a) P-values of χ^2 tests for electric power adaptations vs. explanatory variables (at significance level=0.05, dark gray=direct effect, light gray=negative effect) 95

Table 4.5. (b) P-values of χ^2 tests for water supply adaptations vs. explanatory variables (at significance level=0.05, dark gray=direct effect, light gray=negative effect) 97

Table 4.6. Matrix of lift for all electric power adaptations (bold: Texas, not bold: Los Angeles) 101

Table 4.7. Matrix of lift for all water adaptations (bold: Texas, not bold: Los Angeles) 103

Table 4.8. Unhappiness model for Texas with corresponding values for LA 107

Table 4.9. Confusion matrix for the Texas unhappiness model 108

LIST OF FIGURES

Figure 1.1: Framework of the CRISP project 4

Figure 1.2: Study area (a) LA city and its water pipeline network map (b) map of customers without power in the 2021 winter storm (from: https://www.nytimes.com/interactive/2021/02/16/us/winter-storm-texas-power-outage-map.html) 9

Figure 2.1. A multihazard scenario 16

Figure 2.2. Main steps of multihazard optimization-based probabilistic scenario (OPS) 20

Figure 2.3. (a) Map of ground failure incidents from Stewart et al. (1996) (b) Map of liquefaction for 1994 Northridge Earthquake 33

Figure 2.4. Traces of 15 considered faults for surface rupture hazard 34

Figure 2.5. Cumulative contribution versus number of earthquake scenarios included 37

Figure 2.6. (a) MHCEG and MHCEL; and (b) average probability errors, both as functions of Nmr, the number of multihazard scenarios in the final reduced set 39

Figure 2.7. Map showing the faults and area sources considered and those selected in the final reduced set of 351 multihazard scenarios 41

Figure 2.8. Comparison of true and reduced set hazard curves, for the sites for which 90% of matches are worse, for (a) ground motion; and (b) liquefaction. 42

Figure 2.9. Histograms of probability errors for (a) ground motion; and (b) liquefaction. 43

Figure 2.10. Maps of (a) "true" ground motion $S_{a(0.2s)}$, (b) ground motion $S_{a(0.2s)}$ based on 351 reduced set multihazard scenarios, and (c) ground motion hazard curve errors, $HCEG, i, 100$, between map (a) and (b), for 100-year and 475-year return periods. 44

Figure 2.11. Maps of (a) "true" ground motion $S_{a(0.2s)}$, (b) ground motion $S_{a(0.2s)}$ based on 351 reduced set multihazard scenarios, and (c) ground motion hazard curve errors, $HCEG, i, 100$, between map (a) and (b), for 1000-year and 2500-year return periods. 45

Figure 2.12. Maps of (a) liquefaction potential, LPI, (b) liquefaction potential, LPI, based on 351 reduced set multihazard scenarios, and (c) liquefaction hazard curve errors, $HCEL, i, 475$, between map (a) and (b), for 100-year and 475-year return periods. 46

Figure 2.13. Maps of (a) liquefaction potential, LPI, (b) liquefaction potential, LPI, based on 351 reduced set multihazard scenarios, and (c) liquefaction hazard curve errors, $HCEL, i, 475$, between map (a) and (b), for 1000-year and 2500-year return periods. 47

Figure 2.14. Comparison of probability distributions of number of damaged pipes based on conventional MCS with 343,891 multihazard scenarios and reduced set of 198 and 351 multihazard scenarios. 49

Figure 3.1. Schematic summary of output of damage scenario development method. 56

Figure 3.2. Histogram of the number of damaged pipes, assuming current resistance levels. 65

Figure 3.3. Exceedance probability of damaged, assuming current resistance levels. . 66

Figure 3.4. One example damage scenario, (a) associated ground motion and rupture map (PGV), (b) Liquefaction Potential Index map (LPI), (c) damaged pipes for current resistance level, (d) damaged pipes assuming moderate resistance level, (e) damaged pipes assuming low resistance level. 68

Figure 4.1. Histograms of the number of adaptations implemented by each respondent for (a) Texas electric power; (b) LA SP electric power; (c) LA RP electric power; (d) Texas water; (e) LA SP water; (f) LA RP water 89

Figure 4.2. (a) Percentage of respondents who said they did/would do each electric power adaptation in Texas, Los Angeles (RP), and Los Angeles (SP) (b) Percentage of respondents who said they did/would do each water adaptation in Texas, Los Angeles (RP), and Los Angeles (SP) 92

Figure 4.3. Empirical probability mass function for Unhappiness by dataset for (a) electric power and (b) water supply 104

Figure 4.4. Extent to which concerns are considered in evaluating unhappiness 109

LIST OF NOTATIONS

Chapter 2:

Notation	Explanation
a_{max}	Peak horizontal ground acceleration (PGA)
$C_{G,j}$	Ground motion contribution factor for earthquake scenario j
$C_{L,j}$	Liquefaction contribution factor for earthquake scenario j
CSR_k	Cyclic stress ratio for layer *k*
CRR_k	cyclic resistance ratio for layer *k*
D_e	"true" number of damaged pipes with annual exceedance probability *e*
$\widehat{D}_e$	Number of damaged pipes from the reduced set with annual exceedance probability *e*
D_n	Expected number of damaged pipes in the multihazard scenario *n*
$e^+_{G,ir}$	Overestimation ground motion error for site *i* and return period *r*
$e^-_{G,ir}$	Underestimation ground motion error for site *i* and return period *r*
$e^+_{L,ir}$	Overestimation liquefaction error for site *i* and return period *r*
$e^-_{L,ir}$	Underestimation liquefaction error for site *i* and return period *r*
$e^+_{s,f}$	Overestimation surface fault rupture error for fault *f*
$e^-_{s,f}$	Underestimation surface fault rupture error for fault *f*
f	Fault index
F	User-specified set of faults considered important for surface fault rupture hazard
G	Ground motion hazard index
$HCE_{G,ir}$	Ground motion hazard curve error at return period *r* and site *i*
$HCE_{L,ir}$	Liquefaction hazard curve error at return period *r* and site *i*
h_k	Soil level *k* thickness
i	Site index
I_G	Ground motion set of sites
I_L	Liquefaction set of sites
j	Earthquake scenario index
J_f	Set of all earthquake scenarios with at least one segment on fault *f*
J_r	Number of earthquake scenarios in the final reduced set
k	Soil level index

k_G	User-specified constant to specify the importance of ground motion hazard
k_L	User-specified constant to specify the importance of liquefaction hazard
k_S	User-specified constant to specify the importance of surface fault rupture hazard
L	Liquefaction hazard index
l_{ij}	Liquefaction potential at site *i* caused by earthquake scenario *j*
LPI	Liquefaction Potential Index
LRI	Liquefaction Resistance Index
$MDCE$	Mean damage curve error
$MHCE_G$	Mean ground motion hazard curve error
$MHCE_L$	Mean liquefaction hazard curve error
$MSCE_G$	Mean spatial correlation error for ground motion
M_w	Earthquake moment magnitude
n_e	Number of probabilities evaluated
N_j	Number of multihazard scenarios associated with each earthquake scenario *j*
N_{mc}	User-specified candidate multihazard scenarios
N_{mr}	Number of multihazard scenarios in the final reduced set
N_{qc}	The candidate set of earthquake scenarios
N_{qr1}	Number of earthquake scenarios in the reduced set after contribution
N_{qr2}	Number of earthquake scenarios in the reduced set after optimization
N_t	Number of pipe segments of type *t* in each grid cell
n	Multihazard scenario index
P_j	annual occurrence probability of earthquake scenario *j*
P_n	Annual probability for each multihazard scenario *n*
p_{tin}	Probability a pipe segment of type *t* in grid cell *i* breaks in multihazard scenario *n*
r	Return period index
R_G	Ground motion return period set
R_L	Liquefaction return period set
$\rho_{i_1,i_2}^{reduced}$	Weighted correlation coefficient of the ground motions at sites i_1 and i_2, for the reduced set
ρ_{i_1,i_2}^{true}	Weighted correlation coefficient of the ground motions at sites i_1 and i_2, for the "true" set
ρ_{bulk}	Bulk density
ρ_{dry}	Dry soil density (above water table)
ρ_m	soil density of layer *m*
ρ_{sat}	Saturated soil density
ρ_w	density of water
s	Surface fault rupture hazard index

$\sigma'_{v,k}$	effective overburden stress at depth z_k
$\sigma_{v,k}$	total overburden stress at depth z_k
t	Pipe segment type index
T	Total contribution factor
V_{s30}	shear-wave velocity over the top 30 m of soil
$V_{s,k}$	Average shear-wave velocities for layer *k*
$V_{s1,k}$	Stress-corrected shear-wave velocity for layer *k*
$V^*_{s1,k}$	Upper limit of $V_{s1,k}$
$\omega_{G,ir}$	User-specified ground motion weight to site *i* and/or return period *r*
$\omega_{L,ir}$	User-specified liqueafction weight to site *i* and/or return period *r*
$w_{S,f}$	User-specified weight for surface fault rupture effect including fault *f*
$x_{PGV,in}$	Peak ground velocity for grid cell *i* and multihazard scenario *n*
$x_{LRI,in}$	Liquefaction resistance index (LRI) for grid cell *i* and multihazard scenario *n*

Chapter 3:

Notation	Explanation
α	Lower bound for $P_{q\|j}$
d	Damage state index
d_j	Number of damaged components in the network associated with multihazard scenario *j*
D_n	Number of damaged components in the network associated with return period *n*
e^+_{ird}	The positive difference between the "true" and estimated probability (based on the reduced set of *Q* damage scenarios) component *i* in resistance level *r* is in damage state *d*
e^-_{ird}	The negative difference between the "true" and estimated probability (based on the reduced set of *Q* damage scenarios) component *i* in resistance level *r* is in damage state *d*
i	Component (pipe) index
j	Multihazard scenario index
J	Number of multihazard scenarios
m_{ird}	"true" probability that component *i* in resistance level *r* is in damage state *d*
P_j	Adjusted annual occurrence probability of multihazard scenario *j*
$P_{q\|j}$	Adjusted occurrence probability of damage scenario *q* sourced by multihazard scenario *j*
q	Damage scenario index
Q	Total number of damage scenarios

Q_j	Number of damage scenarios for multihazard scenario *j*
r	Resistance level index
w_{irdq}	Binary variable that is 1 if component *i* in resistance level *r* and damage scenario *q* is in damage state *d*

Chapter 4:

Notation	Explanation
α_k	Thresholds separating the *k* categories (in the regression model)
$\vec{\beta}$	The vector of regression parameters
i	Individual index
k	Unhappiness category index
K	Total number of categories for unhappiness
pik	The probability that unhappiness of individual *i* is in category *k*
$\vec{\theta}_i$	Random subject effect associated with individual *i* on their repeated assessments
$\vec{x}_i$	Covariate vector for individual *i*
Zi	Unhappiness ordinal variable for individual *i* that indicates the *k*th ordered category

ABSTRACT

This dissertation makes three major contributions to the development of a new method to describe the earthquake risk to civil infrastructure systems in terms of societal (household) impact. The overall method is the focus of an interdisciplinary research project funded by the National Science Foundation, Critical, Resilient Infrastructure Systems, and Processes (CRISP) program. The contributions of this dissertation specifically are summarized as follows. First, we developed the Multihazard Optimization-Based Probabilistic Scenario (multihazard OPS) method and applied it to Los Angeles. To present a computationally efficient set of multihazard scenarios including the effects of three different co-occur hazards (e.g., ground motion, liquefaction and surface fault rupture), we applied mixed-integer linear programming from the Extended OPS-based method and extended the objective function for multiple hazards. The application to Los Angeles shows that while more scenarios are necessary for the multihazard analysis to obtain similarly small errors as for an analysis of ground motion alone, errors small enough for practical reasons may still be achieved with only a few hundred multihazard scenarios.

Second, we developed a computationally efficient set of probabilistic earthquake damage scenarios for the Los Angeles water transmission system. We applied a damage model for the water pipeline system assuming different design levels (given specific system objectives) of the components to estimate the damages due to the final reduced set of multihazard scenarios achieved by the first contribution. In addition, applying a mixed-integer nonlinear program ensured us that the method is

computationally efficient enough to be implemented to a real network for many risk management strategies. The application to the Los Angeles water transmission system demonstrates how a set of probabilistic earthquake damage scenarios can support the design and analysis of spatially distributed infrastructure systems to achieve a specific system performance. These damage scenarios can assist in making informed component replacement decisions because they indicate the damage state of each network component under different resistance levels.

Third, household adaptations to and impacts of electric power and water supply outages were examined. We deployed a web-based survey for the Texas 2021 winter storm and built statistical models to investigate the effects of household and event attributes, household risk experience and perception, and social connectedness on household impact and adaptation adoption. The results from this study were compared to findings from Los Angeles (both revealed and stated preferences) studies to explore the patterns and generalizability of the results. The findings revealed a similar frequency of implemented adaptations to those in Los Angeles, but predictors of adaption and the household impact that were somewhat different. These findings provide insight to comprehend the degree of societal impact and adaptation adoption due to service interruptions, which can facilitate efficient emergency management.

Chapter 1

INTRODUCTION

1.1 Introduction

Infrastructure systems such as water supply, electric power, transportation, and communications are vital to the functioning of society. They must be resilient to protect security, the economy, and social welfare. In many countries, such as the United States, however, they are at risk of experiencing major damage and disruption from all forms of natural hazards, including hurricanes, storms, wildfires, and earthquakes. These interruptions in the services of infrastructure systems have the potential to yield many negative consequences for households, businesses, and other organizations. Thus, understanding how infrastructure systems can be damaged and can negatively impact societal functioning can help to create more reliable and prepared infrastructures and communities.

One of the complexities in assessing the damage in spatially distributed infrastructure networks is the spatial correlation among the components. This correlation relates the damage and performance level of components to each other. Another significant issue in quantifying the infrastructure system risk is the need to make sure the effects of concurrent hazards are considered (e.g., in the case of earthquakes, that includes ground shaking, liquefaction, and surface fault rupture). The reason is concurrent hazards can combine and exacerbate total risk.

When infrastructure systems are damaged, the service they provide is often interrupted as well. Because of the importance of those services in enabling daily

activities, the risk of interruption plays a vital role in determining the resiliency of a community. Nevertheless, the way these services meet societal needs and how interruptions of those services impair the ability to meet those needs are not well-understood (Sattar et al. 2021). Addressing this knowledge gap requires better understanding the types, prevalence, and effects of adaptive strategies that system users take to meet their needs when disrupted; the typical user needs that can not be met through adaptive strategies; and how adaptations and the ultimate effects on daily life vary depending on who is receiving the service and under what circumstances the lack of service occurred.

The research presented in this dissertation is part of a larger research project funded by the National Science Foundation Critical, Resilient Infrastructure Systems, and Processes (CRISP) program. After briefly introducing the CRISP project, the main objectives and contributions of this dissertation are described in Sections 1.3 and 1.4, respectively. Section 1.5 introduces the two case study areas, and the Chapter concludes with an outline of the remainder of the dissertation.

1.2 CRISP framework

The CRISP project aims to improve understanding of the relationship between infrastructure systems functioning and societal functioning, and how to design, manage, and operate these systems to maximize societal functioning. With a focus on earthquake hazard and electric power and water supply systems, it involves four main goals:

(1) Develop a probabilistic scenario-based model of the risk of multiple infrastructure systems to earthquakes with the ability to evaluate alternative risk management strategies.

(2) Integrate the complementary strengths of social media, household surveys, and economic impact analyses to empirically assess societal objectives, users' adaptive strategies in responding to disruptions, and the relationships between them and traditional measures of system functioning.

(3) Develop an optimization model to optimize risk management to meet societal objectives.

(4) Apply models through a case study application for electric power and water in Los Angeles.

The CRISP project is structured around a conceptual framework that relates traditional risk modeling of infrastructure systems to societal functioning (Figure 1.1). Within the framework (Fig. 1.1), Step (A) is to generate a computationally efficient set of probabilistic hazard scenarios associated with earthquakes while considering multiple effects of seismic hazards. Step (B) generates a computationally efficient set of probabilistic damage scenarios corresponding to each hazard scenario in Step (A). Step (C) computes the system functioning of the damaged system for each damage scenario in Step (B). In Step (D), the system functioning for each scenario from Step (C) is modified based on implementation of adaptive strategies by service users. Steps (G) and (F) help understand the effects of adaptive strategies on system functioning, which depends on the types implemented, their prevalence, and the effect of each. Those, in turn, depend on attributes of system users, uses, and the disruptive event. The modified system functioning is then translated into societal functioning in Step (E), which is then optimized in Step (H).

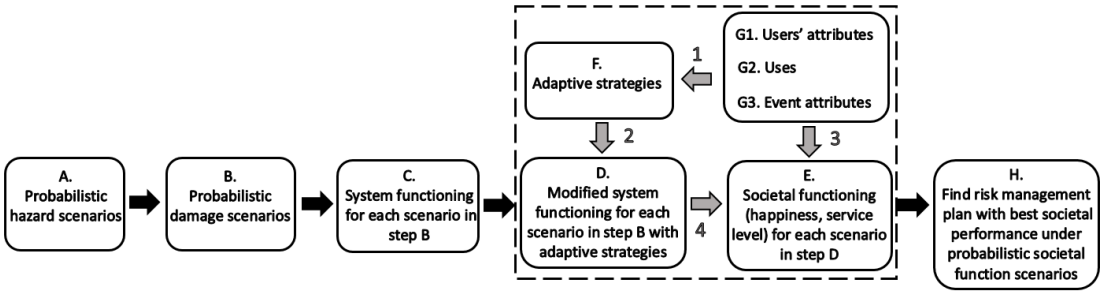

Figure 1.1: Framework of the CRISP project

1.3 Objectives

This dissertation focuses on achieving Steps A and B, and contributing to Steps E and F in the CRISP framework (Fig. 1.1). Specifically, the objectives are as follows:

(1) **Develop the Multihazard Optimization-Based Probabilistic Scenario (multihazard OPS) method and apply it to Los Angeles.** This method should create an ensemble of multihazard scenarios that can be used for efficient evaluation of spatially distributed infrastructure. Each multihazard scenario offers a possible realization of the co-occurring multiple hazard effects associated with a single earthquake, and together, when the small set of multihazard scenarios are combined with their computed weights, they represent the probabilistic hazard in a way that captures spatial correlation, includes multiple hazards, and is computationally-efficient based on run-time and memory.

(2) **Develop a computationally efficient set of probabilistic earthquake damage scenarios for the Los Angeles water transmission system.** This objective aims to produce a relatively small set of probabilistic damage

scenarios that capture the damage consistently for all possible components of the system and are computationally efficient for subsequent system-level risk analysis, such as evaluation of the post-disaster system functionality. We build on a previously available method, but apply it for a new infrastructure system type (water supply instead of highways) that includes many more components (pipe segments instead of bridges), consider ground motion, liquefaction and surface fault rupture (not just ground motion), and conduct the analysis for a full set of multihazard scenarios (rather than a single earthquake scenario).

(3) **Describe the adaptation to and household impact of electric power and water supply outages during the 2021 Texas Winter Storm.**

This objective adds to the very limited available quantitative empirical knowledge about household adaptations to and impacts of infrastructure service interruption. That is, it investigates the effects of household and event attributes, risk experience and perception, and social connectedness on the impact to households and adaptation adoption. Importantly, it aims to begin to evaluate the extent to which findings of a recent previous study in Los Angeles which was based on revealed and stated preference data (also part of the CRISP project) are generalizable to this new event and location.

1.4 Contributions

The main contributions in this dissertation are:

(1) **Develop the Multihazard Optimization-Based Probabilistic Scenario (multihazard OPS) method and applying it to Los Angeles**. This research contributes to the literature by combining two lines of research—computationally efficient probabilistic approaches to spatially distributed

infrastructure and risk assessment with multiple hazards. It builds on the Extended Optimization-based Probabilistic Scenario (OPS) method from Han and Davidson (2012) and Manzour et al. (2016), but expands it to make it multihazard for the first time, specifically to include ground motion, liquefaction, and surface fault rupture hazards in an integrated way. The full-scale application to Los Angeles examines if including multiple hazards requires more scenarios to match the probabilistic hazard than when ground motion alone is addressed. Importantly, it evaluates how developing an ensemble of multihazard scenarios by matching one hazard type indirectly leads to a good match for others.

(2) **Develop a computationally efficient set of probabilistic earthquake damage scenarios for the Los Angeles water transmission system.** To develop damage scenarios, we applied a mixed-integer nonlinear optimization model based on Brown et al. (2013) for a more complicated network, a water pipeline system. Further, we assumed the components' different design levels (given specific system objectives) to support future informed decisions such as pipe replacement. Notably, we considered ground motion and liquefaction (not just ground motion) and conducted the analysis for a complete, computationally efficient set of multihazard scenarios developed in this dissertation (Objective 1).

(3) **Examine the adaptation to and household impact of electric power and water supply outages during the 2021 Texas Winter Storm**. The case study contributes to the relatively small empirical literature on household impact and adaptation adoption through a survey-based data analysis for households

affected by the 2021 Texas winter storm. We asked the same questions as Abbou et al. (2022) and Stock (2020) did for Los Angeles county. The Texas study was more based on revealed behavior of households in a recent major event, while Los Angeles study focused on stated preference responses and revealed preference responses for each respondent's longest outage experience (not a single event, and mostly of relatively short duration). The results from this case study were compared to findings from the Los Angeles studies to explore the patterns and generalizability of the results.

1.5 Case study

This dissertation uses two case study areas to demonstrate the application of key contributions in this research—Los Angeles, California and the area affected by the 2021 winter storm that was centered on North Texas. The probabilistic multihazard scenario method and the probabilistic damage scenario analysis were both applied to Los Angeles, the latter to the Los Angeles water supply transmission network in particular. The analysis of adaptation adoption and household impact due to service interruptions was conducted for the area affected by the 2021 Texas winter storm and compared to a similar analysis based on data from Los Angeles.

The first case study area is Los Angeles city, a Southern California city with a population of nearly 4 million in an area of 1,300 Km^2 (US Census Bureau 2019). This city is one of the most seismically active cities in the U.S. (Chen et al. 2016). A new earthquake forecasting model for California predicts that in the next 30 years, there is a 60% chance this city will experience one or more earthquakes with magnitude 6.7 or greater (Field et al. 2014). The Los Angeles Department of Water and Power (LADWP) water transmission network includes approximately 2,200 Km

of pipes serving 680,000 customers. This indicates the wide extent and complexity of this network (Fig. 1.2a).

The second case study focuses on a winter storm that affected parts of Texas and surrounding areas on February 13-17, 2021 and disrupted power and/or water supply for 4.5 million homes and businesses at its peak (Fig. 1.2b). Snow and ice paired with extremely low temperatures caused widespread road closures and unsafe travel conditions due to this storm. This storm contributed to 246 fatalities (Texas DSHS 2021). From a financial viewpoint, the storm's economic toll is estimated to be as high as $295 billion (Watson et al. 2021). This case study area was chosen because the severe interruptions in the electric power and water supply systems due to the winter storm offered an opportunity to investigate the revealed behavior of households, which could then complement a previous analysis based primarily on a stated preference data for Los Angeles (Abbou et al. 2022, Stock 2020).

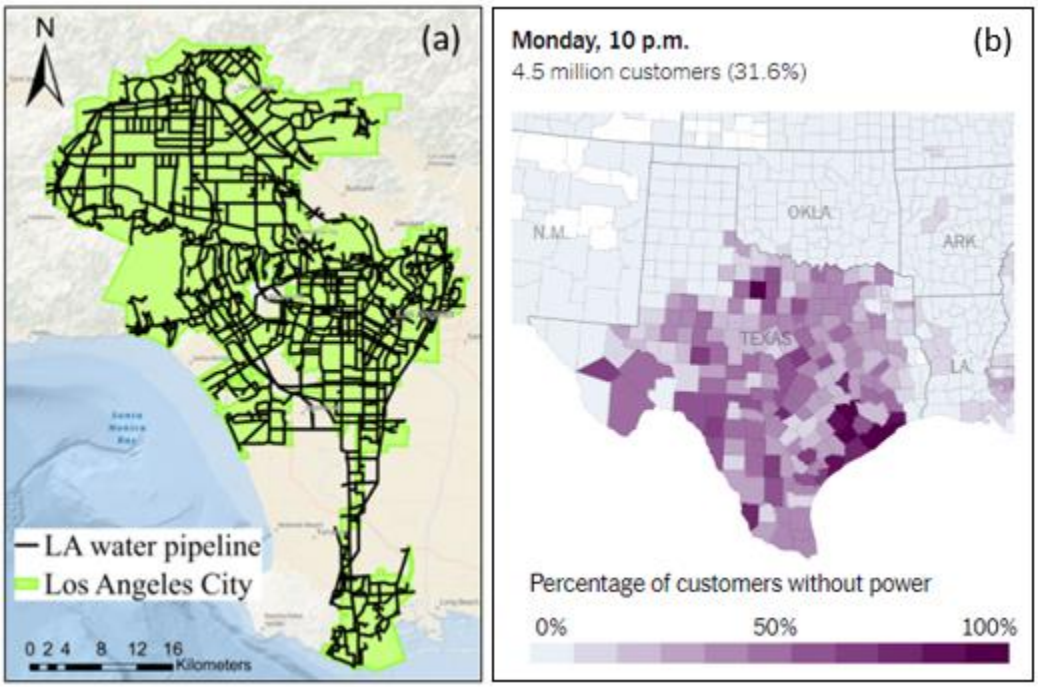

Figure 1.2: Study area (a) LA city and its water pipeline network map (b) map of customers without power in the 2021 winter storm (from: https://www.nytimes.com/interactive/2021/02/16/us/winter-storm-texas-power-outage-map.html)

1.6 Outline of dissertation

This dissertation consists of five chapters. Chapter 2 describes the new multihazard optimization-based probabilistic scenario method for spatially distributed infrastructures. A full-scale case study for earthquake risk in Los Angeles city is conducted to illustrate the application of this model. Chapter 3 presents application of the probabilistic multihazard based damage scenario model for the Los Angeles water transmission network. Chapter 4 introduces analysis of the household impact and adaptation adoption during the Texas 2021 winter storm. Chapter 5 summarizes the conclusions and possible future extensions of this research.

Chapter 2

PROBABILISTIC MULTIHAZARD SCENARIO BASED MODEL FOR SPATIALLY DISTRIBUTED INFRASTRUCTURES

2.1 Introduction

Recognizing their importance in community resilience, spatially distributed infrastructure, such as water supply and electric power networks, have received increasing attention within the earthquake engineering community. Seismic risk assessments of these infrastructures ideally (1) capture spatial correlation, (2) are probabilistic, (3) are computationally efficient, and (4) address the multiple hazards that co-occur in an earthquake. Unlike risk assessment of a single-location facility, the analysis must address the spatial correlation of the components that comprise an infrastructure system, and thus scenario-based approaches, in which the joint performance of all facilities is assessed for one earthquake at a time, are preferred (Crowley and Bommer 2006, Han and Davidson 2012). As with single-location facilities, probabilistic risk assessment is required to support resource allocation and other decisions because the best designs or policies often differ depending on which earthquake occurs. Although probabilistic seismic hazard analysis methods have been available for years, combining it with scenario-based analysis leads to computational challenges. The most straightforward way to accomplish probabilistic scenario-based analysis is using conventional Monte Carlo simulation, in which a rupture, ground motion, facility damage, and system performance are simulated in turn; the process is repeated many times; and the results are combined. To capture the more intense, less

frequent events, however, requires many replicates. With computationally intensive models of system performance (e.g., traffic model for the highway system), this approach becomes highly inefficient if not intractable. Finally, in many regions and for some infrastructure types, liquefaction, surface fault rupture, and landslide can cause substantial damage in addition to ground motion. For buried pipelines and roads, in particular, these collateral hazards have represented a major portion of the damage (e.g., O'Rourke et al. 2014). For a complete risk assessment, all relevant hazards should be included.

Recent work has addressed the first three issues—spatial correlation, probabilistic analysis, and computational efficiency—by developing methods to identify a computationally efficient set of earthquake rupture or ground motion scenarios, each with a hazard-consistent annual occurrence probability, that can be used for probabilistic analysis of spatially distributed infrastructure (Section 2.2.1). The methods perform well, but almost always address only ground motion. In parallel, research has expanded typical ground motion analyses to include collateral hazards like landslide and liquefaction (Section 2.2.2), but those studies have not been fully probabilistic. This study contributes to the literature by integrating these two lines of research to develop a method for multihazard probabilistic seismic hazard analysis for spatially distributed infrastructure. It builds on the Extended Optimization-based Probabilistic Scenario (OPS) method from Han and Davidson (2012) and Manzour et al. (2016), but expands it to make it multihazard, specifically to include ground motion, liquefaction, and surface fault rupture hazards in an integrated way. The method is applied to the City of Los Angeles, California. In the case study, we demonstrate the method, examine if including multiple hazards requires more

scenarios to match the probabilistic hazard than when ground motion alone is addressed, and assess the extent to which developing an ensemble of multihazard scenarios by matching one hazard type indirectly achieves a good match for others.

Key strengths of the new Multihazard Optimization-based Probabilistic Scenario (multihazard OPS) method include the following. First, it generates a relatively small, user-specified number of multihazard scenarios, each with an associated hazard-consistent annual occurrence probability, and each of which represents a physically realistic description of ground motion, liquefaction, and surface fault rupture that could co-occur in a single event. Together, the set of multihazard scenarios (on the order of a few hundred for a large, seismically-active city) are determined so as to minimize the error between (a) the probabilistic ground motion, liquefaction, and surface fault rupture hazard based on the reduced set and (b) that based on a full conventional Monte Carlo simulation. Second, the tradeoff between the error and the number of multihazard scenarios included in the reduced set is explicit, allowing the user to decide the appropriate balance for a given application. Third, once the reduced set of multihazard scenarios is determined for a city or region, it can be used for seismic risk analyses for all aspects of the city (e.g., utility and transportation networks, buildings) to ensure consistency and minimize repetition of effort. Following a summary of the relevant literature in Section 2.2, the new Multihazard OPS method is presented in Section 2.3. Section 2.4 describes a case study for Los Angeles, and the chapter concludes with suggested avenues of future research.

2.2 Literature review

2.2.1 Computationally efficient probabilistic approaches for spatially distributed infrastructure

Recognizing the computational demands of conventional Monte Carlo simulation (MCS), Chang et al. (2000) introduced the idea of selecting a relatively small set of earthquake scenarios (defined by a source-magnitude combination) and assigning each a *hazard-consistent* annual occurrence probability. That set is then used for a risk analysis instead of the full set of simulated scenarios. Each hazard-consistent annual occurrence probability can be thought of as a weight. It is not the actual likelihood of occurrence of the associated earthquake, but rather an artificial probability assigned so that the probabilistic combination of the selected set of earthquake scenarios matches hazard maps based on a full probabilistic seismic hazard analysis using a typical discretization approach (which we call PSHA) or conventional MCS.

Jayaram and Baker (2010) extended the idea to include selection of a reduced set of ground motion scenarios with associated hazard-consistent occurrence probabilities. They also advanced it by introducing importance sampling to efficiently generate the candidate sets of earthquake scenarios and ground motion maps, and using a k-means clustering approach to simultaneously select the reduced set of ground motion maps and assign the hazard-consistent annual occurrence probabilities. The Extended Optimization-based Probabilistic Scenario (OPS) method further advanced the idea, providing a reproducible method based on a mixed integer linear program that guarantees the minimum error between the reduced set of ground motion scenarios and a full PSHA, and that explicitly characterizes the magnitude and nature of those errors (Vaziri et al. 2012, Han and Davidson 2012, Manzour et al. 2016)).

Zolfaghari and Peyghaleh (2016) offered a similar application for Tehran, Iran, and Apivatanagul et al. (2011) applies a similar method to hurricane wind and coastal flooding. Christou et al. (2018) describes Hazard Quantization, a method similar to k-means clustering but derived from the concept of continuous random fields. Finally, Miller and Baker (2015) extend these ideas to probabilistic damage scenarios that can further improve efficiency in a risk analysis for spatially distributed infrastructure, using exceedance rates instead of exceedance probabilities.

These methods accomplish the goal of computationally tractable, scenario-based, probabilistic seismic hazard analysis. Using the Extended OPS method in an application in the highly seismic area of Christchurch, New Zealand, just 125 ground motion scenarios matched the hazard curves and loss exceedance curves based on a million-year simulation with errors insignificant for practical purposes (Manzour et al. 2016). With the exception of Du and Wang (2013), which applies the Extended OPS method with the addition of slope displacement, all of these studies address only the transient ground movement hazard. In this dissertation, we build on the Extended OPS method.

2.2.2 Risk assessment with multiple hazards

Other research is developing methods to address multiple hazards. These multihazard approaches include two distinct situations—combining diverse hazards (e.g., earthquake, wildfire, hurricane) because they can occur in the same region (e.g., Greiving 2006, Salman and Li 2018), and integrating hazards because one triggers another or they co-occur (e.g., earthquake ground motion triggering landslide or liquefaction) (Kappes et al. 2012). For the latter, the multiple hazards can be part of a single complex event.

Recent efforts to address multiple hazards in the context of spatially distributed infrastructure systems include analyses of ground motion, flood, and landslide hazards for transportation networks in Europe (Clarke and Obrien 2016, INFRARISK 2019); ground motion, liquefaction, post-earthquake fire hazards for gas pipelines in Tehran (Omidvar and Kivi 2016); ground motion and hurricane wind hazards for electric power transmission systems (Salman and Li 2018); and earthquake ground motion, liquefaction, and landslide hazards for gas pipelines (De Risi et al. 2018). With a focus on integrating the models of different hazards, however, these studies have not typically emphasized an effort to simultaneously make the analysis efficiently probabilistic. Instead, De Risi et al. (2018) and Omidvar and Kivi (2016), for example, limit their analyses to a single earthquake scenario or fault, including uncertainty in ground motion and component damage, but not rupture. As the former notes, they are appropriate for post-event analysis, but for a long-term risk analysis that considers all possible ruptures, they would be too computationally intensive. Even with importance sampling, a seismic analysis for Christchurch, New Zealand resulted in approximately 75,000 rupture scenarios (Manzour et al. 2016). At the almost 20 min. per run for one rupture that De Risi et al. (2018) reports, it would be infeasible to apply for all of them.

2.3 Multihazard Optimization-based Probabilistic Scenario (multihazard OPS) method

The Multihazard OPS method is similar to that in Manzour et al. (2016), but modified to address multiple, co-occurring earthquake-related hazards. Whereas Manzour et al. (2016) and other methods aimed to produce a set of *earthquake scenarios* (defined by source and magnitude) and/or *ground motion scenarios*, the

Multihazard OPS method output is a small set of multihazard scenarios, each with an associated hazard-consistent annual occurrence probability. A *multihazard scenario n* is a map depicting a possible realization of the multiple hazard effects associated with a single earthquake, including ground motion intensity, liquefaction potential, and surface fault rupture (Fig. 2.1). The hazard-consistent annual occurrence probability P_n can be thought of as a weight. Together, when the small set of multihazard scenarios are combined with their weights, they represent the probabilistic hazard in a way that captures spatial correlation, includes multiple hazards, and is computationally efficient.

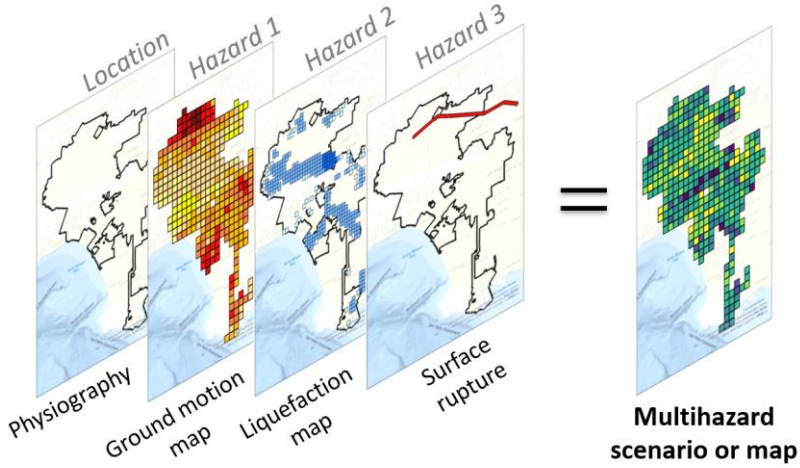

Figure 2.1. A multihazard scenario

Specifically, for ground motion, the reduced set of multihazard scenarios match as well as possible the "true" hazard curves (i.e., those based on a conventional PSHA or MCS) and the "true" spatial correlation (i.e., that based on a conventional MCS). The matches are defined at a set of specified sites i, and a set of specified

points on the hazard curves (defined by the corresponding return periods r). Similarly, for liquefaction, the reduced set of multihazard scenarios match as well as possible the "true" liquefaction hazard curves and spatial correlation, although the specified sites and return periods may or may not be the same as those for ground motion. For surface fault rupture, the reduced set of multihazard scenarios match as well as possible the "true" probability of rupture on specified critical faults. The method also provides errors in the hazard curve, spatial correlation, and rupture probability matches.

We consider ground motion, liquefaction, and surface fault rupture hazards, three of the most consequential hazards. The method could be extended further, however, to consider additional collateral hazards, such as landslide or tsunami inundation. We expect that as more hazards are included, more multihazard scenarios will be required to achieve the same match.

2.3.1 Component hazard models

Including multiple hazards requires a component hazard model for each. Any metric can be used for ground motion intensity (e.g., peak ground acceleration, spectral acceleration) as long as there is a model to compute it. Ground motion prediction equations (GMPEs) will typically be used, although the method could be adapted to apply physics-based models.

A second model is required to compute liquefaction potential and/or intensity at each site in the region for a specified earthquake and ground motion scenario. Liquefaction susceptibility describes characteristics of the soil that make it more or less prone to liquefaction. When subjected to sufficiently strong ground motion, liquefaction can be triggered in susceptible soil, subsequently potentially producing

permanent ground deformation (PGD). Liquefaction potential depends on the combination of liquefaction susceptibility and ground motion. Metrics that could be used to describe liquefaction potential or intensity include probability that liquefaction occurs (e.g., Zhu et al. 2017, Kayen et al. 2013, NIBS and FEMA 2003), liquefaction potential index, LPI (Iwasaki et al. 1984, Maurer et al. 2014), factor of safety for liquefaction (e.g., Mayfield et al. 2010), a binary indicator variable (liquefaction/no liquefaction), and PGD caused by liquefaction (e.g.,Baska 2003, Youd et al. 2002). The liquefaction model employed should: (1) be able to predict liquefaction potential/intensity at each site in the study region as accurately as possible, (2) describe liquefaction in terms of the desired metric, and (3) be applicable throughout the whole study region, which means that all required input data are available throughout the region. If the intent is to use the multihazard scenarios to estimate damage to pipelines or buildings, the liquefaction measure used must be the same as (or able to be translated into) that used in the damage model. Since most methods require site-specific geotechnical data such as cone penetration test (CPT) or standard penetration test (SPT) results, which are not typically available for an entire region, this final requirement can be limiting.

Although it is often omitted in favor of focus on more geographically widespread effects like ground motion, the surface fault rupture hazard can be important, especially for long ruptures that could simultaneously damage pipelines or other infrastructure in multiple places in a single event. Surface fault rupture hazard differs from ground motion and liquefaction because it is localized along the length of a fault rupture, and therefore must be modeled differently. Multiple earthquakes can cause ground motion and/or liquefaction at a site, allowing the method to match the

probabilistic hazard by determining hazard-consistent probabilities in a way that eliminates some earthquakes and weighs others heavily. By contrast, at a particular site, typically only one earthquake-generating source could cause the permanent ground deformation associated with fault rupture. Thus, the only way to match the probability of surface rupture displacement at a site is to include a rupture on that fault in the final reduced set of multihazard scenarios. It is impossible, therefore, to match the surface fault rupture hazard everywhere in the study area with a small set of scenarios. Instead, we focus on a small user-identified set of faults that are of particular concern and we require the reduced set of multihazard scenarios to match the probability of rupture on those faults only. Surface fault rupture intensity can be measured as a binary variable (occurs or not) or in terms of the resulting permanent ground displacement (e.g., Petersen et al. 2011). As with liquefaction and ground motion, the best surface fault rupture hazard model depends on predictive power, availability of the required input data, and output metric required for use in subsequent analyses.

2.3.2 Step-by-step implementation

The Multihazard OPS method includes 5 main steps, adapted from Manzour et al. (2016) (Fig. 2.2): (1) generate a candidate set of earthquake scenarios (ruptures), (2) reduce the set of earthquake scenarios based on their contribution to the ground motion and liquefaction hazards, (3) reduce it and assign hazard-consistent annual occurrence probabilities using a mixed integer linear program (MILP), (4) generate multihazard scenarios for each earthquake scenario in the reduced set in a way that minimizes sampling variability, and (5) reduce the multihazard scenarios using the

same MILP from Step 3. Han and Davidson (2012) and Manzour et al. (2016) include additional detail; this section highlights aspects that are new.

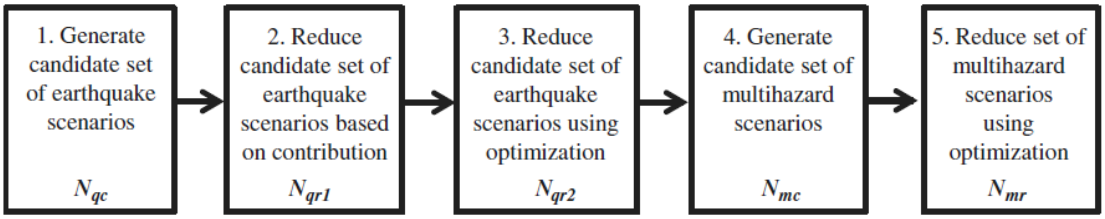

Figure 2.2. Main steps of multihazard optimization-based probabilistic scenario (OPS)

2.3.2.1 Step 1. Generate candidate set of earthquake scenarios

We first generate an initial candidate set of N_{qc} earthquake scenarios. In general, this is done by sampling events for each earthquake fault or area source based on the associated magnitude-frequency distribution, using importance sampling of the magnitudes to more efficiently include higher magnitude events of greatest consequence (Han and Davidson 2012). (Note that, as described in Section 2.4.1, in the case study herein, we use a different earthquake scenario generation approach for fault sources so as to be consistent with the recent 2014 National Seismic Hazard Map.) The user also identifies and includes in the candidate set any particular earthquake scenarios that are of interest due to their potential surface fault rupture hazard. Importantly, there is no single best candidate set of earthquake scenarios, so the method used is not critical (Vaziri et al. 2012). The candidate set should include only physically realistic earthquakes and should be sufficiently large and diverse that the hazard curves can be matched. Beyond that, it does not matter since only a small number will be included in the final reduced set anyway.

2.3.2.2 Step 2. Reduce candidate set of earthquake scenarios based on contribution

In Step 2, we reduce the candidate set of earthquake scenarios by removing any that are not among those that contribute most to the ground motion or liquefaction hazard. The contributions, $C_{G,j}$ and $C_{L,j}$, of each earthquake scenario *j* to the ground motion and liquefaction hazard, respectively, are defined as:

$$C_{G,j} = \frac{1}{I_G R_G} \sum_{i=1}^{I_G} \sum_{r=1}^{R_G} \frac{P_j P(y_{ij} \geq Y_{ir})}{\sum_{j=1}^{J} P_j P(y_{ij} \geq Y_{ir})} \quad (2.1)$$

$$C_{L,j} = \frac{1}{I_L R_L} \sum_{i=1}^{I_L} \sum_{r=1}^{R_L} \frac{P_j P(l_{ij} \geq L_{ir})}{\sum_{j=1}^{J} P_j P(l_{ij} \geq L_{ir})} \quad (2.2)$$

where P_j is the annual occurrence probability of earthquake scenario *j*; Y_{ir} is the "true" ground motion for return period *r* at site *i*; y_{ij} is the ground motion at site *i* caused by earthquake scenario *j*; L_{ir} is the "true" liquefaction potential for return period *r* at site *i*; l_{ij} is the liquefaction potential at site *i* caused by earthquake scenario *j*; J is the number of earthquake scenarios (same as N_{qc} in Section 2.3.2.1); $0 \leq \omega_{G,ir} \leq 1$ and $0 \leq \omega_{L,ir} \leq 1$ are user-specified weights that can be used to give extra weight to certain sites and/or return periods if desired, such that $\sum_{ir} \omega_{G,ir} = 1$ and $\sum_{ir} \omega_{L,ir} = 1$; I_G and I_L are the number of sites for the ground motion and liquefaction hazard, respectively; and R_G and R_L are the number of return periods for the ground motion and liquefaction hazard, respectively. The $P(y_{ij} \geq Y_{ir})$ are computed by integrating over the ground motion prediction equations. (Note that although the P(yij>=Yir) values are conditional probabilities more completely written as $P(y_{ij} \geq Y_{ir} | Scenario\ j)$, for brevity and to remain consistent with Han and Davidson (2012) and Manzour et al. (2016), we use the notation $P(y_{ij} \geq Y_{ir})$). Uncertainty in l_{ij} depends only on earthquake magnitude and ground motion intensity (Section 4.1.2), so

to compute $P(l_{ij} \geq L_{ir})$, for each possible magnitude, we calculate the ground motion intensity $Y_{L_{ir}}$ associated with L_{ir} and then find $P(y_{ij} \geq Y_{L_{ir}})$.

To ensure earthquake scenarios are retained if they contribute greatly to either the ground motion or liquefaction hazard, all candidate earthquake scenarios are ranked from largest to smallest based on $\max(C_{G,j}, C_{L,j})$. Only those that together account for the top *T*% of total ground motion contribution and the top *T*% of liquefaction contribution are retained. At the end of Step 2, N_{qr1} earthquake scenarios remain. Note that different thresholds *T* could be used (Manzour et al. 2016). Conceptually, Step 2 is not required since Step 3 will reduce the candidate set of earthquake scenarios again anyway. It is recommended, however, since it makes the optimization in Step 3 easier to solve computationally, the scenarios omitted in Step 2 contribute so little to the hazard curves that their removal has little effect, and it adds little time since the required probabilities, $P(y_{ij} \geq Y_{ir})$ and $P(l_{ij} \geq L_{ir})$, have to be computed for Step 3 anyway.

2.3.2.3 Step 3. Reduce candidate set of earthquake scenarios using optimization

In Step 3, a mixed-integer linear program is used to further reduce the candidate set of N_{qr1} earthquake scenarios to a smaller user-specified N_{qr2} and to assign a hazard-consistent annual occurrence probability, P_j, to each remaining earthquake scenario (Eqs. 2.3-2.13). The optimization is like that in Han and Davidson (2012) and Manzour et al. (2016) except that new constraints are added to define errors in liquefaction and surface fault rupture hazard, and those errors are added to the objective function so that the optimization aims to reduce them as well as errors in the ground motion hazard curves.

$$Minimize: k_G \sum_{i\in I_G}\sum_{r\in R_G} w_{G,ir}\left(e^{+}_{G,ir} + e^{-}_{G,ir}\right) + k_L \sum_{i\in I_L}\sum_{r\in R_L} w_{L,ir}(e^{+}_{L,ir} + e^{-}_{L,ir}) + k_s \sum_{f\in F} w_{S,f}(e^{+}_{s,f} + e^{-}_{s,f}) \quad (2.3)$$

The objective (Eq. 2.3) is to minimize the weighted errors in the ground motion, liquefaction, and surface fault rupture hazards subject to several constraints (Eq. 2.4-2.13). The user-specified constants, k_G, k_L, and k_S, allow the user to stipulate the relative importance of matching the three types of hazard.

$$\sum_{j=1}^{J}\left\{P_j * P\left(y_{ij} \geq Y_{ir}\right)\right\} - e^{+}_{G,ir} + e^{-}_{G,ir} = 1 - e^{-1/r} \qquad \forall i \in I_G,\ r \in R_G \quad (2.4)$$

$$\sum_{j=1}^{J}\left\{P_j * P\left(l_{ij} \geq L_{ir}\right)\right\} - e^{+}_{L,ir} + e^{-}_{L,ir} = 1 - e^{-1/r} \qquad \forall i \in I_L,\ r \in R_L \quad (2.5)$$

$$\sum_{j\in J_f} P_j - e^{+}_{s,f} + e^{-}_{s,f} = P_{t,f} \qquad \forall f \in F \quad (2.6)$$

$$\sum_{j\in J_f} z_j \geq 1 \qquad \forall f \in F \quad (2.7)$$

$$P_j \leq z_j \qquad \forall j \quad (2.8)$$

$$\sum_{j=1}^{J} z_j \leq J_r \quad (2.9)$$

$$e^{+}_{G,ir}, e^{-}_{G,ir} \geq 0 \qquad \forall i \in I_G, r \in R_G \quad (2.10)$$

$$e^{+}_{L,ir}, e^{-}_{L,ir} \geq 0 \qquad \forall i \in I_L, r \in R_L \quad (2.11)$$

$$e^{+}_{s,f}, e^{-}_{s,f} \geq 0 \qquad \forall f \in F \quad (2.12)$$

$$0 \leq P_j \leq 1,\ z_j \in \{0,1\} \qquad \forall j \quad (2.13)$$

As in Manzour et al. (2016) and Han and Davidson (2012), the ground motion error term is the weighted sum of errors over all sites *i* and return periods *r*, between points on the "true" ground motion hazard curves and the corresponding points on hazard curves developed with the reduced set of earthquake scenarios and the hazard-consistent annual occurrence probabilities. The first term in Equation 2.4 is the annual probability of exceeding Y_{ir} as estimated based on the reduced set of multihazard scenarios. Thus, $e^{+}_{G,ir}$ and $e^{-}_{G,ir}$ are the errors resulting from overestimating and

underestimating, respectively, the "true" annual exceedance probability, 1-exp(-$1/r$), for return period *r* at site *i*. The errors $e^{+}_{G,ir}$ are positive if the "true" values are overestimated and zero otherwise; $e^{-}_{G,ir}$ are positive if the "true" values are underestimated and zero otherwise. The liquefaction error term is analogous to the ground motion error term. The liquefaction potential errors, $e^{+}_{L,ir}$ and $e^{-}_{L,ir}$, are similarly the over- and underestimation of liquefaction potential for return period *r* at site *i* (Eq. 2.4). Note that the sites and return periods used to match ground motion and liquefaction need not be the same. Since liquefaction will likely be physically impossible at some locations and vary more locally than ground motion in others, the set of sites considered in matching liquefaction potential, I_L, will likely be smaller than that for ground motion, I_G. The user-specified weights $w_{G,ir}, w_{L,ir} \geq 0$ are typically set to $w_{G,ir} = w_{L,ir} = r$ to give equal weight to each error as a percentage of its true exceedance probability (Manzour et al. 2016). If desired, they could be set to vary by site to indicate locations that are more or less important to match (as in Legg et al. 2010).

The surface fault rupture error is defined differently than ground motion and liquefaction errors because at a particular site, typically only one earthquake generating source could cause the permanent ground deformation associated with fault rupture. Thus, we define the surface fault rupture error in terms of the difference, for each fault in *F*, between the "true" annual occurrence probability, $P_{t,f}$, and the hazard-consistent annual occurrence probability based on the reduced set, $\sum_{j \in J_f} P_j$ (Eq. 2.6), where *F* is the user-specified set of faults considered important for surface fault rupture hazard and J_f is the set of all earthquake scenarios *j* with at least one segment on fault *f*. The user-specified weight $w_{S,f} \geq 0$ should typically be set to $w_{S,f} = 1/P_{t,f}$

to normalize the surface fault rupture errors so they are approximately the same order of magnitude as the ground motion and liquefaction errors and the *k* weights can represent relative importance of the different hazards. With z_j defined as a binary variable that indicates whether earthquake scenario *j* is included in the reduced set of events, Equation 2.7 (which is optional depending on user preferences) ensures that at least one earthquake is included for each fault in J_f; and Equations 2.8 and 2.9 limit the number of earthquake scenarios *j* included in the final reduced set to a user-specified number $J_r = N_{qr2}$.

The optimization provides as output values for the decision variables P_j, which define the new hazard-consistent annual occurrence probability for earthquake scenario *j*. If $P_j = 0$, scenario *j* is not included in the reduced set. It also provides values of all the errors—$e^+_{G,ir}$, $e^-_{G,ir}$, $e^+_{L,ir}$, $e^-_{L,ir}$, $e^+_{s,f}$, and $e^-_{s,f}$, which can be used to ensure that they are of an appropriate size and character for the intended purpose.

2.3.2.4 Step 4. Generate candidate set of multihazard scenarios

In Step 4, we generate a user-specified N_{mc} candidate multihazard scenarios. Each multihazard scenario is a map that includes (Fig. 2.1): (1) the surface rupture from the associated earthquake scenario, (2) ground motion contours, and (3) liquefaction potential contours. The ground motion contours are computed using the ground motion prediction equations, and sampling values for the residuals. The liquefaction potential contours are computed using the information about the earthquake scenario (e.g., magnitude) and the sampled ground motion map, so that all hazards described in the scenario are internally consistent.

Equation (2.14) is used to determine N_j, the number of multihazard scenarios associated with each earthquake scenario *j*. As derived in Han and Davidson (2012),

employing Equation (2.14) minimizes the variability in the estimated probability of exceeding ground motion Y_{ir}, while ensuring a total of $N_{mc} \cong \sum_j N_j$ candidate multihazard scenarios are sampled. Using this approach, more multihazard scenarios are sampled from those earthquake scenarios *j* for which the probability of exceeding a specified ground motion varies a lot across ground motion scenarios. Unlike Manzour et al. (2016), which included fewer earthquake scenarios, here we allow N_j to be zero when rounded.

$$N_j = N_{mc}\left[\frac{P_j\sqrt{P(y_{ij}\geq Y_{ir})*[1-P(y_{ij}\geq Y_{ir})]}}{\sum_{j'} P_{j'}\sqrt{P(y_{ij'}\geq Y_{ir})*[1-P(y_{ij'}\geq Y_{ir})]}}\right] \quad (2.14)$$

Ground motion is used to determine the number of multihazard scenarios associated with each earthquake scenario in this step since the variability across multihazard scenarios for a specified earthquake scenario is associated with ground motion. In any case, as in Step 1, there is not just one best candidate set. The candidate set need only be large enough and represent enough variability that a reduced set of multihazard scenarios can be identified in Step 5 that minimizes the errors to an acceptable degree.

2.3.2.5 Step 5. Reduce candidate set of multihazard scenarios using optimization

The optimization in Step 3 (Eqs. 2.2 to 2.13) is applied again in Step 5 to reduce the candidate set of N_{mc} multihazard scenarios to a user-specified set of N_{mr} multihazard scenarios that together minimize the error between the description of hazards based on the reduced set and the "true" description of hazards. The only differences in applying the optimization in this step is that: (1) we replace earthquake scenario *j* with multihazard scenario *n*, (2) the user-specified number of scenarios in

the reduced set, J_r, is now N_{mr}, and (3) the values of $P(y_{in} \geq Y_{ir})$ and $P(l_{in} \geq L_{ir})$ are binary (zero or one) values since there is no uncertainty in the ground motion or liquefaction potential at site *i* in multihazard scenario *n*.

2.3.3 Evaluation metrics

Results are evaluated using four types of metrics. First, we present the average of the errors for each hazard type in terms of probabilities—Average $e^{+/-}_{G,ir}$, Average $e^{+/-}_{L,ir}$, and Average $e^{+/-}_{s,f}$—the quantities directly being minimized. Second, for errors that are easier to interpret, we use the mean ground motion hazard curve error, $MHCE_G$, and mean liquefaction hazard curve error, $MHCE_L$. $MHCE_G$ is the same metric that was known as *MHCE* in Han and Davidson (2012) and Manzour et al. (2016). It is the mean over all sites *i* and return periods *r* of the ground motion hazard curve errors, $HCE_{G,ir}$, defined as the horizontal distance at return period *r* from the reduced set hazard curve to the "true" hazard curve for location *i* (Eqs. 2.15-2.16). $MHCE_L$ is the analogous metric defined for the liquefaction hazard (Eqs. 2.17-2.18).

$$(HCE)_{G,ir} = (Y_{ir} - \hat{Y}_{ir})/Y_{ir} \tag{2.15}$$

$$MHCE_G = \frac{1}{I_G R_G} \sum_{r_G}^{R_G} \sum_{i_G}^{I_G} |(HCE)_{G,ir}| \tag{2.16}$$

$$(HCE)_{L,ir} = (L_{ir} - \hat{L}_{ir})/L_{ir} \tag{2.17}$$

$$MHCE_L = \frac{1}{I_L R_L} \sum_{r_L}^{R_L} \sum_{i_L}^{I_L} |(HCE)_{L,ir}| \tag{2.18}$$

where Y_{ir}, $\hat{Y}_{ir}$, L_{ir} and $\hat{L}_{ir}$ are the "true" and reduced set ground motion intensities, and "true" and reduced set liquefaction potential index values at site *i* and return period *r*, respectively.

Third, we define spatial correlation errors for ground motion and liquefaction hazards as in Han and Davidson (2012, Eqs. 15-16). Equations (2.19-2.20) define the

mean spatial correlation error for ground motion, $MSCE_G$, where ρ_{i_1,i_2}^{true} and $\rho_{i_1,i_2}^{reduced}$ are the weighted correlation coefficients of the ground motions at sites i_1 and i_2, for the "true" and reduced set, respectively, and the weight for each scenario is its annual occurrence probability. An analogous definition holds for the mean spatial correlation error for liquefaction, $MSCE_L$.

$$(SCE)_{G,i_1,i_2} = \rho_{i_1,i_2}^{true} - \rho_{i_1,i_2}^{reduced} \tag{2.19}$$

$$MSCE_G = \frac{1}{I_G^2 - I_G} \sum_{i_1}^{I_G} \sum_{i_2 \neq i_1}^{I_G} |(SCE)_{G,i_1,i_2}| \tag{2.20}$$

Finally, to examine the practical implications of replacing a full set of scenarios developed using conventional MCS with a reduced set based on the multihazard OPS method, we compare estimates of number of damaged water pipes from each. Any relevant damage or loss model for any type of infrastructure could be used; this was chosen for our case study as an example because it relies on both ground motion and liquefaction potential. Specifically, using D_n, the expected number of damaged pipes in multihazard scenario *n* and annual probability P_n for each multihazard scenario *n*, an empirical CDF of damage is created. The mean damage curve error (*MDCE*) is then defined as the average absolute error as a percentage, over all exceedance probabilities, where D_e and $\widehat{D}_e$ are the "true" and reduced set number of damaged pipes with annual exceedance probability *e*, and n_e is the number of probabilities evalauted (every 0.0001 from 1/2500 to 1/100 in the case study).

$$MDCE = \frac{1}{n_e} \sum_e \left| (D_e - \widehat{D}_e)/D_e \right| \tag{2.21}$$

2.4 Case study

2.4.1 Input

The aim of this case study is to demonstrate the multihazard method and examine the effect of considering multiple hazards. The City of Los Angeles, a seismically-active region with 4.0 million people in an area of 1300 km^2, serves as the case study region (US Census Bureau 2019). The city was partitioned into I_G =369 2 km by 2 km grid cells. Since liquefaction varies at a higher geographic resolution, those ground motion grid cells in areas with nonzero liquefaction susceptibility were partitioned into I_L =367 1 km by 1 km grid cells. The liquefaction susceptible areas were identified based on liquefaction hazard zone 7.5-minute quadrangle maps prepared by the California Geologic Survey which in turn were used to develop the 21 liquefaction susceptibility maps covering the City of Los Angeles over the period 2001 to 2003 (SCG 2001-2003). The hazard curve values for matching both ground motion and liquefaction were calculated at the same four return periods of r =100, 475, 1000 and 2500 years, as in Han and Davidson (2012). In Step 2, the weights $\omega_{G,ir}$ are assumed to all be equal; same for $\omega_{L,ir}$. For the base case, the user-specified relative hazard weights were $k_G = k_L = k_S = 1/3$, corresponding to an assumption of equal importance across all three hazard types. Other values were tested in the sensitivity analysis (Section 2.4.3.2).

2.4.1.1 Earthquake sources

All earthquake source and ground motion inputs were identified so as to be consistent with the most recent 2014 National Seismic Hazard Map (NSHM), which is based on the Uniform California Earthquake Rupture Forecast v3 (UCERF3) (Petersen et al. 2014, Field et al. 2014, Powers 2015). To relax fault segmentation assumptions

and include multifault ruptures, UCERF3 makes a substantial departure from previous methods (including those used in Han and Davidson 2012). Rather than constructing a magnitude-frequency distribution model for each fault separately then adding background seismicity, in UCERF3, all fault sections are divided into small equal-length subsections, all plausible combinations of two or more contiguous fault subsections are considered possible ruptures, and the rates of all ruptures are computed simultaneously using the inversion method (Field et al. 2014). UCERF3 results in 250,000+ possible ruptures compared to <8000 in UCERF2. In this case study, we directly used the 186,716 ruptures from the earthquake rupture forecast that are within 200 km of Los Angeles in the candidate set of earthquake scenarios. In addition, consistent with the 2014 NSHM, background sources are represented as gridded seismicity at 0.1° longitude by 0.1° latitude following truncated Gutenberg–Richter relationships. Including only those within 200 km of Los Angeles resulted in 2,505 background sources.

2.4.1.2 Component hazard models

Ground motion was modeled using the five ground motion prediction equations and weights for the Western U.S. from the 2014 NSHM (Table 16 of Petersen et al. 2011). In the case study, we used the ground motion intensity parameter spectral acceleration at 0.2s, $S_{a,0.2s}$, though another could be substituted.

We compute the liquefaction hazard using the LPI3 model in Kongar et al. (2017). This model was chosen because the data are available to apply it to a large region unlike methods that require CPT, SPT, or other detailed geotechnical data, and because, based on the comparison in Kongar et al. (2017) and our own comparison for the 1994 Northridge earthquake in the following paragraphs, it offers accuracy that is

reasonable for regional analysis like that targeted by the multihazard OPS method. The LPI3 method estimates liquefaction potential in terms of the liquefaction potential index (LPI), which Maurer et al. (2014) interprets as corresponding to no (LPI<4), marginal (4≤LPI<8), moderate (8≤LPI<15), and severe (LPI≥15) liquefaction. The method, which is based on the average shear-wave velocity over the top 30 m of soil, V_{s30}, is a combination of previous work by Seed and Idriss(1971), Andrus and Stokoe (2000), Juang et al. (2005), and Boore (2004). At each location, the soil is partitioned into layers, each h_k =5 m thick, where z_k is the depth to the bottom of layer *k* and k =1 is the top layer. It requires computing for each layer *k*: (1) Average shear-wave velocities, $V_{s,k}$, and stress-corrected shear-wave velocity, $V_{s1,k}$ (Eqs. 2.24-2.25); (2) cyclic stress ratio, CSR_k (Eqs. 2.26-2.29); and (3) cyclic resistance ratio, CSR_k (Eq. 2.30). We then use Eq. (2.31) to compute *LPI*.

$$V_{s,k} = \begin{cases} 10^{\left(\frac{log\, V_{S30} - 0.042062}{1.0292}\right)} & \text{for } z_k \le 10 \\ 2\left[10^{\left(\frac{log\, V_{S30} - 0.025439}{1.0095}\right)}\right] - 10^{\left(\frac{log\, V_{S30} - 0.042062}{1.0292}\right)} & \text{for } 10 < z_k \le 20 \end{cases} \tag{2.24}$$

$$V_{s1,k} = \mathrm{V_{s,k}}\left(\frac{100}{\sigma'_v}\right)^{0.25} \tag{2.25}$$

Where $\sigma'_{v,k}$ is effective overburden stress at depth $z_k$in $\mathrm{N/m^3}$. We proceeded with the following equations, to compute the cyclic stress ratio, CSR_k; and cyclic resistance ratio, CSR_k:

$$r_d = \begin{cases} 1 - 0.00765 z_k & \text{for } z_k < 9.2\ m \\ 1.174 - 0.0267 z_k & \text{for } z_k \ge 9.2\ m \end{cases} \tag{2.26}$$

$$\sigma_{v,k} = \sum_{m=1}^{k} \rho_m h_m g \tag{2.27}$$

$$\sigma'_{v,k} = \begin{cases} \sigma_{v,k} & \text{for } z_k \le z_{wt} \\ \sigma_{v,k} - \rho_w (z_k - z_{wt}) g & \text{for } z_k > z_{wt} \end{cases} \tag{2.28}$$

$$CSR_k = 0.65\left(\frac{a_{max}}{g}\right)\left(\frac{\sigma_{v,k}}{\sigma'_{v,k}}\right)r_d \tag{2.29}$$

$$CRR_k = \left(0.022\left(\frac{V_{s1,k}}{100}\right)^2 + 2.8\left(\frac{1}{V^*_{s1,k} - V_{s1,k}} - \frac{1}{V^*_{s1,k}}\right)\right)\left(\frac{M_w}{7.5}\right)^{-2.56} \tag{2.30}$$

$$LPI = \sum_{k=1}^{4}\left(1 - 1.4\frac{CRR_k}{CSR_k}\right)(10 - 0.5z_k) \tag{2.31}$$

where r_d is a shear stress reduction coefficient; $\sigma_{v,k}$ is total overburden stress at depth $z_k$in $\mathrm{N/m^3}$; $\sigma'_{v,k}$ is effective overburden stress at depth $z_k$in $\mathrm{N/m^3}$; ρ_m is soil density of layer m in $\mathrm{kg/m^3}$; $\rho_w = 1000\ \mathrm{kg/m^3}$ is density of water; z_{wt} is water table depth in m; a_{max} is peak horizontal ground acceleration (PGA) in $\mathrm{m/s^2}$; g is acceleration of gravity; V^*_{s1} is the limiting upper value of V_{s1} for cyclic liquefaction occurrence, assumed to be 200 $\mathrm{m/s}$ for all sites; and M_w is earthquake moment magnitude. Following Anbazhagan et al. (2016), we assume soil density is $\rho_{dry} = 0.523V_s^{0.193}$ for layers above the water table and $\rho_{sat} = \rho_{bulk} = 0.412V_s^{0.262}$ for those below. The input data required is thus only V_{s30}, z_{wt}, a_{max}, and M_w. The V_{s30} data was taken from Wills and Clahan. (2006); z_{wt} was obtained by spatially interpolating over data from California Department of Water Resources (2019); and a_{max} and M_w are from the earthquake scenario.

Stewart et al. (1996) reported numerous locations of ground failure caused by the 1994 Northridge earthquake, which led to thousands of pipe breaks in Los Angeles and provided a map to locate these incidents (Fig. 2.3a). As mentioned, we implemented LPI model for the 1994 Northridge Earthquake to evaluate its accuracy compared to the reported incidents from Stewart et al. (1996) (Fig. 2.3b). The LPI results in Zones A, B and the left side of C revealed marginal to moderate liquefaction, consistent with reported ground failures and high ground water depths. Likewise for low liquefaction potential situation, the results from LPI model ($LPI < 4$) confirms the

reported indices of shallow ground water depth without potential of liquefaction. This comparison suggests that the *LPI* model can present a good estimation of the liquefaction potential in the area of interest.

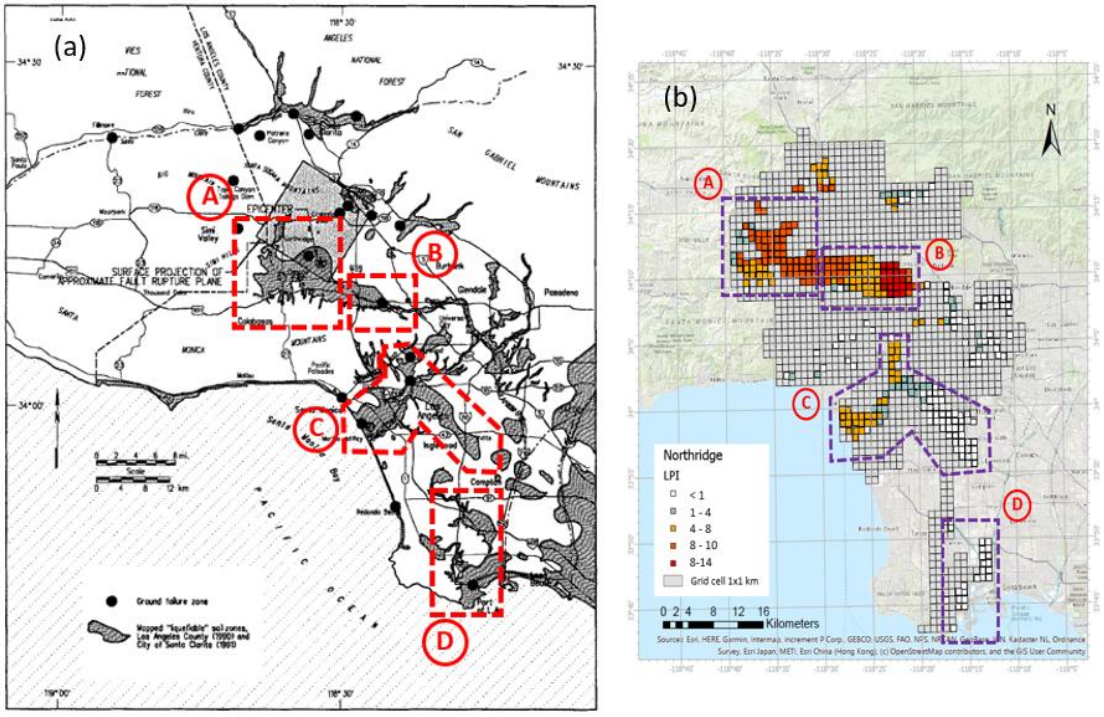

Figure 2.3. (a) Map of ground failure incidents from Stewart et al. (1996) (b) Map of liquefaction for 1994 Northridge Earthquake

The user-specified set of faults considered important for surface rupture hazard, F, was defined with input from the Los Angeles Department of Water and Power (Davis 2019). It was taken to include the following 15 faults (with number of earthquake scenarios in associated set J_f): Hollywood (771), Malibu Coast (alt1 (460) and extension (364)), Mission Hills (160), Newport Inglewood alt1 (520), Northridge Hills (1595), Palos Verdes (169), Raymond (639), Santa Monica (783), Santa Susana

(east (256) and alt1 (388)), Sierra Madre (494), Sierra Madre–San Fernando (84), Verdugo (608), and Hollywood-Raymond-Santa Monica combination (730). These faults include earthquakes of magnitudes 5.80 to 8.05 (Fig. 2.4).

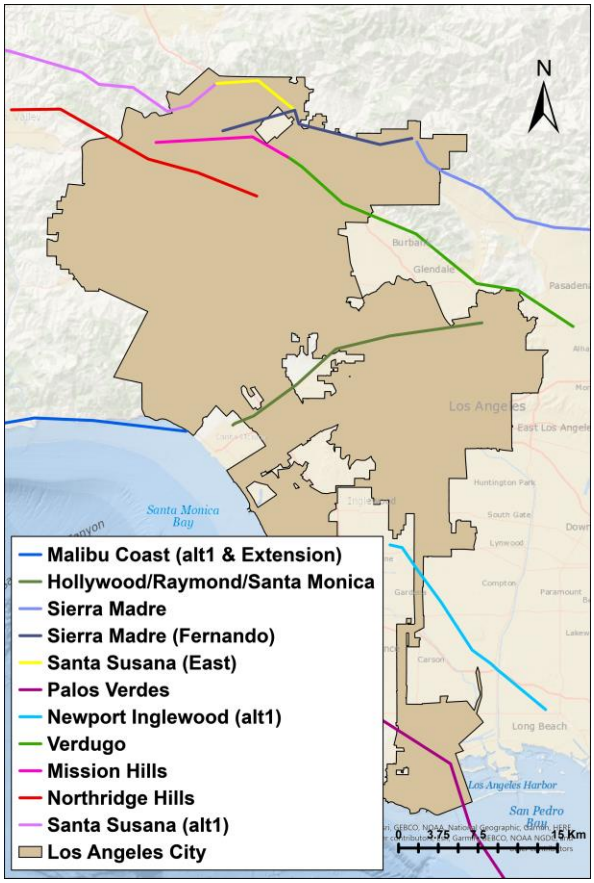

Figure 2.4. Traces of 15 considered faults for surface rupture hazard

2.4.1.3 "True" hazards

The "true" ground motion and liquefaction hazard were based on conventional MCS because unlike PSHA, MCS allows comparison of the spatial correlation error (Han and Davidson 2012). However, the "true" ground motion and liquefaction hazard

were computed in two parts. The 186,716 UCERF3 fault rupture scenarios were included directly (Section 2.4.1.1), and a conventional MCS over 200,000 years was applied to generate 157,175 background source scenarios to add to the set.

2.4.1.4 Pipe damage model

To compute the method performance in terms of error in damage estimates, we apply the logistic regression model labeled R3 in Bagriacik et al. (2018) to estimate the expected number of damage pipe segments (Eqs. 2.33-2.34), where p_{tin} is the probability a pipe segment of type *t* in grid cell *i* breaks in multihazard scenario *n*; $x_{PGV,in}$ and $x_{LRI,in}$ are the peak ground velocity and liquefaction resistance index (LRI) in grid cell *i* for multihazard scenario *n*, respectively; and x_{CI}, x_{AC}, x_{DI}, and x_S are binary variables that are one if the pipe is cast iron (CI), asbestos cement (AC), ductile iron (DI), or steel (S) respectively, and zero otherwise.

$$Z = -2.39 + 0.014\left(x_{PGV,in}\right) - 0.677\left(x_{LRI,in}\right) + 0.014(25) - 0.885x_{CI} - 0.522x_{AC} - 1.74x_{DI} - 0.739x_S \quad (2.33)$$

$$p_{tin} = \frac{\exp(Z)}{1+\exp(Z)} \quad (2.34)$$

The Los Angeles Department of Water and Power (LADWP), which operates the water supply system in the study area, has approximately 11,800 km of distribution mains (LADWP 2017). For simplicity, we assume they are evenly distributed across the city; that each pipe segment, defined as the length between intersections with other pipes, is 25 m long; and that the distribution of materials is the same as at the time of the Northridge earthquake in 1994, 72% CI, 9% AC, 8% DI, and 11% S (O'rourke et al. 2014). For these purposes—examining the effect of using a reduced set of multihazard scenarios instead of a full set from conventional MCS on pipe damage—these simplifications are reasonable. An evaluation of system functionality would

require the actual network. To obtain the $x_{LRI,in}$ values, we save the *CRR* values while computing LPI (Section 2.4.1.2) and map CRR to LRI as defined in Cubrinovski et al. (2011). The expected number of damaged pipes in multihazard scenario *n* is $D_n = \sum_{i,t} p_{tin} N_t$, where N_t is the number of pipe segments of type *t* in each grid cell.

2.4.2 Application of multihazard OPS method

The method was implemented using Python 3.5 (www.python.org) to create and call the optimization model in Steps 3 and 5, and Matlab R2017b (www.mathworks.com) for everything else. The optimizations were solved using Gurobi 8.1, a commercial solver (gurobi.com). To help interpret the results of this analysis, we compare to them to those in Han and Davidson (2012) and Manzour et al. (2016), which apply the ground-motion-only version of the Extended OPS method to Los Angeles and Christchurch, New Zealand, respectively. Han and Davidson (2012) also differs in that it does not include Step 2, and it used input from the 2008 NSHM instead of the substantially modified 2014 NSHM used here.

2.4.2.1 Step 1. Generate candidate set of earthquake scenarios

Due to the new way the 2014 NSHM generated earthquake scenarios (Section 2.4.1.1), we did not have to simulate earthquake scenarios from fault sources. Rather, we directly used the 186,716 ruptures from the 2014 NSHM earthquake rupture forecast that are within 200 km of Los Angeles in the candidate set of earthquake scenarios. Additional candidate earthquake scenarios were generated from the background sources using importance sampling as in Han and Davidson (2012) and Manzour et al. (2016). In doing so, the magnitude range was divided into bins of width

0.1. This approach led to 147,470 background source earthquake scenarios. In total, $N_{qc} = 334{,}186$ candidate earthquake scenarios.

2.4.2.2 Step 2. Reduce candidate set of earthquake scenarios based on contribution

The first reduced set included N_{qr1} =19,154 earthquake scenarios, which was based on ensuring we retained at least T =85% of the total contribution for both ground motion and liquefaction hazard. The actual percentages of contribution included for ground motion and liquefaction were 97% and 85%, respectively (Fig. 2.5). By comparison, in Manzour et al. (2016) 99% of the contribution was retained because that resulted in only 6500 earthquake scenarios. For both Los Angeles and Christchurch (Manzour et al. 2016) the cumulative contribution curves are much steeper than for liquefaction (Fig. 2.5). A scatterplot of $C_{L,j}$ vs. $C_{G,j}$ suggests that they are highly correlated (ρ =0.96), but the average contribution of each earthquake scenario to the liquefaction hazard is 65% that of the average contribution of each to the ground motion hazard.

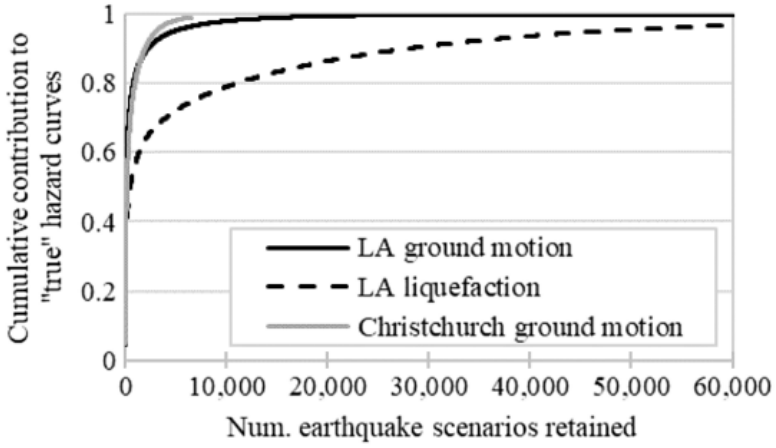

Figure 2.5. Cumulative contribution versus number of earthquake scenarios included

2.4.2.3 Step 3. Reduce candidate set of earthquake scenarios using optimization

The maximum number of earthquake scenarios allowed in the second reduced set was taken to be N_{qr2} =1000, but the optimization selected only $N_{qr2(actual)}$ =815, suggesting that including additional earthquake scenarios would not reduce the error further. The mean errors at this intermediate step were $MHCE_G$ =0.025 and $MHCE_L$ =0.061 meaning that on average, the reduced set ground motion hazard curve based on those 815 earthquake scenarios differed from the "true" ground motion hazard curve by 2.5%. Similarly, on average, the reduced set liquefaction hazard curve differs by 6.1%. In terms of probabilities, the average absolute value errors were $e_G = 9.3 \times 10^{-7}$, $e_L = 1.6 \times 10^{-6}$, and $e_S = 0$.

By comparison, at this stage in Han and Davidson (2012), the method selected only 143 earthquake scenarios resulting in $MHCE_G$ =0.025 and in Manzour et al. (2016), 83 earthquake scenarios were selected with $MHCE_G$ =0.001. Both those studies considered only ground motion hazard, so they could achieve smaller errors with fewer earthquake scenarios. Nevertheless, these multihazard results were on par with the earlier results at this step, and these intermediate errors appear small enough for practical purposes.

2.4.2.4 Step 4. Generate candidate set of multihazard scenarios

We tried five values for the number of candidate multihazard scenarios, N_{mc}(900, 2000, 3000, 5000, 10,000). Ultimately, we set N_{mc} =900 (with the actual number generated $N_{mc(actual)}$ =805), fewer than the N_{mc} =2000 and N_{mc} =3000 used in Manzour et al. (2016) and Han and Davidson (2012), respectively. The reasons for the choice were that using N_{mc} =900 resulted in errors small enough for most practical purposes (see full error discussion in Section 2.4.3.1), and the Step 5

optimization did not converge for $N_{mr} \leq 300$ if N_{mc} was higher (e.g., for $N_{mc} = 5{,}000$ and $N_{mr} = 200$ the gap was above 50% after 4 days). One could explore other solution algorithms to allow for larger N_{mc} values if desired, but that was not necessary for this study.

2.4.2.5 Step 5. Reduce candidate set of multihazard scenarios using optimization

Finally, the maximum number of multihazard scenarios allowed in the final reduced set was varied N_{mr} =200 to 600 to examine the tradeoff between the error introduced and the final number of multihazard scenarios. Figure (2.6), which depicts the tradeoffs, suggests that N_{mr} =400, which resulted in $N_{mr(actual)}$ =351, represents a reasonable point in the tradeoff, and thus we use that as the base case discussed in Section 2.4.3.

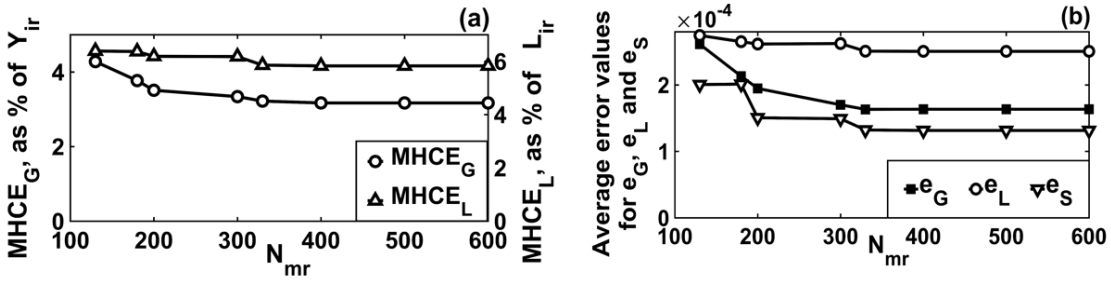

Figure 2.6. (a) MHCEG and MHCEL; and (b) average probability errors, both as functions of N_{mr}, the number of multihazard scenarios in the final reduced set

2.4.3 Results

2.4.3.1 Final recommended set of probabilistic multihazard scenarios

The base case run can be summarized as follows (Fig. 2.2): N_{qc} =334,186 candidate earthquake scenarios, N_{qr1}=19,154 earthquake scenarios after reduction based on 85% contribution, N_{qr2} =1000 earthquake scenarios allowed after reduction using the optimization, ($N_{qr2(actual)} = 815$), N_{mc} =900 candidate multihazard scenarios specified ($N_{mc(actual)}$ =815), N_{mr} =400 multihazard scenarios allowed in the reduced set ($N_{mr(actual)} = 351$). The resulting 351 multihazard scenarios range from magnitude of 5.2 to 7.9, and the adjusted annual occurrence probabilities from 6.065×10^{-7} to 2.464×10^{-3}. They include 338 multihazard scenarios from fault sources and 13 from background sources (Fig. 2.7).

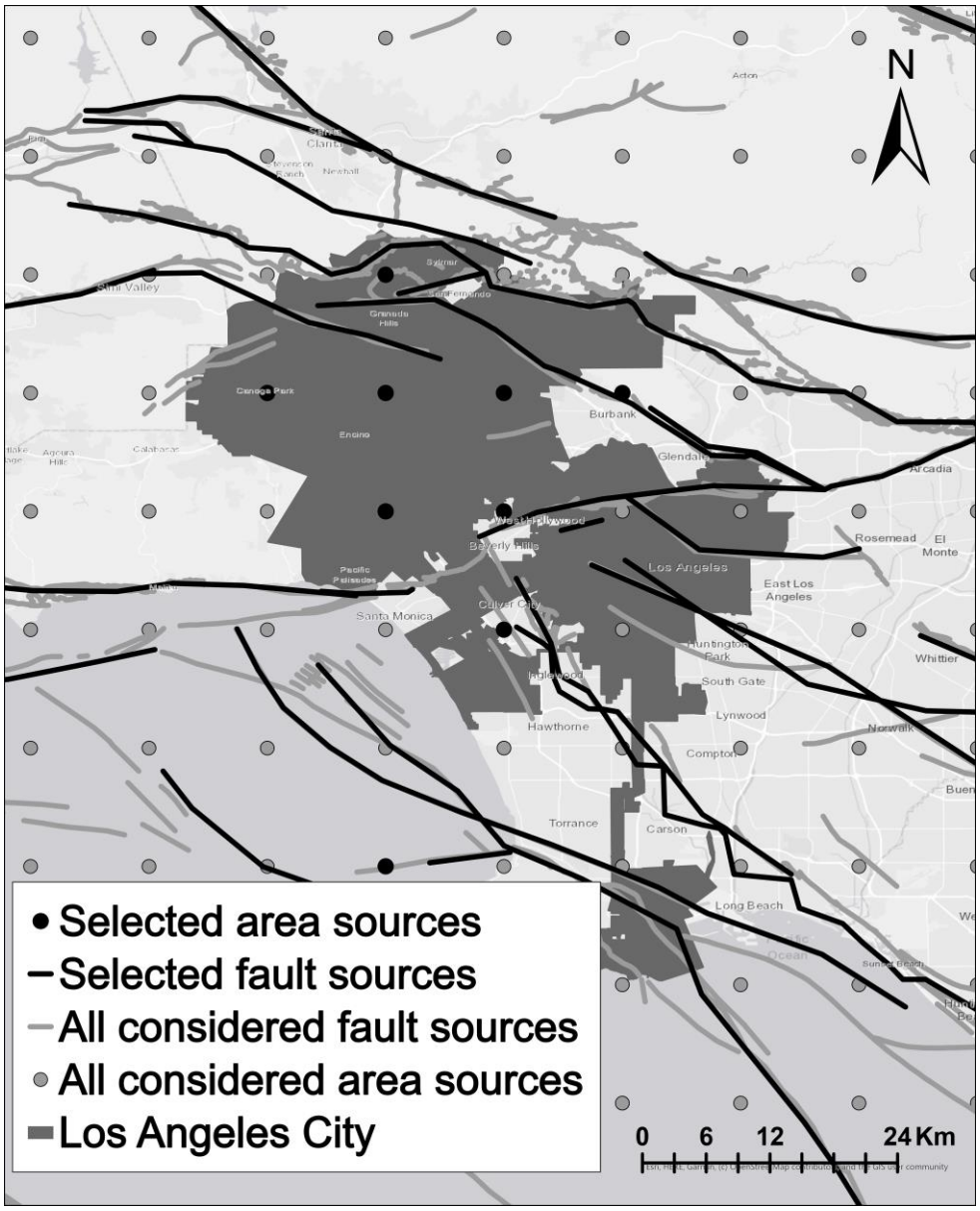

Figure 2.7. Map showing the faults and area sources considered and those selected in the final reduced set of 351 multihazard scenarios

2.4.3.2 Method performance

To determine how well this reduced set of 351 multihazard scenarios captures the true ground motion, liquefaction, and surface fault ruptures hazards, we examine the evaluation metrics (Section 2.3.3). The probability errors introduced by using the reduced set of 351 multihazard scenarios are: Average $e_G = 1.634 \times 10^{-4}$, average $e_L = 2.506 \times 10^{-4}$ and average $e_S = 1.615 \times 10^{-4}$. These values are small and useful for comparing across runs. Metrics that are easier to interpret are $MHCE_G = 3.2\%$, $MHCE_L = 5.8\%$, which indicate the reduced set ground motion and liquefaction hazard curves differ from the "true" ones in the horizontal direction by 3.2% and 5.8% on average across all sites *i* and return periods *r*. For comparison, Han and Davidson (2012) resulted in 194 ground motion scenarios with $MHCE_G = 0.84\%$, and Manzour et al. (2016) resulted in 124 ground motion scenarios with $MHCE_G = 0$. Spatial correlation errors are $MSCE_G = 0.088$ and $MSCE_L = 0.026$, compared to $MSCE_G = 9.4 \times 10^{-4}$ and $MSCE_G = 0.031$ for Han and Davidson (2012) and Manzour et al. (2016), respectively. To offer some intuition about the magnitude of error introduced, Figure 2.8 shows a comparison of the "true" and reduced set hazard curves for the sites for which 90% of matches are worse.

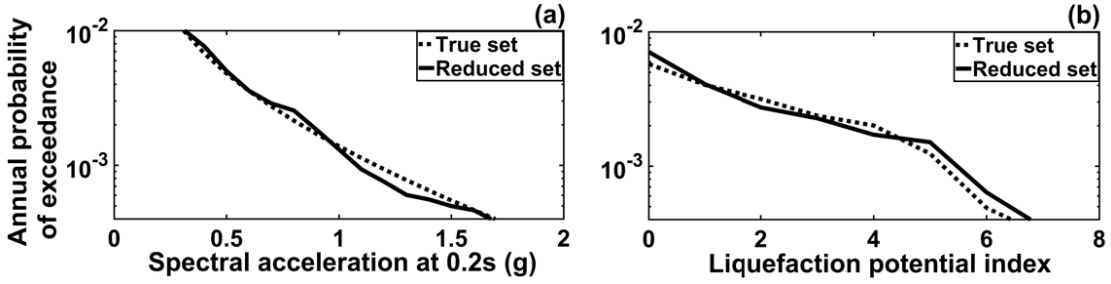

Figure 2.8. Comparison of true and reduced set hazard curves, for the sites for which 90% of matches are worse, for (a) ground motion; and (b) liquefaction.

The errors also should not introduce bias. Figure 2.9 shows histograms of the errors, suggesting no notable bias.

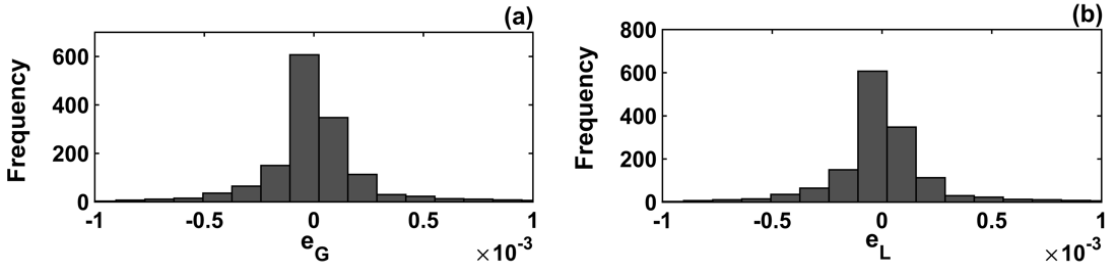

Figure 2.9. Histograms of probability errors for (a) ground motion; and (b) liquefaction.

Maps of the ground motion and liquefaction errors at 100, 475, 100 and 2500 year, return period (Figs. 2.10-2.13), suggest no geographic bias either.

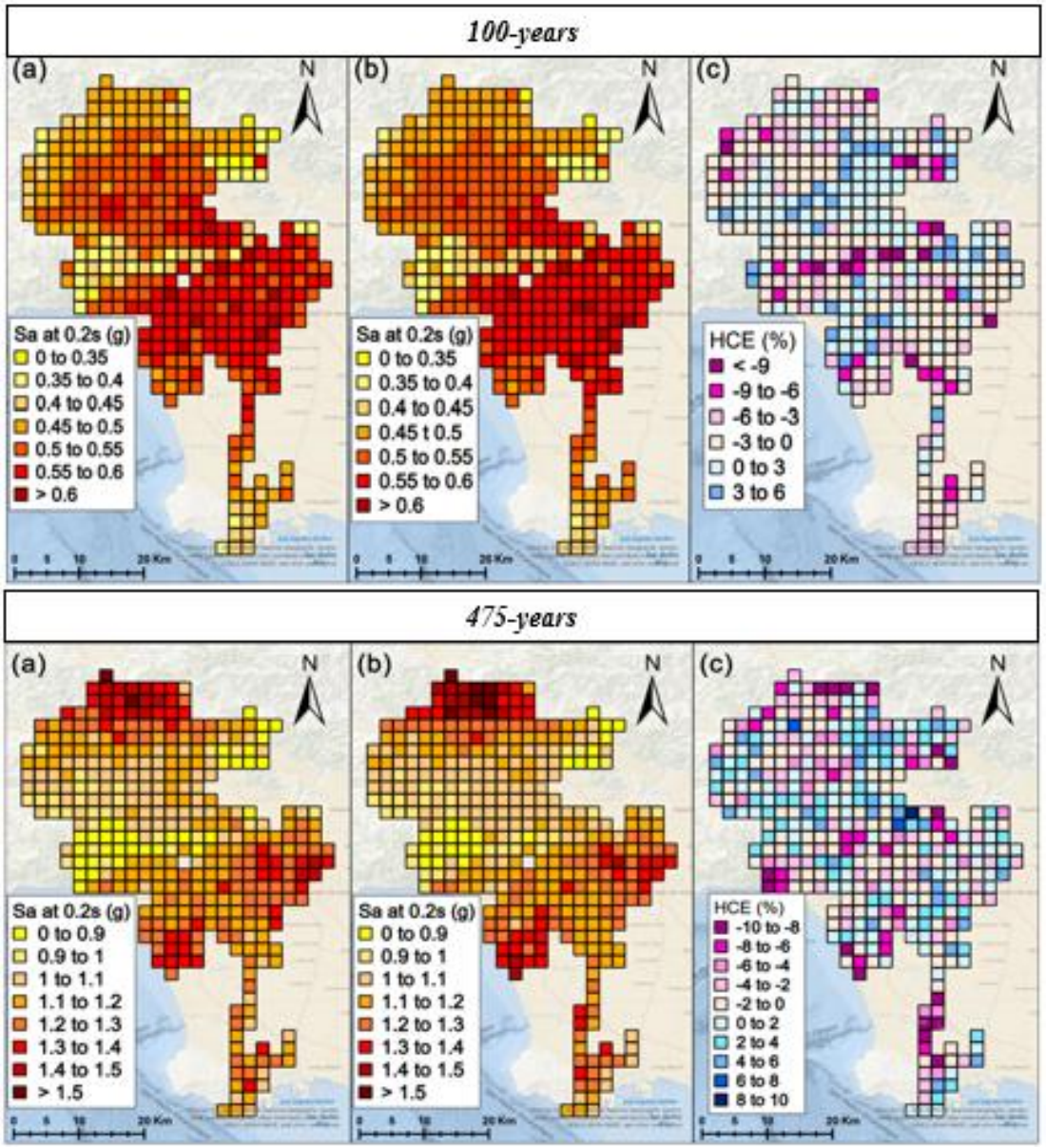

Figure 2.10. Maps of (a) "true" ground motion $S_{a(0.2s)}$, (b) ground motion $S_{a(0.2s)}$ based on 351 reduced set multihazard scenarios, and (c) ground motion hazard curve errors, $HCE_{G,i,100}$, between map (a) and (b), for 100-year and 475-year return periods.

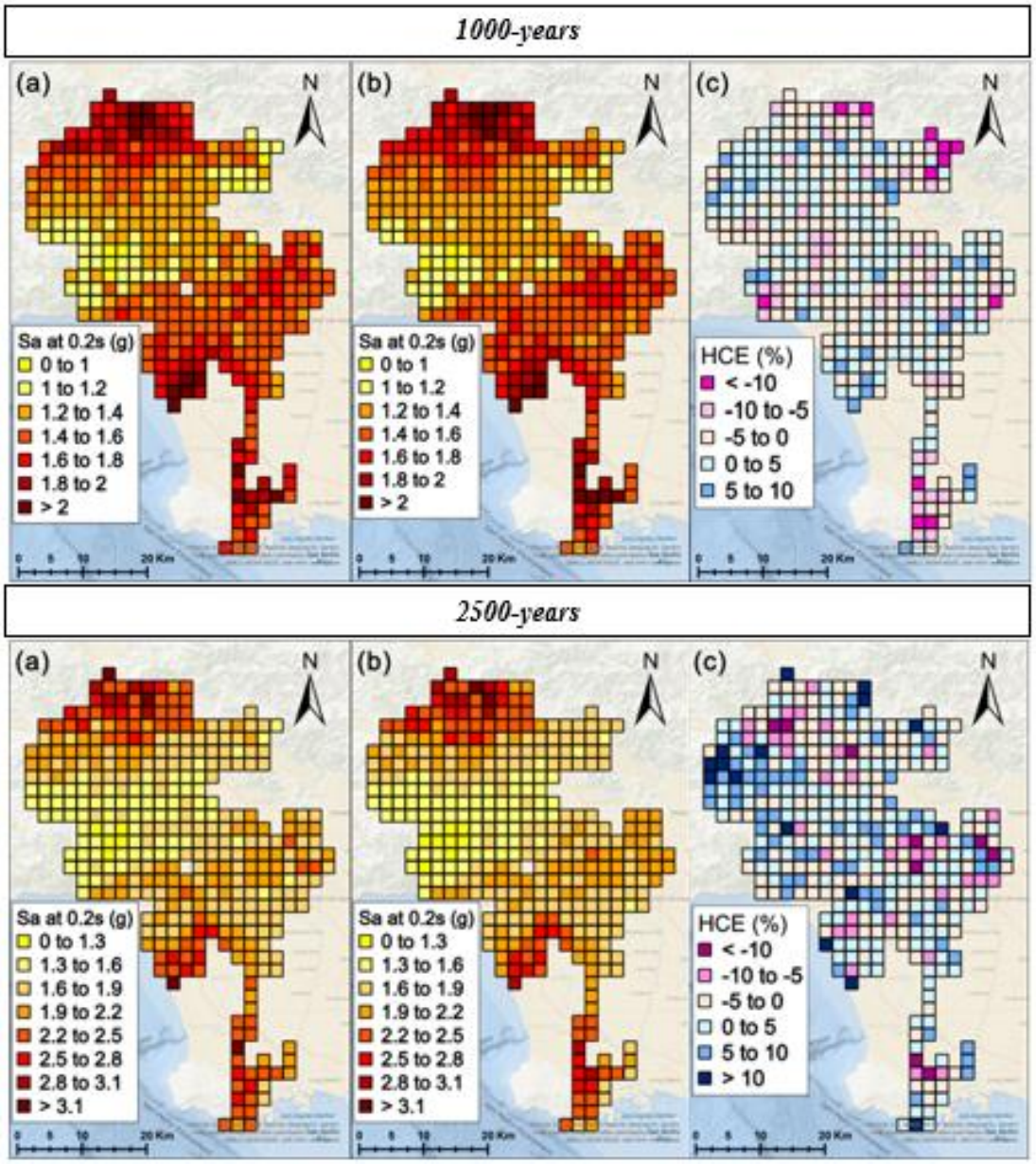

Figure 2.11. Maps of (a) "true" ground motion $S_{a(0.2s)}$, (b) ground motion $S_{a(0.2s)}$ based on 351 reduced set multihazard scenarios, and (c) ground motion hazard curve errors, $HCE_{G,i,100}$, between map (a) and (b), for 1000-year and 2500-year return periods.

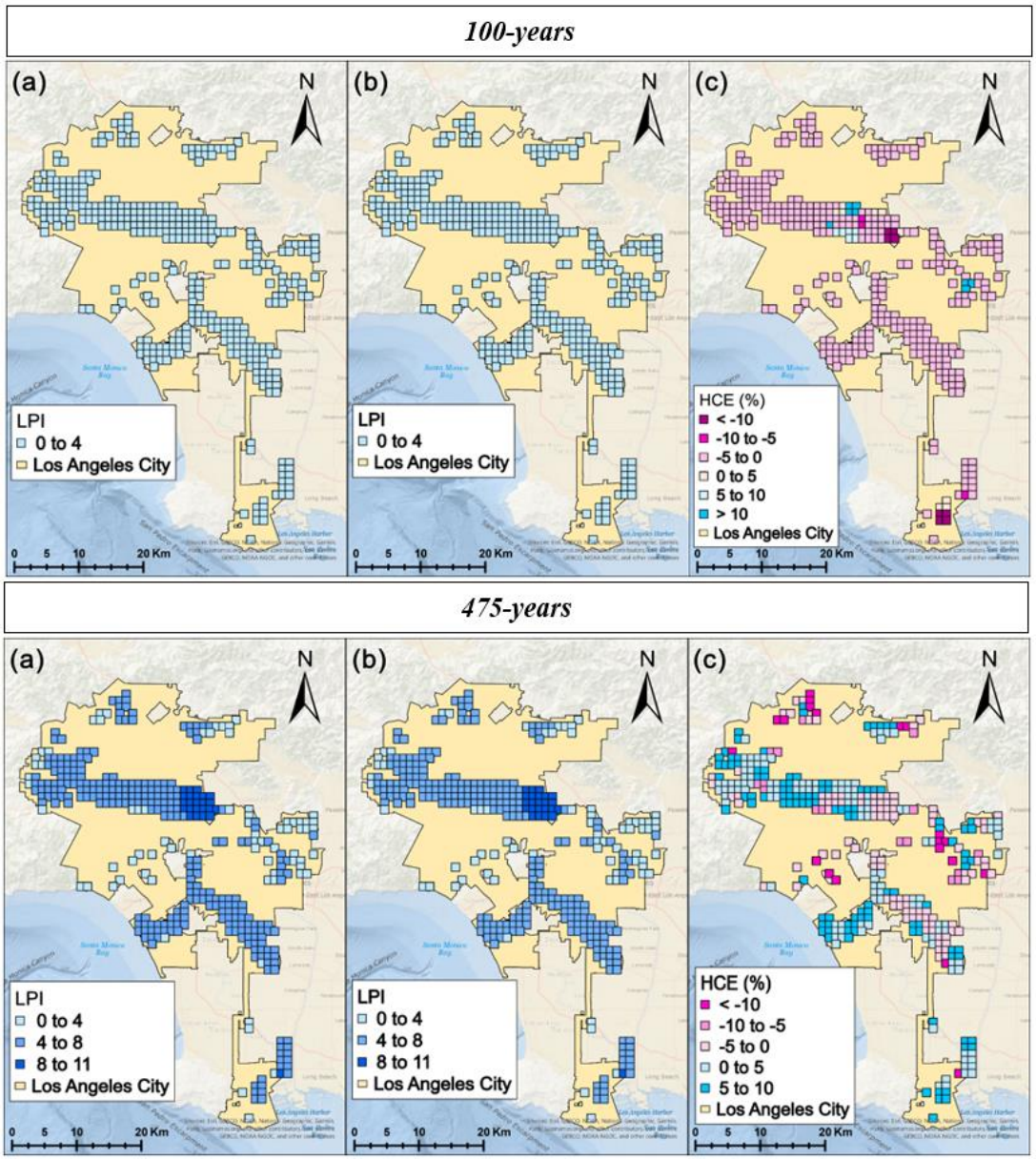

Figure 2.12. Maps of (a) liquefaction potential, LPI, (b) liquefaction potential, LPI, based on 351 reduced set multihazard scenarios, and (c) liquefaction hazard curve errors, $HCE_{L,i,475}$, between map (a) and (b), for 100-year and 475-year return periods.

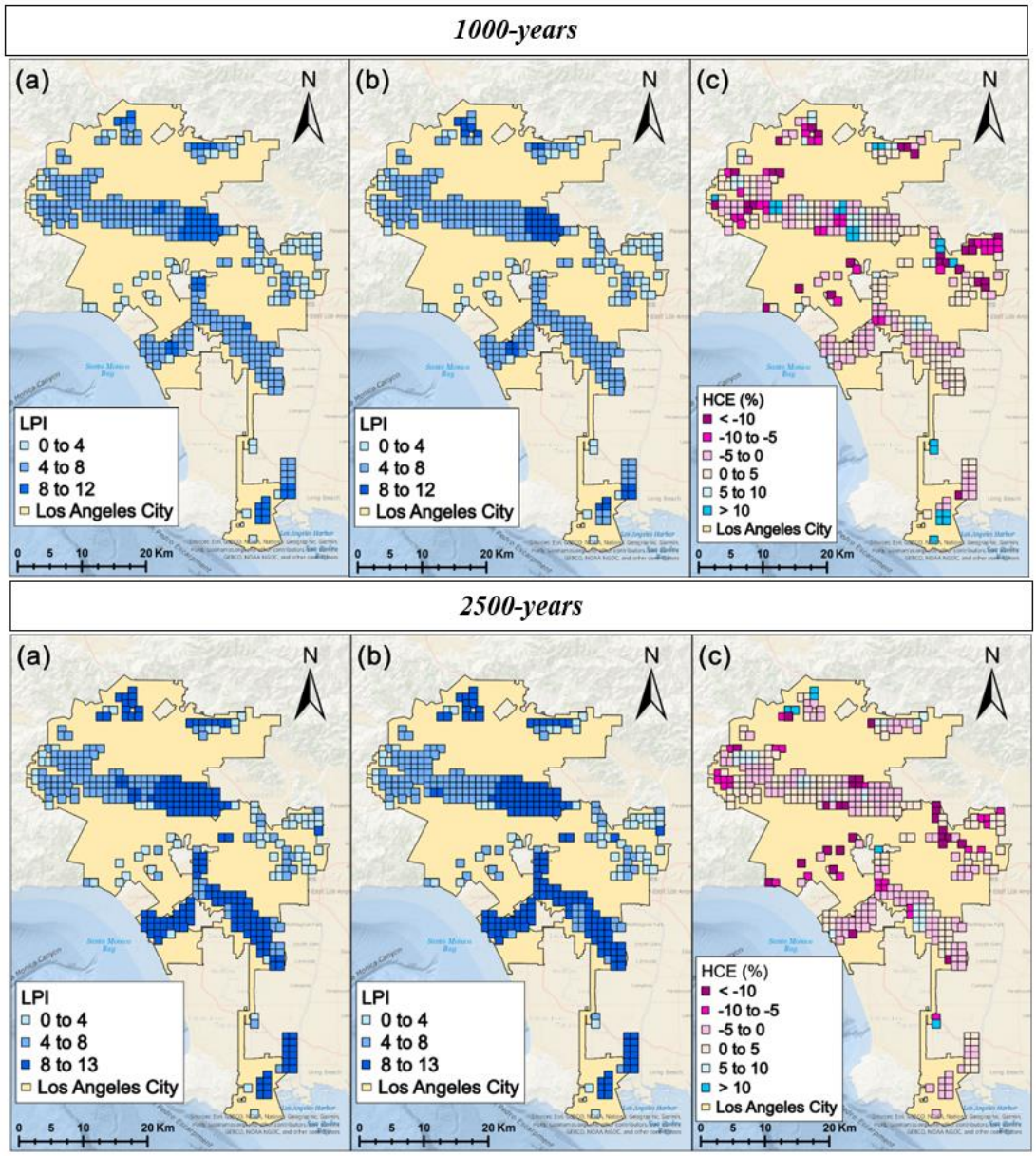

Figure 2.13. Maps of (a) liquefaction potential, LPI, (b) liquefaction potential, LPI, based on 351 reduced set multihazard scenarios, and (c) liquefaction hazard curve errors, $HCE_{L,i,475}$, between map (a) and (b), for 1000-year and 2500-year return periods.

Finally, Figure 2.14 shows the results of the damage analysis. It compares the annual probability distributions of the number of damaged pipes in Los Angeles based on the conventional MCS with 343,891 multihazard scenarios and based on reduced sets of 198 and 351 multihazard scenarios, suggesting relatively small differences compared to the vast reduction in computational demand. The mean damage curve error (MDCE) is 0.028 for the reduced set of 351 multihazard scenarios. Overall, given other uncertainties in a damage or loss analysis, these errors are reasonable for many applications. More or fewer multihazard scenarios could be included in the final set, however, depending on the desired tradeoff between error and computational efficiency. The set of sites *i* and/or return periods *r* could be modified to achieve fewer scenarios or smaller errors as well. While computational savings will depend on the particulars of the case study and hardware, in this case computing the pipe damage required approximately 3.5 hours for the full set of 343,891 multihazard scenarios when parallelized across 35 nodes on a computing cluster (approximately 120 hours without parallelization). It only required 9 minutes for the reduced set of 351 multihazard scenarios.

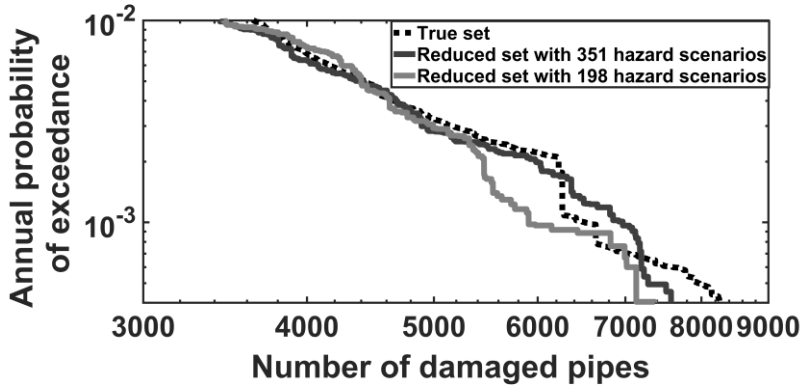

Figure 2.14. Comparison of probability distributions of number of damaged pipes based on conventional MCS with 343,891 multihazard scenarios and reduced set of 198 and 351 multihazard scenarios.

2.4.4 Sensitivity analysis

To examine the effect of considering multiple hazards, we conducted sensitivity analysis on the hazard weights, k_G, k_L, and k_S. Specifically, we did 10 runs in which the weight for each hazard was varied from zero (the hazard was not considered at all) to one (it was the only hazard considered) (Table 2.1). Not surprisingly, as the weight for a specified hazard (e.g., ground motion) was increased, the errors associated with that hazard decreased. Runs 1, 2, and 3 provide the minimum error possible for ground motion, liquefaction, and surface fault rupture, respectively. Runs 1 to 6 also suggest that when the weight for a specified hazard goes to zero, the errors can be quite large for that hazard. That is, matching one hazard has an effect on matching the other hazards, but it does not match them very well. When k_G =0 in Runs 2, 3, and 6, for example, the $MHCE_G$ is on the order of 25% to 57% compared to 2.7% when k_G =1.

Table 2.1. Results of sensitivity analysis for hazard weights

Run	k_G	k_L	k_S	N_{mr}	$MHCE_G$	$MHCE_L$	Avg. e_G	Avg. e_L	Avg. e_S	MDCE
1	1	0	0	324	0.027	0.271	$1.08(10^{-4})$	0.080	1.07	0.054
2	0	1	0	259	0.571	0.051	1.75	$1.80(10^{-4})$	1.73	0.619
3	0	0	1	15	0.323	0.508	0.246	0.031	0	0.052
4	0.5	0.5	0	306	0.032	0.057	$1.64(10^{-4})$	$2.52(10^{-4})$	1.47	0.046
5	0.5	0	0.5	335	0.029	0.284	$1.11(10^{-4})$	0.075	$0.62(10^{-4})$	0.032
6	0	0.5	0.5	245	0.254	0.048	1.54	$1.92(10^{-4})$	$3.38(10^{-4})$	0.100
7	0.5	0.25	0.25	334	0.032	0.058	$1.47(10^{-4})$	$2.64(10^{-4})$	$2.07(10^{-4})$	0.024
8	0.25	0.5	0.25	294	0.036	0.056	$1.88(10^{-4})$	$2.41(10^{-4})$	$2.77(10^{-4})$	0.054
9	0.25	0.25	0.5	310	0.032	0.058	$1.63(10^{-4})$	$2.51(10^{-4})$	$1.03(10^{-4})$	0.041
10	1/3	1/3	1/3	351	0.032	0.058	$1.63(10^{-4})$	$2.51(10^{-4})$	$1.61(10^{-4})$	0.028

Nevertheless, the results also suggest minimal difference in errors for each hazard when the weight is between 0.25 and 0.5.Overall, Table 2.1 indicates that as long as the weight for each hazard is at least 0.25, the errors for all hazards are kept small enough for practical purposes.

2.5 Conclusion

In this research, we introduce a new multihazard version of the optimization-based probabilistic scenario (OPS) method of developing a computationally efficient, set of hazard scenarios for use in analysis of spatially distributed infrastructure. It retains the general approach of the previous version (Manzour et al. 2016), but includes liquefaction potential and surface fault rupture in addition to ground motion. The application to Los Angeles indicates that while more scenarios are required for the multihazard analysis to achieve a similar match in a ground motion only analysis, it is still possible to achieve errors small enough for practical purposes with on the order of a few hundred multihazard scenarios. In addition, the sensitivity analysis suggests that developing an ensemble of multihazard scenarios by matching one hazard type does not necessarily indirectly achieve a good match for others. However, as long as the weight for each hazard is at least 0.25, the errors for all hazards are kept small enough for practical purposes.

Opportunities for future research remain. Improved liquefaction and surface fault rupture component models could be incorporated. Additional co-occurring hazards, such as landslide, could be included in a similar way. More applications in more places may strengthen the conclusion that the method can apply excellent results anywhere. Finally, although it was not considered necessary in this case study, it could be useful to develop a new solution algorithm for the Step 5 optimization for cases

when there is a larger number of candidate multihazard scenarios and a small number allowed in the final reduced set.

Chapter 3

SELECTION OF MULTIHAZARD-BASED DAMAGE SCENARIOS FOR THE LOS ANGELES WATER TRANSMISSION NETWORK

3.1 Introduction

The seismic performance of infrastructure systems depends on the joint damage state of all its components, which in turn is dependent on their spatial correlation. As a result, lifeline networks are typically analyzed using a scenario-based approach. In the most common method, conventional Monte Carlo simulation (MCS), a rupture, ground motion, component damage, and system performance are simulated in turn; the process is repeated many times; and the results are combined (Han and Davidson 2012). While MCS is effective and conceptually straightforward, it is computationally inefficient, if not infeasible, because it requires so many expensive simulations to capture the full probabilistic distribution of performance. Recent methods have been developed to instead identify a relatively small, computationally efficient set of ground motion hazard scenarios, each with an associated adjusted annual occurrence probability, so that when probabilistically combined they represent the hazard accurately and efficiently (e.g., Jayaram and Baker 2010, Han and Davidson 2012, Zolfaghari and Peyghaleh 2016, Manzour et al. 2016). Similarly, Brown et al. (2011, 2013), Gearhart et al. (2011, 2014), and Miller and Baker (2015) describe methods to develop a computationally efficient set of damage scenarios, each with an associated adjusted occurrence probability.

In this research, we apply the Brown et al. (2013) method to develop a computationally efficient set of damage scenarios for the Los Angeles water transmission system. We chose this method because it has the benefit of including, within each damage scenario, all the information necessary to evaluate every possible combination of component retrofit or replacement strategies. Each damage scenario describes, for each pipe segment (or other component) in the network, both its damage state assuming it is in its current condition and its damage state if it were to be replaced with a pipe of a different resistance level. That makes it easy to use the results in a subsequent optimization to determine what pipes to retrofit/replace and how so as to meet some system-level objectives. Damage scenarios can be used for subsequent flow modeling and to improve the decisiveness for reducing consequences resulting from the infrastructure hazard exposure. The damage scenario also includes the corresponding multihazard scenario and an associated adjusted annual occurrence probability. Each multihazard scenario includes effects of multiple earthquake-related hazards, specifically ground motion, liquefaction and surface rupture. Having a set of multihazard scenarios as well allows use of that same set of multihazard scenarios for analyses of different infrastructure systems within the same geographic region so they are consistent. Unlike Brown et al. (2013), we apply the method for a water transmission system (not a highway network), consider ground motion and liquefaction (not just ground motion), and conduct the analysis for a full, computationally efficient set of multihazard scenarios developed using the Manzour et al. (2016) method.

3.2 Damage scenario development method

3.2.1 Objective and assumptions

The goal of the damage scenario selection method is to compute a relatively small set of Q damage scenarios to be used for subsequent system-level risk analysis. Each damage scenario q defines the damage state d of each system component i for each possible resistance level r it might have. Each damage scenario also includes an associated adjusted occurrence probability $P_{q|j}$ such that for multihazard scenario j, $\sum_q P_{q|j} = 1$. When probabilistically combined with the adjusted occurrence probabilities, the damage distributions for each component conditional on the hazard, computed using the set of Q damage scenarios (which we will call the "reduced set" of scenarios) should match the "true" damage distributions.

The annual occurrence probability of the damage scenario q is $P_j P_{q|j}$, the product of the annual occurrence probability of the multihazard scenario j and the conditional probability of damage scenario q given multihazard scenario j. Each damage scenario also includes the associated multihazard scenario j that generated the damage. Finally, the method computes the errors between the "true" and reduced set marginal damage distributions for each component i and resistance level r, so the tradeoff between reduced error relative to the "true" damage probabilities and increased computational efficiency for subsequent analyses (lower Q) can be examined explicitly. Figure 3.1 provides a schematic summary of the type of output provided by the damage scenario development method for a set of J multihazard scenarios each of which has Q_j damage scenarios associated with it such that $\sum_j Q_j \leq Q$. Note that 'no earthquake' at bottom of Figure 3.1 is one damage scenario, and there may be slightly fewer than Q damage scenarios total due to rounding.

Multihazard scenarios		**Damage scenarios**									
					Damage state d of component i in resistance level r in hazard scenario j, w_{irdq}						
					Component i=1			…	Component l		
Multihazard scenario	Annual occurrence probability of multihazard scenario j	Damage scenario	Conditional probability of damage scenario q	Annual occurrence probability of damage scenario q	Resistance level r=1	…	Resistance level r	…	r=1	…	Resistance level r
j	P_j	q	$P_{q\|j}$	$P_q=P_j(P_{q\|j})$	w_{1111}	…	w_{1r11}	…	w_{l111}	…	w_{lr11}
1	0.0001	1	0.05	0.000005	1	…	1	…	0	…	0
		2	0.01	0.000001	0		1		0		0
		…			0		0		1		1
		Q_1	0.002	0.0000002	1		1		1		1
…	…	…	…	…	…	…	…	…	…	…	…
J	0.0002	1	0.04	0.000008	0	…	1	…	0	…	1
		2	0.02	0.000004	1		1		0		0
		…			1		1		0		1
		Q_J	0.01	0.000002	0		0		0		0
No earthquake	0.4	1	1	0.4	0	…	0	…	0	…	0

Figure 3.1. Schematic summary of output of damage scenario development method.

3.2.2 Overall framework of the methodology

The method involves three main steps: (1) generating a set of J multihazard scenarios, (2) determining Q_j, the number of damage scenarios q for each multihazard scenario j; and (3) using the damage scenario optimization to generate the set of damage scenarios q and determine the adjusted occurrence probability of each, $P_{q|j}$ so as to match the marginal damage function for each system component (e.g., pipe) i.

3.2.2.1 Step 1. Generate a set of J multihazard scenarios

The first step is to generate a relatively small, computationally efficient set of J multihazard scenarios, such that when combined with their associated adjusted annual occurrence probabilities, P_j, the hazard curves they produce match the "true" hazard curves as defined by probabilistic seismic hazard analysis or a conventional MCS. We applied the method introduced in Chapter 2, although another could be used.

3.2.2.2 Step 2. Determine Q_j, the number of damage scenarios q for each multihazard scenario j

The next step is to determine how many damage scenarios Q_j to generate for each multihazard scenario j. The simplest approach is to simulate the same number of damage scenarios for each multihazard scenario. Assuming a desire to end up with a total of Q damage scenarios, that means Q/J damage scenarios for each multihazard scenario. Alternatively, to be as efficient as possible, we can vary the number of damage scenarios Q_j to generate for each multihazard scenario j so as to minimize the variance in the estimated system-wide damage exceedance probabilities. For multihazard scenarios with very high (or very low) intensities, the probability of exceeding a specified level of system damage does not vary as much across damage

scenarios, so there is no need to sample many of them. Using a method analogous to the one used to determine the number of ground motion scenarios for every earthquake scenario derived in Han and Davidson (2012, Section 4.3.3), we use Eq. (3.1) to determine the number of damage scenarios, Q_j, to generate for each multihazard scenario j so as to end up approximately a user-specified total of Q damage scenarios across all multihazard scenarios. To ensure each multihazard scenario includes at least one associated damage scenario, we required $Q_j \geq 1$ after rounding.

$$Q_j = \frac{Q}{N} \sum_n \left[\frac{P_j \sqrt{P(d_j \geq D_n) * [1 - P(d_j \geq D_n)]}}{\sum_j P_j \sqrt{P(d_j \geq D_n) * [1 - P(d_j \geq D_n)]}} \right] \quad (3.1)$$

Where P_j is the probability of multihazard scenario j, D_n is the number of damaged components in the network associated with return period n in multihazard scenario j, $\mathrm{P}(d_j \geq D_n)$ is the probability of exceeding D_n in multihazard scenario j, and N is the number of return periods n at which the damage exceedance probabilities are computed (four in the case study).

To compute the D_n values, a conventional MCS is used to simulate a large number of hazard scenarios and a damage scenario for each. A probability of exceedance vs. number of damaged components in the system curve is generated, and the values of D_n read from it (Note that the hazard portion of the MCS may have been done as part of Step 1, as in the case study). To compute $\mathrm{P}(d_j \geq D_n)$, for each multihazard scenario j, a large number of damage scenarios are simulated and then $\mathrm{P}(d_j \geq D_n)$ is computed as the proportion for which the number of damaged components is at least D_n. If Eq. (3.1) is used (rather than assuming the same number of damage scenarios for each multihazard scenario), a damage model is required to compute D_n and $\mathrm{P}(d_j \geq D_n)$. There are many available, including, for example, ,

Lanzano et al. (2014), Toprak et al. (2017), and Bagriacik et al. (2018). The same damage model should be used in Step 2 and Step 3. The choice depends on what form of system damage is required for the application and available data.

3.2.2.3 Step 3. Generate the set of damage scenarios using the damage scenario optimization

For each multihazard scenario *j*, use the damage scenario optimization (see Damage scenario optimization section below) to generate the set of damage scenarios *q* and determine the adjusted occurrence probability of each, $P_{q|j}$, so as to match the component damage functions. Keep track of which multihazard scenario *j* goes with each damage scenario *q*. Results include (a) a set of approximately *Q* damage scenarios, each of which identifies the damage state *d* of each component *i* for each possible resistance level *r* it might have, its annual occurrence probability ($P_j P_{q|j}$), and the multihazard scenario that generated the damage (Fig. 3.1); (b) errors between the "true" and reduced set marginal damage distributions for each component *i* and resistance level *r*.

Equations (3.2-3.8) describe the optimization formulation applied in Step 3. It is almost the same as that in Brown et al. (2013), except that we omit the constraint that requires the reduced set damage correlation to equal the "true" damage correlation. In our application, because we (1) incorporate spatial correlation in developing multihazard scenarios, and (2) assume there is no correlation in the component damage conditional on hazard, we do not need to retain the constraint. The spatial correlation in multihazard scenarios is considered through ground motion and liquefaction (using soil type) intensities calculation. Note that it is possible that the latter assumption is not true due to similarities in the design and construction between

pipe segments, but there is little data on what those correlations should be and it is likely less important than correlations due to hazard.

$$\text{Min} \sum_{ird}(e_{ird}^{+} + e_{ird}^{-}) \tag{3.2}$$

$$\sum_{q} P_{q|j} w_{irdq} - e_{ird}^{+} + e_{ird}^{-} = m_{ird} \quad \forall i, r, d \tag{3.3}$$

$$\sum_{d} w_{irdq} = 1 \quad \forall i, r, q \tag{3.4}$$

$$\sum_{q} P_{q|j} = 1 \tag{3.5}$$

$$e_{ird}^{+}, e_{ird}^{-} \geq 0 \quad \forall i, r, d \tag{3.6}$$

$$w_{irdq} = \{0,1\} \quad \forall i, r, d, q \tag{3.7}$$

$$\alpha \leq P_{q|j} \leq 1 \quad \forall j, q \tag{3.8}$$

In the formulation, Constraint (3.3) defines the errors terms as the difference between m_{ird}, the "true" probability that component *i* in resistance level *r* is in damage state *d* and the estimated probability component *i* in resistance level *r* is in damage state *d* based on the reduced set of *Q* damage scenarios. If the reduced set probability overestimates the "true" probability, e_{ird}^{+} will be positive and e_{ird}^{-} will be zero; if it underestimates, e_{ird}^{-} will be positive and e_{ird}^{+} will be zero. The objective function (Eq. 3.2) minimizes the sum of those errors. Note that if desired, one could include weights in the objective function to ensure especially small errors for particular pipes, damage states, or resistance levels. Constraint (3.4) requires that for each damage scenario *q*, each component *i* in resistance level r must be in exactly one damage state. Constraint (3.5) represents the assumption that exactly one damage scenario ultimately occurs for each multihazard scenario, so the sum of the conditional damage scenario probabilities is one. By providing lower bound α for $P_{q|j}$ in constraint (3.8), we aim to have more common damage scenarios.

The optimization is a nonlinear mixed integer program since Equation (3.3) includes the product of two decision variables, $P_{q|j}$ and w_{irdq}. We solve it using the iterative heuristic algorithm described in Gearhart et al. (2014). Briefly, it includes the following four steps: (a) Assume that the values of all the variables P_q are $1/\sum_j Q_j$ and solve the resultant linear mixed-integer program for the variables w_{irdq} using a local search algorithm where initially pipes are randomly assigned to damage states under each damage scenario; (b) Fix the values for w_{irdq} using the solution identified in Step *a* and solve the resultant linear program for the variables $P_{q|j}$; (c) Fix the variables $P_{q|j}$ and again solve the mixed-integer linear program for the variables w_{irdq} for each pipe using the local search algorithm; and (d) Iterate between Steps *b* and *c* (where Step *b* uses the values for the variables w_{irdq} identified in Step *c* until the solution converges. The local search algorithm used in Steps *a* and *c* is as follows. We define a neighboring solution to an existing solution as one for which all w_{irdq} are the same except two and those two are the result of moving a single pipe from one damage state to another under a single damage scenario. To compute the value of a neighboring solution requires only computation of the errors in the marginal distribution for the single pipe under this swap. The algorithm stops when there are no moves of this nature that improve the objective function. The method is implemented in Python 3.5 and the optimizations are solved by Gurobi 6.0, a commercial solver (www.gurobi.com), with all multihazard scenarios solved in parallel.

3.3 Case study

3.3.1 Input

The damage scenario development method was applied to the Los Angeles Department of Water and Power (LADWP) water transmission network, as it existed in 2007. The LADWP system in this analysis includes approximately 2,200 km of pipe serving 680,000 customers representing 4 million people in a service area of approximately 1300 Km^2.

In applying the method to the LADWP system, we considered damage only to pipes in the transmission network for multihazard scenarios including ground motion and liquefaction. There are 57,581 pipe segments of 50m or less. One could consider pump stations or other network components if desired. We used Bagriacik et al. (2018, Table 8) damage model to compute the probability of damage to each pipe segment as a function of peak ground velocity (PGV), liquefaction resistance index (LRI) (Cubrinovski et al. 2011), pipe length, diameter, and pipe material (e.g., steel, cast iron). Since we have very large diameter pipes in our data set, we refitted the data like R4 model (considered PGV, LRI, pipe length, pipe diameter and pipe material variables) by considering diameter a binary rather than continuous variable, equal to one when pipe diameter is greater than or equal to 300 mm and zero otherwise. Consistent with the formulation of the damage model, two damage states *d* were considered, damaged or not. In Step 2, we assumed four values of return period *n*—72, 475, 975, 2475 years. The value of D_n, the number of damaged components in the network associated with return period *n*, was obtained by a conventional MCS over 100,000 years. To compute the exceedance probability $P(d_j \geq D_n)$ in Equation 1, 10,000 damage scenarios were simulated for each multihazard scenario. The analysis

was run assuming J=351 and Q=750. Also, the lower bound α for $P_{q|j}$ in Constraint (3.8) is assumed to be 0.01.

In this application, we define each pipe resistance level r as a P(damage|hazard) vs. hazard curve, with hazard expressed in terms of return period of PGV. Specifically, we consider four resistance levels r—low, moderate, high, and current state (Table 3.1).

Table 3.1. Resistance levels low, moderate, high

Return period	High	Moderate	Low
2475	0.005	0.01	0.05
975	0.001	0.005	0.01
475	0.00075	0.001	0.005
72	0.0005	0.00075	0.001

The low, moderate, and high resistance levels are defined by assuming a set of specified damage probabilities for each of four return periods (72, 475, 975, 2475 years). We assume, for example, that if designed to moderate resistance, a pipe segment should have a probability of damage of 0.00075, 0.001, 0.005, and 0.01 if it experiences the PGV with a 72-, 475-, 975-, or 2475-year return period, respectively. For the current state, the curve is different for each pipe, as determined by application of the damage model. To compute the m_{ird} values for a specified multihazard scenario j, i.e., the "true" probability that component i in resistance level r is in damage state d when subjected to multihazard scenario j, we found the PGV for pipe i in multihazard

scenario *j*, determined the return period it corresponds to, then used the curve for the appropriate resistance *r* to determine the probability of damage, m_{ird}. This format for defining resistance levels is consistent with the performance-based design thinking as described in Davis (2019a, 2019b).

3.3.2 Results

For Step 1 in the case study, we used the 351 multihazard scenarios developed in Chapter 2. The ground motion hazard was based on the 2014 National Seismic Hazard Map, in turn based on the Uniform California Earthquake Rupture Forecast v3 (UCERF3) (Petersen et al. 2011, Field et al. 2014, Powers 2015) and the liquefaction hazard was based on the LPI3 liquefaction model in Kongar et al. (2017) and liquefaction susceptibility maps from Southern California Gas Company (2001-2003). The final reduced set included 710 damage scenarios derived from those 351 multihazard scenarios (less than Q=750 due to rounding of the Q_j values). Among these 351 scenarios, 285 multihazard scenarios (81%) have one or two damage scenarios, 60 multihazard scenarios (17%) have three to ten damage scenarios, and 2% have more than 10 damage scenarios (up to 29).

The total number of damaged pipes varies across damage scenarios. Figure (3.2) shows the distribution for the current resistance level. With 57,581 pipes in the system, 82% of damage scenarios include fewer than 2,500 damaged pipes; and only less than 1% have more than 12,000 damaged pipes.

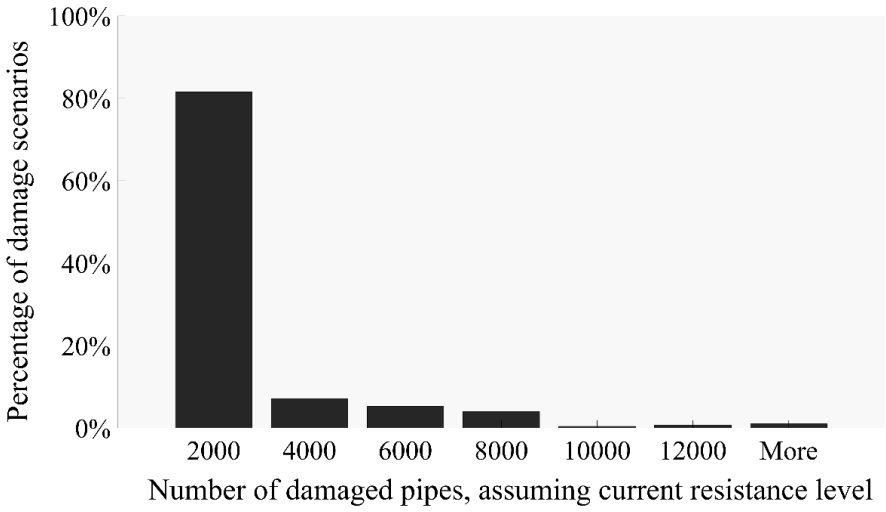

Figure 3.2. Histogram of the number of damaged pipes, assuming current resistance levels.

The adjusted annual occurrence probabilities, P_j, for the multihazard scenarios range from $6.07(10^{-8})$ and $2.50(10^{-3})$. The adjusted annual occurrence probabilities, $P_{q|j}$, for the damage scenarios conditional on the multihazard scenarios are 0.01 to 1.0; and the adjusted annual occurrence probabilities, P_q, for the damage scenarios range from $3.9(10^{-8})$ and $1.4(10^{-3})$. Figure 3.3 indicates the probability of exceedance for the damaged pipes over all damage scenarios, assuming current resistance level.

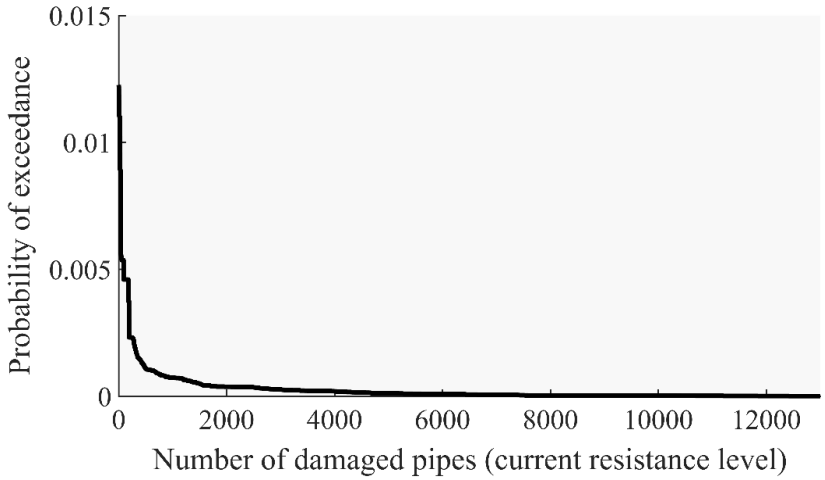

Figure 3.3. Exceedance probability of damaged, assuming current resistance levels.

As an example, Figure 3.4 shows maps associated with one example damage scenario associated with a M6.38 earthquake on the Mission Hill fault. This particular damage scenario has an adjusted annual occurrence probability of $P_q = 1.28(10^{-5})$, based on the product of the adjusted annual occurrence rate of the associated multihazard scenario is $P_j = 2.24(10^{-4})$, and the probability of the damage scenario given the multihazard scenario is $P_{q|j} = 0.057$.

Figures (3.4a) and (3.4b) show maps of the rupture trace and ground motion (PGV), and liquefaction potential index (LPI), respectively. Figure 3.4c shows which pipes are damaged assuming the current resistance levels. Figure 3.4d and 3.4e illustrate those damaged assuming that all are replaced with pipes having a moderate and low resistance level, respectively. The damage scenario also includes information about which pipes would be damaged if they were replaced with pipes designed to low resistance level or high resistance level. That information is not shown due to space limitations. Comparing Figures 3.4c and 3.4d shows the different damage patterns

resulting from the different resistance levels. In particular, while many pipes are damaged in the northern part of the city when assuming the current resistance levels, they are not when we assume they are replaced by pipes with moderate resistance level (as defined in Table 3.1). Note that while these maps show damage patterns assuming all pipes have their current resistance levels or all pipes have moderate or low resistance level, the information for each pipe can be mixed and matched. That is, if, for example, one wanted to do an analysis to see how the system would perform if only the pipes in the northern part of the city were replaced with pipes with moderate resistance, but the rest of the pipes remained in their current resistance level, you would simply use a damage scenario created by selecting the damage state associated with *r=moderate* for the pipes in the northern part and selecting the damage state associated with *r=current* for the remaining pipes.

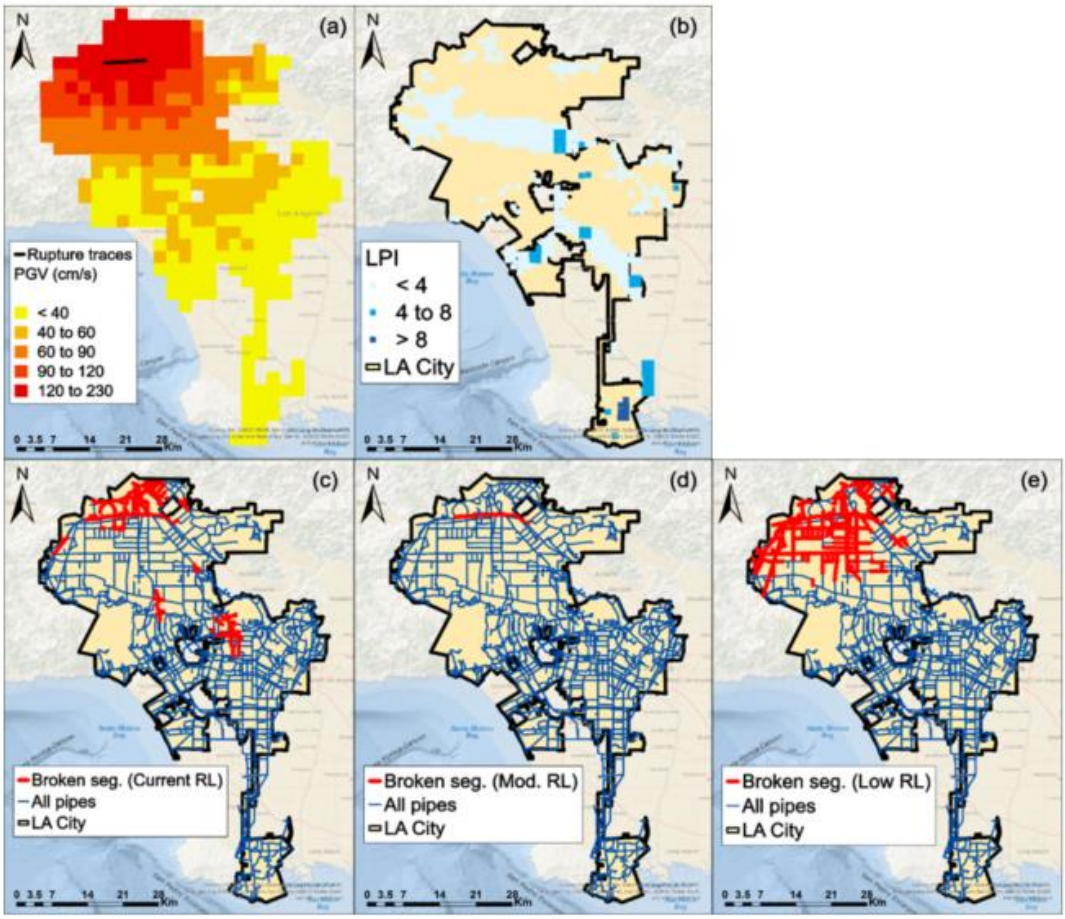

Figure 3.4. One example damage scenario, (a) associated ground motion and rupture map (PGV), (b) Liquefaction Potential Index map (LPI), (c) damaged pipes for current resistance level, (d) damaged pipes assuming moderate resistance level, (e) damaged pipes assuming low resistance level.

To assess how well the set of 710 damage scenarios match the marginal damage distributions associated with each pipe for each resistance level, we can examine the error terms, e^{+}_{ird} and e^{-}_{ird}. The mean of the error terms across all damage scenarios *q*, pipes *i*, resistance levels *r*, and damage states *d* equals $1.39(10^{-10})$, which is close to zero and suggesting no notable bias. To get a sense for the magnitude of the errors, 97% of the absolute values of the error terms are within 1% of the "true" value

of m_{ird} and 99.84% are within 5% of the "true value of m_{ird}, which should be sufficiently small for most practical purposes. For a particular application, the analyst can always conduct a sensitivity analysis by varying the maximum allowable number of multihazard scenarios *J* and the maximum allowable number of damage scenarios *Q* in the reduced set, and examining how the errors change, and select the appropriate computation-error tradeoff for the application. The optimization requires less than 5 minutes to reveal the optimal solution for each damage scenario.

3.4 Conclusion

This chapter describes development of a computationally efficient set of damage scenarios for the Los Angeles water transmission system that considers multiple earthquake hazards. Each damage scenario describes, for each pipe segment (or other component) in the network, both its damage state assuming it is in its current condition and its damage state if it were to be replaced with a pipe of a different resistance level. The damage scenario also includes the corresponding multihazard scenario and an adjusted annual occurrence probability so that when probabilistically combined the set of damage scenarios with their probabilities matches the probabilistic hazard and system functioning (e.g., percentage of demand satisfied) exceedance curves.

Once developed, one can then simulate system functioning for each damage scenario in the reduced set to obtain a fully probabilistic analysis of system functioning that is computationally efficient enough to allow sophisticated hydraulic analysis rather than a more computationally efficient but less accurate connectivity-based system functioning analysis. Since each damage scenario includes for every pipe, both its damage state assuming it is in its current condition and its damage state

if it were to be replaced with a pipe of a different resistance level, the resulting set of damage scenarios can be used in a subsequent optimization to determine what pipes to retrofit/replace and how so as to meet some system-level objectives. Otherwise it would be extremely computationally intensive to do so. Possible future work includes incorporating the effects of surface fault ruptures in the damage modeling; doing sensitivity analysis to understand the tradeoff between including more multihazard scenarios, J, and more damage scenarios per multihazard scenario Q; and including damage to water system components other than pipes (e.g., pump stations).

Chapter 4

HOUSEHOLD ADAPTATIONS TO AND IMPACTS FROM ELECTRIC POWER AND WATER OUTAGES IN THE TEXAS 2021 WINTER STORM

4.1 Introduction

Households rely on infrastructure system services for virtually all aspects of daily life. They use electric power for lighting, heating, and accessing electronic devices, for example, and potable water for drinking, bathing, and cleaning. When those services are interrupted, numerous negative consequences may follow, in terms of health, safety, financial loss, and disruption of daily activities. Thus, unsurprisingly, households typically try to lessen the negative impacts of service outages by adapting in many ways, planned and unplanned. They may purchase and use a power generator to adapt to an electric power outage, use water from a rain barrel during a water outage, or go to a hotel during a gas service interruption. In fact, these adaptations can represent a massive mediating influence on the effect of system outages. Recognizing the importance of such user adaptations and of understanding the implications of service outages for daily life, the study of resilience of infrastructure systems has expanded to include both ideas (NEHRP 2014, ATC 2016).

Nevertheless, quantitative empirical descriptions of household adaptations to and impacts from service outages are still limited. In this research, we ask the same questions as Abbou et al. 2022 and Stock (2020) but using different data. Whereas data in the current study describe actual behavior (revealed preferences) during the February 10-21, 2021 winter storm centered in Texas, USA the previous studies were

based on data from a larger sample of Los Angeles County residents that included a combination of (a) revealed preference responses from each respondent's longest outage experience (not a single event) and (b) questions about intended behavior (stated preference) in hypothetical future outages of specified durations. Both the Texas and Los Angeles datasets, however, used the same questions about household adaptations to and impacts from electric power and water supply outages, allowing direct comparison of the results. In this Chapter, we explore the generalizability of the findings from those Los Angeles-based studies by answering a few research questions. Following a review of the related literature on household adaptations to and impacts of lifeline service outages in Section 4.2, the research questions are defined in Section 4.3. Then we describe the data and methods in Section 4.4. Sections 4.5 addresses each of the six research questions in turn. Finally, we conclude with the implications and limitations of this study.

4.2 Background

4.2.1 Household adaptations to service outages

Although the study of adaptations to service outages includes those by businesses, government agencies, and non-profit organizations, and adaptations to various types of events, here we focus on household adaptations to electric power and water service interruptions in particular. Previous studies have identified many examples of such user adaptations, which we define as an *action taken by the users of an infrastructure service to address their needs with other methods when that service is suspended or substantially reduced*. Heidenstrom and Kvarnlöf (2017), for example, documented use of camping stoves to cook during electric power outages in winter

storms in Norway and Sweden. Following the 2010 earthquake in Chile, some households got water from streams to replace water supply that was interrupted (Moreno and Shaw 2019). Similar examples have been observed in various extreme events and locations, resulting in a list of dozens of different adaptations (Abbou et al. 2022).

The literature has also proposed many variables that may help explain who implements what adaptations under what circumstances. These include variables describing: (1) outage attributes (Zhang 2019), (2) past experiences and risk perception (Heidenstrøm and Throne-Holst 2020, Clay et al. 2020, Martins et al. 2018, FEMA 2013), (3) socio demographics (Osberghaus and Abeling 2022, Moreno and Shaw 2019, Ercumen et al. 2015, Jeandron et al. 2015, Dargin and A. Mostafavi 2020, Klinger et al. 2014), and (4) social connectedness (Wolf et al. 2010). Osberghaus and Abeling (2022) suggested that low-income households are extremely heat sensitive while having lower adaptive capacity than high-income households. Moreno and Shaw (2019) stated older people in Chile could locate ancient streambeds to draw water after experiencing the 2010 earthquake. When households experience water interruptions, they may rely on unsafe water alternatives, affecting their hygiene. A few studies suggest this issue is more prominent for low-income households and households who rely more on tap water (e.g., for drinking) (Ercumen et al. 2015; Jeandron et al. 2015). A study in the UK indicated a strong social bond could perpetuate a specific adaptive action or behavior of the members depending on the shared material in the group (Wolf et al. 2010).

Davidson et al. (in review) recently introduced a typology of household adaptations to service interruptions to help understand them not as isolated, one-off,

workarounds, but as a well-defined phenomenon in which the same or similar types of actions are taken by many people across many events. Despite these advances in knowledge, this body of work includes little quantitative study of the implementation of adaptations. This Chapter aims to build on Abbou et al. (2022), which uses a large survey-based dataset that includes both revealed and stated preference data to develop statistical models of adaptation implementation. Asking the same questions with different data from a different past event, we begin to examine the generalizability of the findings from Abbou et al. (2022).

4.2.2 Household impacts from service outages

Efforts to identify and quantify household impacts of infrastructure system service interruptions can be partitioned into (1) needs-based and (2) reaction-based (Davidson et al. 2022). In the former, a list of needs or uses the infrastructure system service helps a household, business or organization meet are enumerated (e.g., survival, hygiene, earning income, and cooking), and the impact is defined in terms of the extent to which those are met. The needs may be defined more specifically or generally, and their definition may depend on the infrastructure system and location. Yang et al. (2021), for example, focus on individual physiological needs and incorporated adaptive capacity to evaluate the societal impact of disrupted water infrastructure, including a case study for Osaka, Japan. They define five levels of need satisfaction, and then express societal impact as the percentage of the population in each. Tabandeh et al. (2018, 2019) use indicators to represent a person's capabilities, which capture distinct dimensions of an individual's well-being, including for example, meeting physiological needs, earning income, being mobile, and being socially connected.

In reaction-based measures, the impact of the service disruption is captured in terms of the household's reaction to it, how they interpret the severity of the interruption and its implications (e.g., Dargin and Mostafavi 2020, Coleman et al. 2020, Esmalian et al. 2019). These methods typically implicitly include the effect of both any reduced level of service that exists even after adaptations and any (usually negative) experience associated with implementing the adaptations (e.g., money and time spent going to a hotel, effort associated with using water from rain barrels). Most studies using the micro approach have relied on self-reported measures in survey or interview data. Stock (2020) developed two reaction-based measures of societal impacts—willingness to pay (WTP) to avoid service interruptions and a constructed scale of unhappiness. Focusing on electric power and water service interruptions, they use survey-based data from Los Angeles County, to fit regression models of WTP and unhappiness, both as functions of infrastructure type, outage duration, and household attributes. Asking the same questions with different data from a different past event, we begin to examine the generalizability of the findings from Stock (2020).

4.3 Research questions

With the aim of examining the generalizability of the household impact and adaptation adoption findings from the Los Angeles-based studies mentioned in Section 4.1, and in particular, exploring which findings are replicated in Texas for the 2021 winter storm, and which are not, we investigate the same questions as those posed in those Los Angeles-based studies (Abbou et al. 2022, Stock2020), namely:

- *Research Question 1*. How common are different types of household adaptations?

- *Research Question 2*. How does household adaptation implementation vary with (a) infrastructure type, (b) outage duration, (c) uses of the service, and (d) household characteristics?
- *Research Question 3*. Which household adaptations tend to occur together? Which tend not to?
- *Research Question 4*. How unhappy are households when service is interrupted?
- *Research Question 5*. How do household impacts vary with (a) infrastructure system type, (b) outage duration, and (c) household characteristics?
- *Research Question 6*. What are the concerns that influence an individual's level of unhappiness associated with service interruptions?

4.4 Methodology

4.4.1 Data collection

Data was collected through a web-based survey coded in Qualtrics. The survey instrument, which was designed to capture households' experiences during the 2021 Texas winter storm, included questions related to: (1) typical electrical and water uses, (2) interruptions in electricity and/or water service due to the storm (February 10-21), (3) adaptations undertaken to cope with and unhappiness associated with service interruptions, (4) risk attitudes, and (5) socio-demographics. The survey required an average of 7.5 minutes to complete.

The survey was distributed on Facebook in March-May 2021. Relevant groups and pages were chosen that focused on the storm and/or the affected area, including

for example, “Disaster Response, Rescue, and Recovery Resources Network” and “Winter Storm 2021 Nacogdoches, Texas”. Members of the research team joined the pages, requested access to post or requested permission to post when necessary, and posted a link to the survey with an explanation of the study on each page. Institutional review board approval was obtained at the University of Delaware (Appendix B). The link was sharable once deployed. Three weeks after the initial posting, a comment was added to most posts to push them to the top of the page and inform potential respondents of the date the survey would close. We posted the survey to 19 groups which collectively had 183,489 members, although members of those groups likely shared the post within their own social networks. There were 215 useable responses. Benefits of this method of survey deployment, previously used by Farmer and DeYoung (2019), DeYoung et al. (2019), and Mongold et al. (2020), include that it can be done quickly, maximizing the accuracy of recollections, and it is less expensive to deploy and analyze than mail or phone surveys.

To examine the representativeness of the sample, demographic data for the sample were compared to that for the population from which they were drawn. Population demographics were computed using county-level data from the U.S. Census (US Census Bureau, 2019), weighted based on the number of respondents from each county. Overall, the sample is reasonably similar to the population, with a few exceptions. The sample includes more White people (85% in sample vs. 65% in the population), more females (80% sample vs. 56% population), and more with at least a 4-year degree (58% in sample vs. 35% in the population). The sample and population have similar age and income distributions (average age is 50 in sample and

45 in the population; average income is $102,000 in sample and $97,000 in the population).

4.4.2 Data summary

4.4.2.1 Household societal impact, adaptation, and outage duration variables

Questions were included to solicit information about the durations of electricity and water outages respondents experienced (4 for electricity, 4 for water). The questions and {*answer choices*} were as follows: **Q1**: Did you experience a loss of electricity [water service] at your residence at any time from February 10 to February 21, 2021? *{Yes, it went off and on more than once; Yes, it went off just once; No}* **Q2**: Over approximately how much time was your electricity [water] disrupted during that period (i.e., from the first time it was interrupted until the last time it came back on)? *{Enter number of full days and number of hours}* **Q3**: Approximately how long did the longest electricity [water] outage during that period last? **Q4**: Approximately how long did the electricity [water] outage last? For each infrastructure type, if the answer to Q1 was *Yes, it went off and on more than once*, Q4 was not asked; if the answer to Q1 was *Yes, it went off just once*, Q2 and Q3 were not asked; and if the answer to Q1 was *No*, Q2, Q3, and Q4 were not asked.

For those who experienced an outage, additional questions were asked about how they adapted to those outages and the impacts of them. For each outage (electricity and/or water), the were asked: **Q5**: Which of the following did you do, if any, to meet your household electricity [water] needs during the longest outage that you experienced? (Select all that apply) {*list of adaptations*}. For electricity and water, respectively, the 19 and 15 adaptations applicable to the infrastructure type in

Table (4.1) were listed. **Q6**: Considering the actions you took to deal with the longest outage that you experienced, as well as any remaining reduction in service, what level of unhappiness did you feel as a result of the outage? {*Not unhappy*; *Slightly unhappy*; *Moderately unhappy*; *Very unhappy*; *Extremely unhappy*}. **Q7**. To what extent did each of the following concerns influence your level of unhappiness? For each of four concerns—Financial cost, Time or effort to meet household needs, Physical health effects, Stress, there were four choices: {*Not at all, To a minor extent, To a moderate extent, To a major extent*}.

Table 4.1. Number of responses for each adaptation

Adaptation		Electric power		Water supply	
		Y	N	Y	N
y_{gen}	Used a generator	24	130		
y_{candle}	Used candles, flashlight, and/or lantern	130	24		
y_{heater}	Used a non-electric heater and/or fireplace	54	100		
y_{stovew}	Used a gas stove for warmth	24	130		
y_{stove}	Used a gas stove and/or camping stove to cook meals and/or boil water	52	102		
y_{car}	Charged cell phone in the car	77	77		
y_{carw}	Used car for warmth	42	112		
y_{shop}	Charged cell phone, laptop, and/or tablet at work and/or in a coffee shop	16	138		
y_{wifi}	Used wifi somewhere other than home	5	149		
y_{burn}	Burned furniture, driftwood, yard trimmings, or other fuels	9	145		
y_{center}	Went to a warming center	3	151		
y_{lake}	Used water from lakes, rivers, and/or creeks			2	85
y_{govt}	Used water delivered by the government			2	85
y_{comm}	Used water provided by community or neighborhood-based orgs.			11	76
y_{tank}	Used water from private tank &/or rain barrel			4	83
y_{pool}	Used water from a swimming pool			3	84
y_{tub}	Used water stored in the bathtub			36	51
y_{snow}	Melted snow or ice			37	50
y_{bottle}	Purchased bottled water			70	17
y_{red}	Reduced consumption of electricity [water] (e.g., cooked less)	71	83	54	33

Table 4.1. Continued

y_{delay}	Delayed consumption of electricity [water] (e.g., postponed laundry)	86	68	53	34
y_{visit}	Visited a relative's or friend's house for their heat [water]	29	125	15	72
y_{rel}	Stayed at a relative's or friend's house	33	121	23	64
y_{hotel}	Moved to a hotel	7	147	3	84
y_{town}	Traveled out of town	2	152	4	83
y_{other}	Other	10	144	7	80

4.4.2.2 Other explanatory variables

Table 4.2 and 4.3 provide summary statistics for the explanatory variables in the Texas survey, with a comparison to data from the Los Angeles survey. The explanatory variables can be grouped in five main categories: (1) outage attributes (x_{type}, $x_{e.num}$, $x_{w.num}$, x_{notice}, x_{damage}), (2) type of service usage ($x_{e.dev}$, $x_{e.work}$, $x_{e.source}$, $x_{w.dev}$, $x_{w.work}$, $x_{w.source}$), (3) past experiences and risk perception ($x_{l.emer}$, $x_{w.emer}$, $x_{n.emer}$), (4) socio-demographics (x_{gen}, x_{race}, x_{edu}, x_{child}, x_{elder}, x_{pets}, $x_{med.c}$, $x_{med.e}$, x_{own}, x_{house}, x_{employ}, $x_{marital}$), (5) social connectivity ($x_{neighbor}$).

To examine the possible effects of repeated outages ($x_{e.num}$, $x_{w.num}$) and outage duration ($x_{e.dur}$, $x_{w.dur}$), respondents were asked questions Q1 and Q3 and Q4, respectively. Note that when a respondent experienced more than one outage (i.e., the power went off and on), the outage duration was taken to be the longest outage duration (Q3). Respondents also answered the questions "Did you receive prior notice of the blackouts? {*Yes or No*}" and "Did you experience any property damage as a result of any disruption of electricity or water? {*Yes or No*}" to collect data for the prior notice (x_{notice}) and property damage (x_{damage}) variables.

Respondents were asked in what ways they regularly use electricity and water. Of nine possible choices for each, we assumed using the services for medical devices and work purposes are of primary importance, and thus included only those uses ($x_{e.dev}$, $x_{e.work}$, $x_{w.dev}$, $x_{w.work}$). To determine if someone might have a backup source of electric power or water, we asked "Which of the following energy [water] sources does your household use at your place of residence? (Select all that apply)" and coded responses as one source or multiple sources ($x_{e.source}$, $x_{w.source}$).

Three variables were used to capture prior hazard event experiences and risk perception as possible predictors of adaptation to and impact of service outages. Respondents were asked “How likely do you think it is that you and your household will be impacted by emergencies in the next five years?” ($x_{l.emer}$); “How worried are you about the potential threat of you and your household being impacted by emergencies in the next five years?” ($x_{w.emer}$); and “Other than the February 2021 winter storm, have you ever experienced other emergencies that caused some negative impact on your life?” ($x_{n.emer}$). In all three cases, the responses were coded as binary due to the relatively small sample size (Table 4.2). This Preparation (x_{prep}) variable was coded as the number of preparation-based activities respondents took out of 12 possible activities—preparing an evacuation plan, preparing a household reunion plan, searching for preparation information, storing important documents, keeping extra medication, keeping extra cash, gathering emergency numbers, storing three days of water per person, storing non-perishable food and snacks, storing first aid supplies, storing flashlights, and storing a battery-operated radio (Table 4.3).

To elicit the level of social connectedness households feel, we asked “Thinking about your neighborhood, how much do you agree or disagree with each of the following sentences: (1) People in this neighborhood are willing to help neighbors, (2) People in this neighborhood know each other well, (3) People in this neighborhood can be trusted, (4) People in this neighborhood participate in neighborhood organizations, and (5) My neighborhood is a safe place.” The possible choices were *Strongly disagree*, *Disagree*, *Agree*, and *Strongly agree*. We computed the neighbor connectedness variable (x_{neigh}) by assigning values 1 to 4 to each response choice,

respectively, averaging the answers for the five statements, and coding them as 0 for Does not feel connected (≤2.5), and 1 for Feels connected (>2.5).

Table 4.2. Number of respondents associated with each level of categorical variables

Variable	Description	Levels	Num. respondents	
			Texas[1]	LA[2]
Outage attributes				
x_{type}	Infrastructure service type	0: Electric	164	1615
		1: Water	164	1615
$x_{e.num}$	More than one power interruption	0: One interruption	42	n.a.
		1: More than one interruption	112	n.a.
$x_{w.num}$	More than one water interruption	0: One interruption	45	n.a.
		1: More than one interruption	42	n.a.
x_{notice}	Prior notice	0: Not received	110	n.a.
		1: Received	44	n.a.
x_{damage}	Property damage	0: No	114	n.a.
		1: Yes	50	n.a.
Type of service usage				
$x_{e.dev}$	Use electricity for medical devices	0: No	139	1474
		1: Yes	25	141
$x_{e.work}$	Use electricity for work	0: No	57	1205
		1: Yes	107	410
$x_{e,source}$	Multiple sources of energy	0: No	55	418
		1: Yes	109	1197
$x_{w.dev}$	Use water for medical devices	0: No	151	1520
		1: Yes	13	95
$x_{w.work}$	Use water for work	0: No	134	1483
		1: Yes	30	132
$x_{w,source}$	Multiple sources of water	0: No	109	824
		1: Yes	55	791
Past experiences and risk perception				
$x_{l.emer}$	Perceived likelihood of emergency in next 5 years	0: Very unlikely, unlikely, not sure	20	515
		1: Likely or very likely	142	1100
$x_{w.emer}$	Worry about emergency in next 5 years	0: Not at all or slightly worried	55	885
		1: Moderately or extremely worried	106	730
$x_{n.emer}$	Has experienced a negative emergency	0: Had not had negative experience	63	1134

Table 4.2. Continued

		1: Has had a negative experience	95	481
Socio-demographics				
x_{gen}	Gender	0: Female	117	838
		1: Other	28	777
x_{race}	Race	0: White	126	428
		1: Other	21	1187
x_{edu}	Education	0: < 4-year degree	47	1155
		1: 4-year degree+	65	460
x_{child}	Children (<18 yrs) live in household	0: No	40	918
		1: Yes	55	692
x_{elder}	Elders (65+ yrs) live in household	0: No	46	1176
		1: Yes	30	434
x_{pets}	Pets live in household	0: No	29	612
		1: Yes	120	1003
$x_{med.c}$	Anyone with a medical condition in household	0: No	110	1167
		1: Yes	35	448
$x_{med.e}$	Anyone in household relies on medical equipment	0: No	123	1426
		1: Yes	23	189
x_{own}	Homeownership	0: Do not own	44	788
		1: Own	100	827
x_{house}	House type	0: Single-family, duplex, townhome	116	1061
		1: Other	29	554
x_{employ}	Employment status	0: Not traditionally employed	53	720
		1: Employed full-time or part-time	93	895
$x_{marital}$	Marital status	0: Not married	57	928
		1: Married	89	687
Social connectedness				
$x_{neighbor}$	Feels connection to neighborhood	0: Does not feel connected	43	572
		1: Feels connected	108	1043

[1] Not all variables have 164 responses due to missing data
[2] n.a. = not asked in survey

Table 4.3. Descriptive statistics for continuous variables for Texas and LA

Variable	Description (unit)	Num. responses		Mean		St. deviation	
		Texas	LA	Texas	LA	Texas	LA
$x_{e.dur}$	Outage duration, electricity (hours)	122	1302	62.20	18.88	41.64	81.29

Table 4.3. Continued

$x_{w.dur}$	Outage duration, water (hours)	48	522	101.01	25.41	52.76	99.61
x_{prep}	Preparation[b]	155	1615	7.69	7.01	2.93	3.38
x_{age}	Age (years)	135	1611	45.11	41.96	14.01	16.40
x_{inc}	Income[a] ($1000s)	135	1615	101.90	77.47	67.78	65.33
$x_{yr,h}$	Years living at current address	139	1590	10.35	14.20	9.85	12.50
$x_{yr,c}$	Years living in your current county	139	1600	19.89	31.12	14.87	17.78

[a] Income was asked as an interval variable but was coded as a continuous variable with the values in parentheses for each interval: less than $15k ($7.5k), $15k–$35k ($25k), $35k–$50k ($42.5k), $50k–$75k ($62.5k), $75k–$100k ($87.5k), $100k–$150k ($125k), $150k–$250k ($200k), and more than $250k ($300k).

[b] Preparation is a continuous value from 0 to 12.

4.4.3 Imputation

After removing the 51 respondents who did not experience either an electric power or water outage and respondents who had answered fewer than 70% of the survey questions, we had 164 respondents with a total of 241 observations (154 respondents with only an electricity outage, 87 with only a water outage, and 77 with both). The data, however, still included missing values (Tables 4.1 and 4.2) in a patchwork, not monotone, pattern. The most common methods of handling missing data—listwise and pairwise deletion—discard useful data and result in coefficient estimates that are potentially biased (Harrell 2015). In this analysis, therefore, we used multiple imputations because it avoids the problems of deletion methods and unlike single imputation, accounts for the uncertainty introduced by the fact that missing values are being imputed and so does not underestimate the *p*-values (van Buuren 2012), Harrell 2015). In multiple imputations the dataset is imputed multiple times creating m ‘‘complete’’ datasets, the analysis is conducted separately on each, and then the results are combined (van Buuren 2012). Specifically, we used the {mice} package in R, which implements the multivariate imputation using chained equations (MICE)

algorithm (van Buuren and Groothuis-Oudshoorn 2011, van Buuren 2012). We generated 50 imputed datasets, consistent with approximate guidelines in van Buuren (2012) and Harrell (2015). Default settings were used—logistic regression for binary variables, proportional odds for ordered and Bayesian linear regression for continuous variables. We checked to ensure the distributions of the observed and imputed datasets were sufficiently similar, using kernel densities for continuous variables, and histograms for binary variables. Results of all checks suggest that the imputed datasets match the observed data w ell in terms of distributions of variables. Results from the imputed datasets were combined using Rubin's rules (van Buuren 2012, White et al. 2011, Miles 2015).

4.4.4 Comparison to Los Angeles County data

Results of the analysis of the Los Angeles data in Abbou et al. 2022 and Stock (2020) offer a valuable comparison for the results of this study. To facilitate interpretation of those comparisons, we summarize the key differences in Table 4.4; other variables were similar. The questions in the Los Angeles survey were the same as those described in Section 4.4.2, with a few minor differences. The Los Angeles survey did not include the questions associated with the multiple interruptions ($x_{e.num}$, $x_{w.num}$), prior notice (x_{notice}), and property damage (x_{damage}) (Table 4.2), or the following adaptations: Used your gas stove for warmth (y_{stovew}), Used your car for warmth (y_{carw}), Melted snow or ice (y_{snow}), and Used water provided by community or neighborhood-based organizations (y_{stovew}). Note also that in some cases the RP and SP questions in the Los Angeles data exhibit different behavior; in those cases, the results are separated into LA-SP and LA-RP.

Table 4.4. Key differences between Texas and Los Angeles County datasets

	Texas	Los Angeles County
Survey type	Web-based deployed 3/21-5/21	Web-based deployed 5/20-12/20
Sample type, location	Convenience sample identified through social media (66% in Texas)	Census-representative, quota-based sample with all respondents from LA County
Num. responses	241	1615
Type of data	RP related to winter storm of February 2021	RP from each respondent's longest outage experience (not a single event) and SP for hypothetical outages of specified durations (1 day, 3 days, 1 week, 1 month)
Outage durations (hours)	Electric: mean=62; s.d.=42 Water: mean=101; s.d.=53	RP Electric: mean=19; s.d.=81 Water: mean=25; s.d.=100 SP Electric: mean=240; s.d.=283 Water: mean=240; s.d.=283
Respondent demographics	81% are female 86% are White 61% are married 42% have < 4-year degree 81% have pets in the household $102,000 mean annual income	52% are female 27% are White 43% are married 72% have < 4-year degree 62% have pets in the household $77,000 mean annual income
Risk perception/ experience	66% worry a/b emergency in next 5 yrs 60% experienced a negative emergency	45% worry about emergency in next 5 yrs 30% experienced a negative emergency
Use of service	65% use electricity for work	25% use electricity for work

4.5 Analyses and results

4.5.1 Adaptation adoption frequency

The first research question asks *How common are different types of household adaptations?* While all those examined in this study have been observed in previous

events, little is known about how common each is in general. We first address this question by examining adaptation implementation by respondent. Figure (4.1) shows histograms of the number of adaptations each respondent implemented, for the electric power and water supply outages, and for the Texas data, as well as the Los Angeles revealed and stated preference data for comparison. They indicate that adaptations are very common for both electric power and water. The Texas data indicate that each respondent implemented an average of 12 adaptations for electric power and 10 for water. The Los Angeles data suggests fewer adaptations per person, but still multiple, with average of 7 and 5 for electric power and water in the SP data, respectively, and 2 and 2 for electric power and water in the RP data, respectively.

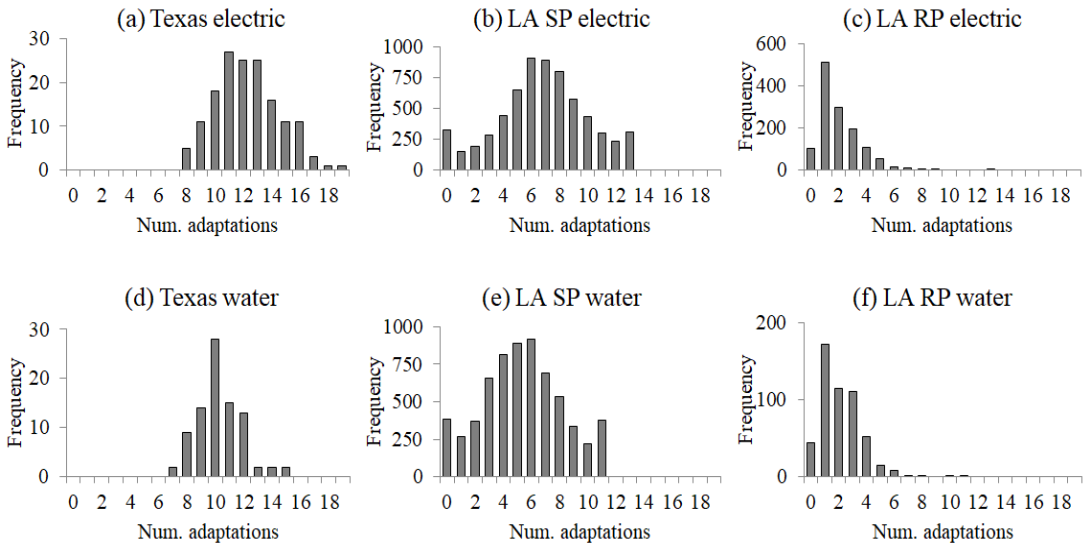

Figure 4.1. Histograms of the number of adaptations implemented by each respondent for (a) Texas electric power; (b) LA SP electric power; (c) LA RP electric power; (d) Texas water; (e) LA SP water; (f) LA RP water

To examine how common specific adaptations are, we examine Figures 4.1a and 4.1b, which show the percentage of respondents who did each adaptation for electric power and water, respectively. For electric power, the most common adaptation in Texas was using candles, flashlight, and/or lantern (84%). Other very common adaptations were delaying consumption (56%), charging the cell phone in the car (50%), and reducing consumption (46%) (Fig. 4.2a). These were also the four most common electric power adaptations in the Los Angeles dataset, although the percentages of people saying they had implemented them in the Los Angeles RP data were smaller, perhaps because the outage durations were shorter in the Los Angeles RP data (Table 4.4). The least common electric power adaptations in both Texas and the Los Angeles RP include going to a coffee shop (10%), a hotel (5%), out of town (1%), or to a warming center (2%). While the most common tend to be relatively inexpensive, the least common involved travel. Notably, for almost all adaptations, the frequency of implementation in the Texas data falls between the lower percentage in the Los Angeles RP data and the higher percentage in the Los Angeles SP data.

For water supply, the most common adaptations in Texas were purchasing bottled water (80%), reducing consumption (62%), and delaying consumption (61%) (Fig. 4.2.b). These were also the most common in the Los Angeles dataset, with similar percentages for the SP data and somewhat lower for the RP data. Among the least common water adaptations in Texas—all implemented by fewer than 13% of respondents—were using water from the government, community organization, a private tank, or a lake; or traveling to a hotel or out of town. Those adaptations were also uncommon in the Los Angeles RP data, but they were quite common in the Los Angeles SP data. This could be due to the fact that it was stated preference data or due

to the longer outage durations associated with the Los Angeles SP data. As with electric adaptations, while the most common tend to be relatively inexpensive and easy to implement, the least common involved travel, help from other people, and/or access to a special resource (e.g., a lake). Interestingly, melting snow was quite common in the Texas data (43%). It was not asked in the Los Angeles survey but would likely not be as common there due to the rarity of snow in that region.

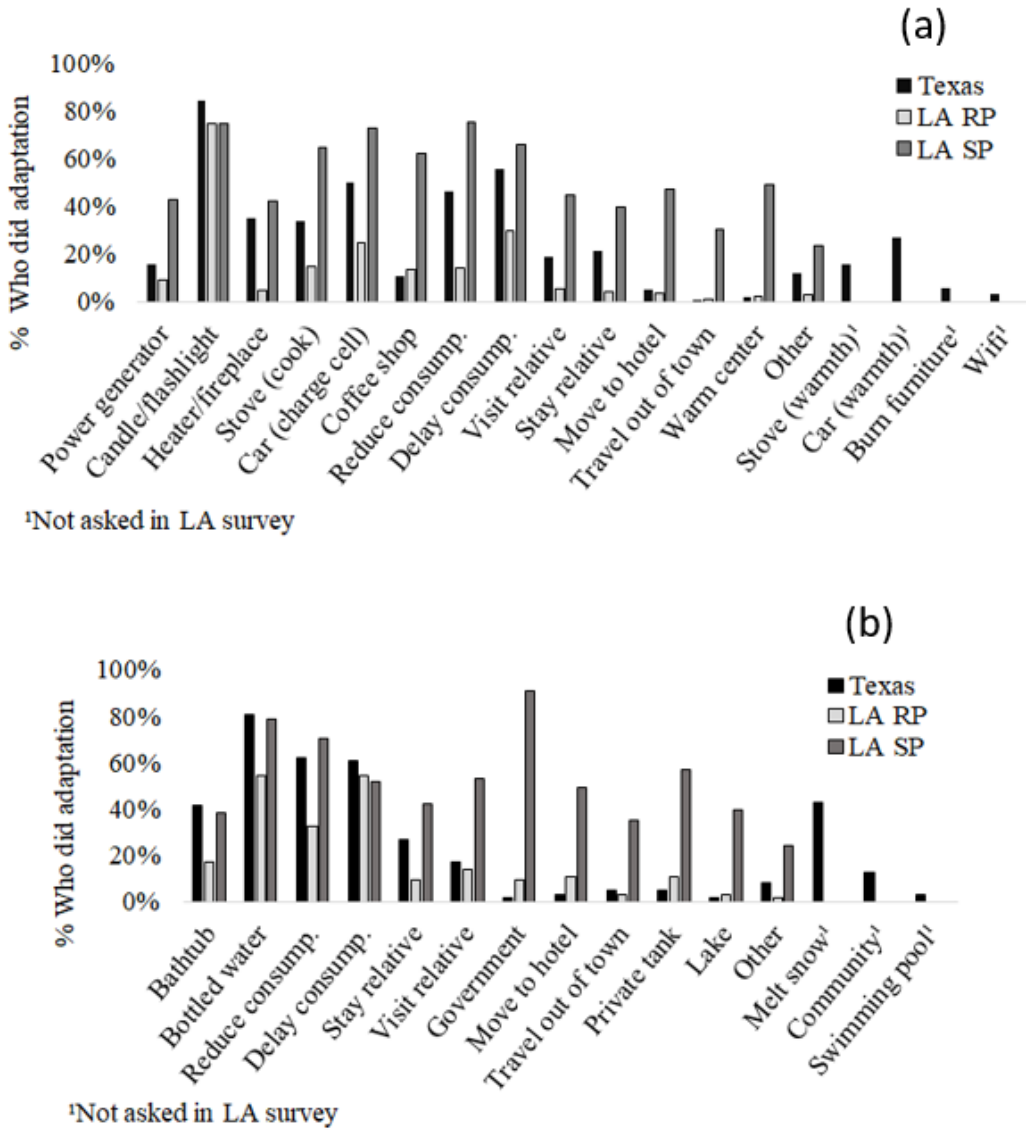

Figure 4.2. (a) Percentage of respondents who said they did/would do each electric power adaptation in Texas, Los Angeles (RP), and Los Angeles (SP) (b) Percentage of respondents who said they did/would do each water adaptation in Texas, Los Angeles (RP), and Los Angeles (SP)

4.5.2 Predictors of adaptation adoption

We used chi-square contingency tests and one-way Analysis of Variance (ANOVA) to identify possible relationships between adaptation decisions (binary variable) and each explanatory variable. While a logistic multiple regression on the adaptation decision would consider the effect of all explanatory variables together (as in Abbou et al. 2022), there was insufficient data to implement that here.

Outage attributes. Results suggest that the longer an electric power outage duration, the more likely someone is to implement the following adaptations: Candle/flashlight (y_{candle}), Heater/fireplace (y_{heater}), Car (charge cell) (y_{car}), Stay relative (y_{rel}), and Car (warmth) (y_{carw}) (Table 5). This agrees with the conclusion about Stay relative (y_{rel}) in the Los Angeles data. However, by contrast, the Los Angeles data suggested that Candle/flashlight (y_{candle}) and Car (charge cell) (y_{car}) are less common as outage duration increases.

Whether an interruption occurred once or more than once ($x_{e.num}$) was one of the variables most related to implementation of adaptations (Table 4.5a). Candle/flashlight (y_{candle}), Heater/fireplace (y_{heater}), Reduce consumption (y_{red}), and Delay consumption (y_{delay}) were all more likely for respondents who experienced more than one outage than those who experienced just one. Respondents who experienced more than one water outage were more likely to implement all adaptations except Used water provided by community or neighborhood-based organizations (y_{comm}). For the Visit relative adaptation (y_{visit}) the p-value is 0.04; for all others it was <0.001. The Los Angeles survey did not ask about multiple interruptions. The results for water supply adaptations are provided in Table (4.5b).

Types of service usage. Table 4.5 indicates evidence ($p<0.001$) that people who use electric power for work or business purposes ($x_{e.work}$) are more likely to adapt by reducing consumption (y_{red}) than those who do not. Examining the data more directly shows a 0.57 probability of reducing consumption for someone who uses power for work, versus a 0.27 probability for someone who does not. A similar relationship was seen in the Los Angeles data.

Table 4.5. (a) P-values of χ^2 tests for electric power adaptations vs. explanatory variables (at significance level=0.05, dark gray=direct effect, light gray=negative effect)

		Adaptive strategy											
	Variable	Power generator	Candle/ flashlight	Heater/ fireplace	Stove (cook)	Car (charge cell)	Coffe e shop	Reduce consump	Delay consump	Visit relative	Stay relative	Stove warmt h	Car warmth
Chi-square test results	Num. of interruption, $x_{e.numint}$	0.60	**0.01**	**0.05**	0.79	1.00	0.94	**0.01**	**0.01**	0.46	0.83	0.98	0.90
	Prior notice, x_{notice}	1.00	0.25	1.00	0.37	0.86	0.53	0.43	1.00	0.42	0.20	1.00	0.62
	Property damage, x_{damage}	1.00	0.80	1.00	0.62	0.08	0.10	0.53	1.00	0.36	0.22	0.81	**0.01**
	Med devices, $x_{e.dev}$	0.23	0.96	1.00	1.00	0.65	1.00	1.00	0.45	0.63	0.43	0.23	0.75
	Work, $x_{e.work}$	0.33	1.00	0.58	0.24	1.00	0.24	**<0.001**	0.05	0.04	0.39	1.00	0.27
	Energy source, $x_{e,source}$	0.89	1.00	**<0.001**	**<0.001**	0.86	1.00	0.85	0.88	0.36	0.11	<0.001	0.64
	Likely emergency, $x_{l.emer}$	0.67	0.32	0.01	1.00	0.81	0.21	0.94	1.00	0.30	0.10	1.00	0.34
	Worry, $x_{w.emer}$	0.41	0.41	0.13	0.02	0.46	0.03	0.86	0.61	0.32	0.05	0.73	0.05
	Negative impact, x_{n_emer}	0.16	0.22	0.30	0.61	0.59	0.40	0.84	0.90	0.21	0.03	1.00	0.99
	Gender, x_{gen}	0.94	0.38	0.80	0.78	0.39	1.00	1.00	0.69	0.95	1.00	0.92	0.98
	Race, x_{race}	0.20	0.29	0.23	0.74	0.17	0.62	0.45	0.51	0.72	0.87	1.00	0.22
	Education, x_{edu}	0.63	0.78	0.25	0.01	1.00	1.00	0.41	0.78	0.20	0.98	0.23	0.40
	Children, x_{child}	0.40	0.78	0.99	0.57	0.54	0.42	0.46	0.90	0.66	0.92	0.60	0.74
	Elders, x_{elder}	0.33	0.06	0.03	0.06	0.41	1.00	<0.001	0.05	0.12	0.78	0.91	0.25
	Pets, x_{pets}	0.93	0.24	0.04	0.69	0.83	0.99	0.11	**0.02**	0.62	0.55	0.71	0.81

Table 4.5. (a) Continued

	Med condition, $x_{med.c}$	0.74	1.00	1.00	0.23	0.88	0.65	0.88	0.70	0.12	0.44	0.93	0.08
	Med equip, $x_{med.e}$	0.71	1.00	0.96	1.00	0.16	0.63	0.87	1.00	0.55	1.00	1.00	0.09
	Ownership, x_{own}	0.02	0.41	<0.001	0.03	0.02	0.25	0.46	0.47	0.03	0.08	0.45	0.13
	House type, x_{house}	0.08	0.54	**0.04**	**0.02**	**0.01**	**0.03**	0.86	0.72	**<0.001**	**<0.001**	0.78	**<0.001**
	Employment, x_{employ}	1.00	0.64	0.36	0.89	0.42	0.91	1.00	1.00	0.25	0.40	0.86	0.32
	Marital, $x_{marital}$	**0.03**	0.29	**<0.001**	1.00	0.17	0.84	0.75	0.79	0.30	0.67	0.48	0.20
	Neighbor connection, $x_{neighbor}$	0.15	0.07	**0.04**	0.98	0.36	0.24	0.61	0.29	0.67	0.53	0.40	0.04
ANOVA test results	Outage duration, $x_{dur,e}$	0.15	**<0.001**	**0.03**	1.00	**<0.001**	0.26	0.13	0.39	0.31	**<0.001**	0.97	**0.02**
	Preparation, x_{prep}	**<0.001**	0.54	1.00	0.47	0.85	0.16	0.43	0.82	0.13	0.18	0.78	0.60
	Age, x_{age}	0.61	0.04	0.08	0.54	0.56	0.74	0.02	<0.001	0.09	0.01	0.07	0.15
	Income, x_{inc}	0.38	0.56	**<0.001**	0.38	0.72	0.25	0.13	0.77	0.99	0.79	0.61	0.60
	Years in house, $x_{yr,h}$	**<0.001**	0.01	0.70	0.95	0.25	0.99	0.06	0.18	0.07	0.07	0.28	0.10
	Years in county, $x_{yr,c}$	**0.02**	0.05	0.94	0.81	0.44	0.68	0.15	0.06	0.19	0.79	0.05	<0.001

Table 4.5. (b) P-values of χ^2 tests for water supply adaptations vs. explanatory variables (at significance level=0.05, dark gray=direct effect, light gray=negative effect)

		Adaptive strategy							
	Variable	Bathtub	Bottled water	Reduce consump.	Delay consump.	Stay relative	Visit relative	Melt snow	Community
Chi-square	Num. of interruption, $x_{w.numint}$	**<0.001**	**<0.001**	**<0.001**	**<0.001**	**<0.001**	**0.04**	**<0.001**	0.53
	Property damage, x_{damage}	0.14	**0.01**	0.23	0.44	0.07	0.14	0.06	0.38
	Med devices, $x_{w.dev}$	0.80	0.58	1.00	1.00	1.00	0.67	1.00	1.00
	Work, $x_{w.work}$	0.66	0.67	0.79	0.58	1.00	0.97	0.85	0.69
	Water source, $x_{w,source}$	0.14	0.90	0.28	0.15	0.09	1.00	0.28	1.00
	Likely emergency, $x_{l.emer}$	0.45	1.00	1.00	0.85	0.42	0.59	0.31	1.00
	Worry, $x_{w.emer}$	0.28	0.41	0.70	0.32	0.99	0.19	**0.04**	0.42
	Negative impact, x_{n_emer}	0.90	0.59	0.56	0.88	0.26	0.60	0.88	0.48
	Gender, x_{gen}	0.35	0.39	0.87	0.86	0.92	0.46	0.38	0.72
	Race, x_{race}	0.25	0.64	0.69	0.93	0.97	**0.03**	0.34	0.92
	Education, x_{edu}	0.36	0.06	0.76	0.43	0.22	0.83	0.51	0.41
	Children, x_{child}	**0.02**	0.66	1.00	0.75	0.55	1.00	0.44	0.60
	Elders, x_{elder}	1.00	0.09	0.30	1.00	0.51	0.89	0.89	1.00
	Pets, x_{pets}	1.00	1.00	1.00	1.00	1.00	0.58	0.73	0.61
	Med condition, $x_{med.c}$	0.94	0.36	0.83	0.74	1.00	0.65	0.37	1.00
	Med equip, $x_{med.e}$	0.10	**0.02**	0.05	**0.04**	0.09	0.27	1.00	0.14
	Ownership, x_{own}	0.06	0.41	1.00	0.34	0.92	0.01	0.03	1.00
	House type, x_{house}	0.01	**0.03**	0.36	0.42	0.94	**<0.001**	**0.01**	1.00
	Employment, x_{employ}	0.33	0.39	0.43	1.00	0.61	1.00	0.60	0.73
	Marital, $x_{marital}$	0.81	0.74	0.33	0.99	1.00	0.05	0.57	0.47

Table 4.5. (b) Continued

	Neighbor connection, $x_{neighbor}$	0.27	0.08	0.56	1.00	0.69	0.01	0.28	1.00
ANOVA	Outage duration, $x_{dur,w}$	0.92	0.10	0.64	0.39	0.50	0.67	0.71	0.67
	Preparation, x_{prep}	**0.01**	0.58	0.59	0.34	0.21	0.95	0.57	0.23
	Age, x_{age}	0.34	0.33	0.90	0.71	0.78	0.36	0.04	0.93
	Income, x_{inc}	0.92	0.30	0.97	0.60	0.63	0.06	0.55	0.84
	Years in house, $x_{yr,h}$	0.52	0.53	0.84	0.35	0.97	0.38	0.19	0.17
	Years in county, $x_{yr,c}$	0.78	0.13	0.10	0.22	0.03	0.30	0.13	0.11

There is also evidence that people who have more than one source of energy in their home ($x_{e.source}$) were more likely to use a non-electric heater and/or fireplace (y_{heater}) or gas stove and/or camping stove (y_{stove}) and less likely to use a gas stove for warmth (y_{stovew}). The first two relationships make sense, as one can only use gas-powered adaptations if one has gas service to the house. Since electric power is the main energy source, those with more than one energy source typically have something in addition to that, often gas. The Los Angeles data provided similar evidence for y_{stove} but not y_{heater}.

Past experiences and risk perception, socio-demographics, and social connectedness. Among the relationships for which the Texas data offers evidence, the most statistically significant ones ($p<0.001$) include the following. Household that include elders (x_{elder}) were less likely to reduce consumption (y_{red}). Those who live in a single-family home, duplex, or townhome (x_{house}) were less likely to visit a relative's or friend's house (y_{visit}) or stay at a relative or friend's house (y_{rel}) than others (e.g., group home, mobile home, apartment, condominium). Those who were more prepared (x_{prep}) and those who have been in their house longer ($x_{yr,h}$) were more likely to use a power generator (y_{gen}). Of these, the only conclusion that agrees with the Los Angeles analysis is that those who were more prepared (x_{prep}) were more likely to use a power generator (y_{gen}).

4.5.3 Adaptation groupings

Given the results in Figure 4.1, which indicate that many people implemented or intend to implement multiple adaptations for a single outage event, we ask *Research Question 3: Which household adaptations tend to occur together? Which*

tend not to? To begin to address this question, we use a symmetric association rule metric called *Lift* defined as (Hahsler et al. 2005):

$$lift(X \Rightarrow Y) = lift(Y \Rightarrow X) \; = \; P(X \cap Y)/P(X)P(Y) \qquad (4.1)$$

Lift measures how many times more often X and Y occur together than expected if they were statistically independent. In this application, X and Y are individual adaptations, and $lift(X \Rightarrow Y)$ is used to measure the extent to which individuals indicating they did (or intend to do) X were less or more likely to indicate they did (or intend to do) Y as well (and vice versa). Tables 4.6 and 4.7 present, for the Texas (bold) and Los Angeles datasets (not bold), the lift values for all combinations of electric power adaptations and water adaptations, respectively.

Table 4.6. Matrix of lift for all electric power adaptations (bold: Texas, not bold: Los Angeles)

	Candles /flashlight	Heater /fireplace	Stove /BBQ	Car (charge cell)	Coffee shop	Reduce consump	Delay Consump.	Visit relative	Stay relative	Stove (warmth)	Car (warmth)
Power generator	**0.88** 1.07	**1.14** 1.64	**1.47** 1.40	**0.60** 1.21	**0.48** 1.33	**1.08** 1.24	**1.07** 1.21	**0.53** 1.48	**0.70** 1.52	**0.64** ---	**0.19** ---
Candles /flashlight	—	**1.28** 1.13	**1.28** 1.14	**1.31** 1.11	**1.24** 1.09	**1.32** 1.10	**1.32** 1.11	**1.22** 1.05	**1.33** 1.00	**1.3** ---	**1.31** ---
Heater /fireplace		—	**1.57** 1.47	**1.28** 1.26	**1.49** 1.38	**1.54** 1.28	**1.39** 1.28	**1.64** 1.48	**1.14** 1.49	**0.85** ---	**1.33** ---
Stove /BBQ			—	**1.42** 1.28	**0.22** 1.30	**1.40** 1.27	**1.32** 1.25	**0.98** 1.31	**0.75** 1.26	**2.36** ---	**1.55** ---
Car (charge cell)				—	**2.09** 1.28	**1.25** 1.24	**1.97** 1.22	**1.57** 1.24	**1.74** 1.21	**1.59** ---	**2.39** ---
Coffee shop					—	**0.97** 1.28	**0.94** 1.24	**2.78** 1.43	**3.48** 1.39	**1.44** ---	**3.09** ---
Reduce consump.						—	**2.05** 1.33	**1.61** 1.36	**1.34** 2.11	**1.08** ---	**1.33** ---
Delay Consump.							—	**1.33** 1.23	**1.10** 1.19	**0.98** ---	**1.2** ---
Visit relative								—	**3.46** 1.96	**0.53** ---	**2.48** ---
Stay relative									—	**0.93** ---	**1.63** ---
Stove (warmth)										—	**1.87** ---

[a] Not included in Los Angeles data

Focusing on the Texas results (bold), Table 4.6 suggests a few points. First, four adaptations (charging cell phone, laptop, and/or tablet at work and/or in a coffee shop (y_{shop}); visiting a relative's or friend's house for their heat (y_{visit}); staying at a relative's or friend's house (y_{rel}); and using your car for warmth (y_{car})) tend to occur together, as indicated by those six pairs having an average lift value of 2.82 (1.63 to 3.48). This could suggest that people switched among multiple efforts to stay warm—going to a coffee shop, relative's or friend's house, and car. The non-bold values in Table 4.6 suggest similar conclusions based on the Los Angeles, although with smaller lift values. Second, a couple lift values suggest that people may use a single piece of equipment to support multiple uses. Charged cell phone in the car (y_{car}) and Used your car for warmth (y_{carw}), both of which make use of one's car, tend to occur together (lift=2.39). Similarly, using your gas stove for warmth (y_{stovew}) and using a gas stove and/or camping stove to cook meals and/or boil water (y_{stove}), both of which make use of a gas stove, tend to occur together (lift=2.36). Third, we note that reducing and delaying consumption are twice as likely to be done by the same household as you would expect if they were independent (lift = 2.05). Finally, several adaptations tend to be less common when one uses a generator (lift values of 0.48 to 0.70). These include visiting a relative's or friend's house for their heat (y_{visit}); staying at a relative's or friend's house (y_{rel}); charging cell phone, laptop, and/or tablet at work and/or in a coffee shop (y_{shop}); using a gas stove for warmth (y_{stovew}); using a car for warmth (y_{carw}); and charging cell phone in the car (y_{car}). This makes sense because a generator can support all power uses and thus other adaptations are less likely to be required. The non-bold values in Table 4.6 suggest a different conclusion based on the

Los Angeles data, i.e., the lift values between generator and the other adaptations are all greater than one.

The lift matrix for the adaptations to water supply interruptions (Table 4.7) offer less evidence that some adaptations tend to occur together and some do not. Across all adaptation pairs, all but one lift value is 0.90 to 1.77. Note that the results shown here do not include information about the timing of adaptations, and in particular, if a person who did two different adaptations did them concurrently or in sequence, and if latter, in what order. Better understanding the timing of multiple adaptations is an area for future research.

Table 4.7. Matrix of lift for all water adaptations (bold: Texas, not bold: Los Angeles)

	Bottled water	Reduce consump.	Delay consump.	Stay relative	Visit relative	Melt snow	Provided by community
Stored water	**0.97** 1.09	**1.30** 1.21	**1.37** 1.28	**0.95** 1.38	**0.97** 1.34	**1.05** ---	**1.10** ---
Bottled water	——	**0.94** 1.14	**1.01** 1.11	**0.97** 1.11	**1.24** 1.14	**1.04** ---	**1.02** ---
Reduce consump.		——	**1.43** 1.27	**0.98** 1.11	**1.07** 1.17	**1.05** ---	**0.88** ---
Delay consump.			——	**0.93** 1.11	**1.09** 1.10	**1.11** ---	**0.90** ---
Stay relative				——	**1.77** 1.62	**1.23** ---	**1.38** ---
Visit relative					——	**1.72** ---	**2.11** ---
Melt snow						——	**1.28** ---

[a] Not included in Los Angeles data

4.5.4 Unhappiness

The last three research questions relate to the impacts of service interruptions on households, specifically in terms of the unhappiness experienced as a result of them. *Research Question 4* asks "How unhappy are households when service is interrupted?" In the Texas survey data, when asked "Considering the actions you took to deal with the electricity [water] disruption that you experienced, as well as any remaining reduction in service, what level of unhappiness did you feel as a result of the outage?" (Q6 in Section 4.4.2.1), the most common response was the highest level of unhappiness, *Extremely unhappy*, for both electric power (43%) and water (44%) outages (Fig. 4.3). Only 6% and 7% of respondents were *Not unhappy* due to electric power and water supply interruptions, respectively. The distribution across unhappiness levels was quite similar for electric power and water. By comparison, respondents in the Los Angeles survey reported lower levels of unhappiness, in both revealed preference and stated preference questions.

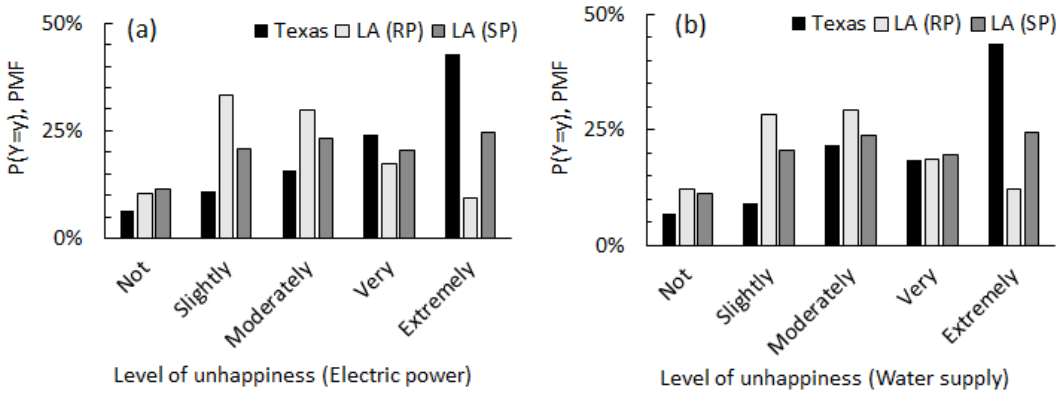

Figure 4.3. Empirical probability mass function for Unhappiness by dataset for (a) electric power and (b) water supply

The lower levels of unhappiness in the Los Angeles RP questions may be explained by the fact that the outage durations reported were shorter in general than those experienced by respondents in Texas. In Texas, the average outage durations for electric power and water were 62 and 101 hours, respectively, versus 19 and 25 hours for Los Angeles RP questions. Interestingly, however, even though the Los Angeles SP data had higher outage durations on average (240 and 240 hours for electric power and water), the unhappiness reported in those were also lower than the Texas data (although higher than the LA RP data). While this finding merits additional study, it could be that while an actual recent outage experience with its associated discomfort (Texas) elicits more emotion and thus reports of unhappiness than a hypothetical future outage (LA SP).

4.5.5 Predictors of household unhappiness related to service interruptions

We used regression, rather than chi-square tests, to examine the relationship between unhappiness and the possible explanatory variables since there was sufficient data. Nevertheless, the sample size is limited, so we restricted the set of explanatory variables to those considered of most interest and those that Stock (2020) found to have a relationship with unhappiness (listed in Table 4.8). The variable Did at least one travel-based adaptation (x_{adapt}) with choices {0=No, 1=Yes} was included to examine if/how implementing adaptations that require travel related to people's unhappiness. The Texas sample included 105 *No* values and 59 *Yes* values. The following adaptations were classified as requiring travel: Charged cell-phone, laptop, and/or tablet at work and/or in a coffee shop (y_{shop}), Used wi-fi somewhere other than home (y_{wifi}), Went to a warming center (y_{center}), Visited a relative's or friend's house

(y_{visit}), Stayed at a relative's or friend's house (y_{rel}), Moved to a hotel (y_{hotel}), and Traveled out of town (y_{town}).

Unhappiness, *z*, is measured on an ordinal scale, meaning the order of the levels is important but the difference between levels is not necessarily constant. In addition, for respondents who experienced both an electric power outage and a water supply outage, there are two observations, one associated with each infrastructure system type (i.e., choice occasion). Thus, we use an ordered logit model with random effects to represent the relationship between unhappiness and the explanatory variables. Specifically, the ordinal response Z_i, takes on a value of *k* when individual *i* falls into the k_{th} ordered category, where $k = 1,...,K$. The probability that individual *i* in category *k* is p_{ik}, and the cumulative probability is $P(Z_i \leq k) = \sum_{l=1}^{k} p_{il}$. The function that links the probability to the linear predictor is the logit link (Eq. 4.2) and the cumulative probability is as in Eq. 3:

$$log\left(\frac{P(Z_i \leq k)}{1-P(Z_i \leq k)}\right) = \alpha_k - \left(\vec{x}_i^T \vec{\beta} + \theta_i\right) \tag{4.2}$$

$$P(Z_i \leq k) = \frac{\exp\left(\alpha_k - \left(\vec{x}_i^T \vec{\beta} + \theta_i\right)\right)}{1+\exp\left(\alpha_k - \left(\vec{x}_i^T \vec{\beta} + \theta_i\right)\right)} \tag{4.3}$$

where the thresholds separating the *k* categories are $-\infty = \alpha_0 < \alpha_1 < \cdots < \alpha_{K-1} < \alpha_K = +\infty$; $\vec{x}_i$ is the covariate vector; $\vec{\beta}$ is the vector of regression parameters; and the unknown random subject effect $\vec{\theta}_i$ represents the influence of individual *i* on their repeated assessments. The models were fitted in R (R Core Team 2022) using the {mixor} package (Archer et al. 2015, Hedeker and Gibbons 1996).

Table 4.8 summarizes the unhappiness model fitted using the Texas data, as well as a similar model based on the Los Angeles data. Note that two variables were not included in the Los Angeles data—number of interruptions and prior notice.

However, we added travel-based adapt to LA survey data and ran the model to reveal its effect. The confusion matrix (Table 4.9) suggests that the model provides a reasonable fit to the data, predicting the unhappiness level correctly for 45% of respondents and within one level for 83% of respondents. The McFadden's R^2 values for the Texas and LA models are 0.145 and 0.207, respectively.

Table 4.8. Unhappiness model for Texas with corresponding values for LA

Explanatory variable	Texas		Los Angeles	
	Estimate (β)	p-value	Estimate (β)	p-value
Type, x_{type}	0.14	0.701	**-0.11**	**<0.001**
Num. interruption (> once), $x_{e.numint}$	**1.61**	**<0.001**		
Prior notice, x_{notice}	-0.34	0.497		
Work, $x_{e.work}$	-0.14	0.773	**0.44**	**0.003**
Worry, $x_{w.emer}$	**2.26**	**<0.001**	**0.69**	**<0.001**
Elders, x_{elder}	-0.62	0.188	**-0.28**	**0.013**
Med condition, $x_{med.c}$	**-1.13**	**0.042**	**0.42**	**<0.001**
Marital, $x_{marital}$	-0.37	0.442	**0.20**	**0.037**
Outage duration, x_{dur}	0.003	0.448	**0.35**	**<0.001**
Preparation, x_{prep}	-0.004	0.961	-0.02	0.088
Income ($1000), x_{inco}	0.002	0.655	**0.002**	**0.006**
Adapt (travel-based), x_{adapt}	**2.10**	**<0.001**	**0.092**	**0.024**
Threshold1	-2.28	0.017	-3.18	<0.001
Threshold2	-0.40	0.337	-0.98	0.051
Threshold3	1.56	0.052	1.02	0.021
Threshold4	3.43	<0.001	3.59	<0.001

Table 4.9. Confusion matrix for the Texas unhappiness model

Unhappiness level		Predicted				
		Not unhappy	Slightly unhappy	Moderately unhappy	Very unhappy	Extremely unhappy
Observed	Not unhappy	0	1	9	5	1
	Slightly unhappy	0	6	14	3	2
	Moderately unhappy	0	3	19	15	6
	Very unhappy	0	2	8	14	29
	Extremely unhappy	0	2	9	23	70

The Texas results suggest that respondents are more unhappy if they experience more than one outage (vs. one) (x_{num}), worry more about an emergency in the next five years ($x_{w.emer}$), did a travel-based adaptation (x_{adapt}), and/or do not include someone with a medical condition in the household ($x_{med.c}$). Of these, only the conclusion about worry agrees with the Los Angeles results. The finding that having someone with a medical condition in the household is associated with less unhappiness conflicts with the results of the Los Angeles model and intuition. The absence of evidence for some variables in the Texas model does not mean that they do not have an effect; only that the Texas data does not provide evidence of it. Nevertheless, it is somewhat surprising that in the Texas model, there is no evidence that outage duration is related to unhappiness. Intuitively, one might think that outage duration would be one of the most important variables. Even when number of interruptions (x_{num}) and prior notice (x_{notice}) are removed, outage duration is not statistically significant (p=0.13) in the Texas model.

4.5.6 Concerns influencing level of unhappiness

The final research question asks "What are the concerns that influence an individual's level of unhappiness associated with service interruptions?" Specifically, respondents were asked to identify the extent to which each of four concerns influenced their assessment of their level of unhappiness—financial, time/effort, health, and stress (Q7). In Texas, as in Los Angeles, for both electric power and water, all four concerns influence the level of unhappiness. In fact, Figure 4.4 shows the extent to which each of the four concerns plays a role are quite similar in Texas and Los Angeles. Considering both electric power and water, in Texas, 33%, 71%, 61%, 80% financial, time/effort, health, and stress concerns were considered to at least a moderate extent, respectively. In Los Angeles, the analogous values are 37%, 59%, 45%, and 63%. Notably, stress and time/effort were especially influential in Texas.

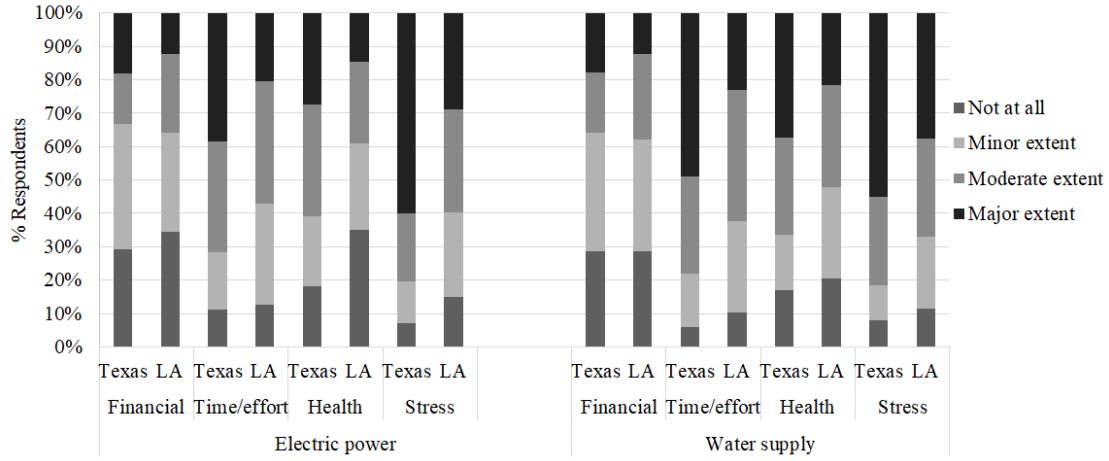

Figure 4.4. Extent to which concerns are considered in evaluating unhappiness

4.6 Conclusion and future work

This study adds to the nascent literature on household adaptations to and impacts from infrastructure system service outages. The analysis of the 2021 Texas winter storm provides additional evidence for a few findings previously reported in the Los Angeles study (Abbou et al. 2022, Stock 2020). First, both studies suggest that adaptations are quite common (RQ1). Almost everyone implements at least one; most implement several. Further, the most common adaptations tend to be relatively inexpensive (e.g., candles, flashlight, and/or lantern; charging the cell phone in the car; bottled water; and delaying or reducing consumption); the least common involve travel (e.g., going to a hotel or friend's or relative's house).

Second, both studies indicate that households experience varied levels of unhappiness, and they tend to be similar for electric power and water supply interruptions (RQ4). The reported levels of unhappiness were notably higher in the Texas data than the Los Angeles data, however, which could be due to a combination of outage durations (which were shorter for the RP Los Angeles data) and actual recent experience versus expected experience (from the SP Los Angeles data). Third, financial, time/effort, health, and stress concerns all have a substantial influence on the extent of unhappiness, and the Texas and Los Angeles analyses suggest they do to similar degrees (RQ6). This suggests that it is critical to consider these harder-to-measure concerns in addition to financial effects of service interruptions.

The results related to the predictors of adaptation implementation and unhappiness, and adaptation groupings (RQ2, RQ3, and RQ5), were more mixed. In general, with a smaller sample, the Texas data provides less evidence of relationships between specified explanatory variables and either adaptations or unhappiness. In some cases, it offers evidence that supports the Los Angeles study (e.g., longer outage

duration is associated with increased likelihood of staying with a relative or friend). In a few cases, it offers contradictory evidence (e.g., having someone in the household with a medical condition is associated with increased unhappiness in Los Angeles, but decreased unhappiness in Texas). The Texas study also introduced the new finding that the number of interruptions can be important in determining both adaptation implementation and unhappiness.

This research includes limitations and opportunities for future extension and improvement. Most importantly, the sample of data from the Texas event is relatively small and more White, female, and educated that the population from which it came. Collecting more data from additional events in different locations would be extremely helpful in further clarifying household experiences in service outages. In general, the survey instrument used in the two deployments discussed here proved to be valuable in addressing the research questions posed and using consistent questions for multiple events facilitates an understanding of generalizability of findings. Nevertheless, this study does suggest a couple modifications to the survey instrument. First, some of the adaptation definitions might be refined so that they do not overlap (i.e., each action is represented by exactly one adaptation, unlike travel out of town and move to hotel, for example); together they represent a relatively complete set of adaptations implemented in most electric power and water supply outages; and they are defined based on use (e.g., warmth, cooking, charging) and/or method (e.g., using car, stove, going to coffee shop) in a consistent way. Second, given the importance of stress and time/effort in determining unhappiness, future work should explore what causes those concerns and how they manifest.

Chapter 5

CONCLUSION AND FUTURE WORK

5.1 Conclusion

This dissertation offers three main contributions: (1) development of a method to generate a set of probabilistic multihazard earthquake scenarios for analysis of spatially distributed infrastructure; (2) development of a computationally efficient set of damage scenarios for the Los Angeles water transmission network; and (3) improvement of understanding of household adaptation to and impact of service interruptions. Each is summarized in turn.

5.1.1 Develop probabilistic multihazard scenarios

In this research, we introduced the multihazard optimization-based probabilistic scenario (multihazard OPS) method to develop an ensemble of multihazard scenarios for the efficient risk assessment of spatially distributed infrastructures, a primary input for subsequent damage and loss analysis. A multihazard scenario from this model depicts a possible realization of the co-occurring multiple hazard effects associated with a single earthquake, including information about ground motion intensity, liquefaction potential, and locations of surface fault rupture. The analysis indicates how one can compute probabilistic hazard in a way that captures spatial correlation, includes multiple hazards, and is computationally efficient.

The method was demonstrated with a case study for Los Angeles city, California. While more scenarios are necessary for the multihazard analysis to obtain a match that is similar to that for analysis of ground motion alone, the application to Los Angeles shows that errors small enough for practical purposes may still be achieved with only a few hundred multihazard scenarios. Importantly, the sensitivity analysis reveals that developing a multihazard scenario ensemble by matching one hazard type does not always result in a satisfactory match for others.

5.1.2 Develop probabilistic damage scenarios

We described the development of a computationally efficient set of probabilistic damage scenarios for the Los Angeles water transmission system. A damage scenario from this model represents damage to the network components and includes the corresponding multihazard scenario and an associated adjusted annual occurrence probability. Since these scenarios are based on the introduced multihazard scenarios, they consider effects of ground motion, liquefaction, and surface fault rupture. The application to the Los Angeles water transmission system depicts how a set of probabilistic earthquake damage scenarios can support the design and analysis of spatially distributed infrastructure systems to achieve a specific system performance. That is, damage scenarios can assist in making informed component replacement decisions because they indicate the damage state of each network component in its current condition and if it were replaced with a component with a different resistance level.

5.1.3 Improve understanding of household impact from and adaptation adoption to infrastructure system service outages

This research contributes to the empirical literature on household adaptations to and impacts from infrastructure system interruptions. We used survey-based data to describe the actual behavior (revealed preferences) during the February 2021 winter storm centered in Texas. By using a survey instrument almost identical to that used in a recent previous study in Los Angeles (Abbou et al. 2022, Stock 2020), and addressing the same set of research questions, we were able to explore the generalizability of the findings from the two studies. The statistical models from this study identify which findings are similar, and which are not. There are a lot of interesting findings based on the comparison between the two studies: (a) both suggest similar common and least common adaptations; (b) the household impact (unhappiness level) in Texas was greater than in Los Angeles, which may be due to longer outage durations and the fact that it was a recent actual (as opposed to hypothetical) experience; (c) in both studies, stress and time/effort had a notable influence on the extent of the household impact (unhappiness level); (d) there are mixed findings from the predictors of adaptation implementation and unhappiness, and adaptation groupings. The Texas study also suggested a novel finding, i.e., that the number of service interruptions (service going on and off repeatedly vs. just once) increases both adaption implementation and unhappiness. The findings of this research can support infrastructure system operators and emergency managers to better understand the degree of societal impact and adaptation adoption due to service interruptions, how they vary across infrastructure systems and community members, and how they depend on outage duration.

5.2 Future work

The development of multihazard optimization-based probabilistic scenarios and damage scenarios described frameworks to make a computationally efficient risk assessment of infrastructure systems. Implementation of these models represents an advance toward more efficiently and realistically capturing the spatial correlation in infrastructure systems. Nevertheless, opportunities exist to extend and overcome some limitations. The component hazard models could be improved and extended for other co-occuring hazards, such as landslides. Further, the solution algorithm for the optimization models could be modified in a way to overcome running time issues due to the increase in the number of scenarios and try to focus on global solution-based algorithms rather than local ones. One also could think of extending the damage scenario optimization model to manage all damage scenarios simultaneously rather than doing the analysis separately for each. Another interesting possible work could be training machine learning models to achieve the adjusted occurrence rate of scenarios to match the true behavior in hazard or damage curve instead of implementing optimization techniques.

The analysis of the Texas winter storm offered improved understanding of household adaptation to and household impact from service outages. Nevertheless, the predictive models from this framework can surely be improved through further data collection in multiple locations and for multiple events. The definitions of the particular adaptations could be refined, for example, to avoid cases in which two adaptations overlap (e.g., go to a hotel, go out of town). One could also ask respondents to indicate their priority of taking each adaptation (order of preference). Investigation of additional explanatory variables (e.g., concerns about employment, losing their current job, shortage in groceries and other essentials) could add more

insight to the research. Further, integrating stated preference data along with the revealed preference data and extend it to other perils could present a holistic framework to estimate the degree of the household impact and adaptation adoption pattern due to outages.

REFERENCES

Abbou, A., Davidson, R., Kendra, J., Martins, V., Ewing, B., Nozick, L., Cox, Z., and Leon-Corwin, M. (2022). "Household adaptations to infrastructure system service interruptions." ASCE Journal of Infrastructure System. Accepted.

Anbazhagan, P., Uday, A., Moustafa, S. S. R., and Al-Arifi, N. S. N. (2016). "Correlation of densities with shear wave velocities and SPT N values." Journal of Geophysics and Engineering, 13(3), 320–341.

Andrus, R. D., and Stokoe, K. H. (2000). "Liquefaction resistance of soils from shear-wave velocity." Journal of Geotechnical and Geoenvironmental Engineering, 126(11), 1015–1025.

Apivatanagul, P., Davidson, R., Blanton, B., and Nozick, L. (2011). "Long-term regional hurricane hazard analysis for wind and storm surge." Coastal Engineering, 58(6), 499–509.

Applied Technology Council (ATC). (2016). Critical Assessment of Lifeline System Performance: Understanding Societal Needs in Disaster Recovery. Prepared for U.S. Department of Commerce, National Institute of Standards and Technology. Redwood City, CA.

Archer, K., Hedeker, D., Nordgren, R., and Gibbons, R. (2015). mixor: an R package for longitudinal and clustered ordinal response modeling.

Bagriacik, A., Davidson, R. A., Hughes, M. W., Bradley, B. A., and Cubrinovski, M. (2018). "Comparison of statistical and machine learning approaches

to modeling earthquake damage to water pipelines." Soil Dynamics and Earthquake Engineering, Elsevier Ltd, 112, 76–88.

Baska, D. (2003). "An analytical/empirical model for prediction of lateral spread displacements." University of Washington, Seatle.

Boore, D. M. (2004). Estimating V ¢ s (30) (or NEHRP Site Classes) from Shallow Velocity Models (Depths 30 m). Bulletin of the Seismological Society of America.

Brown, N. J., Gearhart, J. L., Jones, D. A., Nozick, L. K., Romero, N., and Xu, N. (2011). "Optimizing the Selection Of Scenarios for Loss Estimation In Transportation Networks (No. SAND2011-2150C)." Sandia National Lab.(SNL-NM), Sandia National Lab.(SNL-NM), Albuquerque, NM (United States).

Brown, N. J., Gearhart, J. L., Jones, D. A., Nozick, L. K., Romero, N., and Xu, N. (2013). "Multi-objective optimization for bridge retrofit to address earthquake hazards." Winter Simulations Conference (WSC), IEEE, 2475–2486.

California Department of Water Resources. (2019). "Water Data Library - Groundwater Level Data." <http://wdl.water.ca.gov/waterdatalibrary/groundwater/> (Accessed Jun. 1, 2019).

Chang, S. E., Shinozuka, M., and Moore, J. E. (2000). "Probabilistic Earthquake Scenarios: Extending Risk Analysis Methodologies to Spatially Distributed Systems." Earthquake Spectra, Earthquake Engineering Research Institute, 16(3), 557–572.

Chen, R., Jaiswal, K. S., Bausch, D., Seligson, H., and Wills, C. J. (2016). "Annualized Earthquake Loss Estimates for California and Their Sensitivity to Site Amplification." Seismological Research Letters, 87(6), 1363–1372.

Christou, V., Bocchini, P., Iranda, M. J., and Karamlou, A. (2018). "Effective Sampling of Spatially Correlated Intensity Maps Using Hazard Quantization: Application to Seismic Events." ASCE-ASME Journal of Risk and Uncertainty in Engineering Systems, Part A: Civil Engineering, American Society of Civil Engineers (ASCE), 4(1).

Clarke, J., and Obrien, E. (2016). "A Multihazard Risk Assessment Methodology, Stress Test Framework and Decision Support Tool for Transport Infrastructure Networks." Transportation Research Procedia, Elsevier B.V., 1355–1363.

Clay, L., Goetschius, J., Papas, M., J, T., Martins, N., and Kendra, J. (2020). "Does preparedness matter? The influence of household preparedness on disaster outcomes during superstorm sandy." Disaster Medicine and Public Health Preparedness, 14(1), 71–79. https://doi.org/10.1017/dmp.2019.78.

Coleman, N., Esmalian, A., and Mostafavi, A. (2020). "Equitable resilience in infrastructure systems: Empirical assessment of disparities in hardship experiences of vulnerable populations during service disruptions." Natural Hazards Review, 21(4), 040. https://doi.org/10.1017/dmp.2019.78

Crowley, H., and Bommer, and J. J. (2006). "Modelling seismic hazard in earthquake loss models with spatially distributed exposure." Bull. Earthquake Eng., 4: 249–273.

Dargin, J., and A. Mostafavi. (2020). "Human-centric infrastructure resilience: Uncovering well-being risk disparity due to infrastructure disruptions in disasters." PloS ONE, 15(6):e0234381. https://doi.org/10.1371/journal.pone.0234381

Davis, C. A. (2019a). Performance based seismic design for LADWP water system Report No. AX-747.

Davis, C. A. (2019b). “A Proposed Performance Based Seismic Design Process for Lifeline Systems,” in Earthquake Geotechnical Engineering for Protection and Development of Environment and Constructions.” Proc. 7th International Conference on Earthquake Geotechnical Engineering, (ICEGE 2019), CRC Press Balkema, 1986–1993.

De Risi, R., De Luca, F., Kwon, O. S., and Sextos, A. (2018). “Scenario-based seismic risk assessment for buried transmission gas pipelines at regional scale.” Journal of Pipeline Systems Engineering and Practice, American Society of Civil Engineers (ASCE), 9(4). https://doi.org/10.1061/(ASCE)PS.1949-1204.0000330

DeYoung, S., Sutton, J., Farmer, A., Neal, D., and Nichols, K. (2019). “‘Death was not in the agenda for the day’: Emotions, behavioral reactions, and perceptions in response to the 2018 Hawaii wireless emergency alert.” International Journal of Disaster Risk Reduction, 36, 101078. https://doi.org/10.1016/j.ijdrr.2019.101078

Ercumen, A., Arnold, B. F., Kumpel, E., Burt, Z., Ray, I., Nelson, K., and Jr, J. M. C. (2015). “Upgrading a Piped Water Supply from Intermittent to Continuous Delivery and Association with Waterborne Illness : A Matched Cohort Study in Urban India.” PLoS medicine, 12(10), e1001892. https://doi.org/10.1371/journal.pmed.1001892

Esmalian, A., Ramaswamy, M. Rasoulkhani, K., and Mostafavi, A. (2019). “Agent-based modeling framework for simulation of societal impacts of infrastructure service disruptions during disasters.” Computing in civil engineering 2019: Smart

cities, sustainability, and resilience, American Society of Civil Engineers (ASCE), Reston, VA, 16–23. https://doi.org/10.1061/9780784482445.003

Farmer, A., and DeYoung, S. (2019). “The pets of hurricane Matthew: Evacuation and sheltering with companion animals.” Anthrozoös, 32(3), 419. https://doi.org/10.1080/08927936.2019.1598661

Federal Emergency Management Agency (FEMA). (2013). “‘Build A Kit.’” <http://www.ready.gov/build-a-kit> (Accessed Jul. 28, 2021).

Field, E. H., Arrowsmith, R. J., Biasi, G. P., Bird, P., Dawson, T. E., Felzer, K. R., Jackson, D. D., Johnson, K. M., Jordan, T. H., Madden, C., Michael, A. J., Milner, K. R., Page, M. T., Parsons, T., Powers, P. M., Shaw, B. E., Thatcher, W. R., Weldon, R. J., and Zeng, Y. (2014). “Uniform California Earthquake Rupture Forecast, version 3 (UCERF3) -The time-independent model.” Bulletin of the Seismological Society of America, Seismological Society of America, 104(3), 1122–1180.

Gearhart, J., Brown, N., Jones, D., Nozick, L., Romero, N., and Xu, N. (2014). “Optimization based probabilistic consequence scenario construction for lifeline systems.” Earthquake Spectra, Earthquake Engineering Research Institute, 30(4), 1531–1551.

Gearhart, J. L., Brown, N. J., Jones, D. A., Nozick, L. K., Romero, N., and Xu, N. (2011). Optimization of Scenario Construction for Loss Estimation in Lifeline Networks (No. SAND2011-9200C). Sandia National Lab. (SNL-NM), Albuquerque, NM (United States).

Greiving, S. (2006). Natural and Technological Hazards and Risks Affecting the Spatial Development of European Regions. Geological Survey of Finland, Special Paper.

Hahsler, M., Grün, B., and Hornik., K. (2005). “arules – A computational environment for mining association rules and frequent item sets.” J. Stat. Softw, 14(15).

Han, Y., and Davidson, R. A. (2012). “Probabilistic seismic hazard analysis for spatially distributed infrastructure.” Earthquake Engineering and Structural Dynamics, John Wiley and Sons Ltd, 41(15), 2141–2158.

Harrell, F. (2015). Regression modeling strategies: with applications to linear models, logistic and ordinal regression, and survival analysis. (Springer, ed.), Heidelberg.

Hedeker, D., and Gibbons, R. (1996). “MIXOR: A computer program for mixed-effects ordinal regression analysis.” Computer Methods and Programs in Biomedicine, 49, 157–176.

Heidenstrom, N., and Kvarnlöf, L. (2017). “Coping with blackouts: A practice theory approach to household peparedness.” Journal of contingencies and crisis management, 00, 1–11. https://doi.org/10.1111/1468-5973.12191

Heidenstrøm, N., and Throne-Holst, H. (2020). “Someone will take care of it”. Households’ understanding of their responsibility to prepare for and cope with electricity and ICT infrastructure breakdowns.” Energy Policy, 144, 111676. https://doi.org/10.1016/j.enpol.2020.111676

Iwasaki, T., Arakawa, T., and Tokida, K. I. (1984). “Simplified procedures for assessing soil liquefaction during earthquakes.” International Journal of Soil Dynamics and Earthquake Engineering, 3(1), 49–58.

Jayaram, N., and Baker, J. W. (2010). “Efficient sampling and data reduction techniques for probabilistic seismic lifeline risk assessment.” Earthquake Engineering and Structural Dynamics, John Wiley and Sons Ltd, 39(10), 1109–1131.

Jeandron, A., Saidi, J. M., Kapama, A., Burhole, M., Birembano, F., Vandevelde, T., and … Ensink, J. H. J. (2015). “Water Supply Interruptions and Suspected Cholera Incidence: A Time-Series Regression in the Democratic Republic of the Congo.” PLoS Medicine, 12(10), e1001893. https://doi.org/10.1371/journal.pmed.1001893

Juang, C. H., Yang, S. H., and Yuan, H. (2005). “Model uncertainty of shear wave velocity-based method for liquefaction potential evaluation.” Journal of Geotechnical and Geoenvironmental Engineering, 131(10), 1274–1282.

Kappes, M. S., Keiler, M., von Elverfeldt, K., and Glade, T. (2012). “Challenges of analyzing multihazard risk: A review.” Natural Hazards.

Kayen, R., Moss, R. E. S., Thompson, E. M., Seed, R. B., Cetin, K. O., Der Kiureghian, A., Tanaka, Y., and Tokimatsu, K. (2013). “Shear-Wave velocity-based probabilistic and deterministic assessment of seismic soil liquefaction potential.” Journal of Geotechnical and Geoenvironmental Engineering, American Society of Civil Engineers (ASCE), 139(3), 407–419.

Klinger, C., Landeg, O., and Murray, V. (2014). “Power outages, extreme events and health: a systematic review of the literature from 2011-2012.” PLoS Curr., 6: ecurren. https://doi.org/10.1371/currents.dis.04eb1dc5e73dd1377e05a10e9edde673

Kongar, I., Rossetto, T., and Giovinazzi, S. (2017). “Evaluating simplified methods for liquefaction assessment for loss estimation.” Natural Hazards and Earth System Sciences, Copernicus GmbH, 17(5), 781–800.

LADWP (Los Angeles Department of Water and Power). (2017). 2016-17 WATER INFRASTRUCTURE PLAN Distribution Mainline. Los Angeles.

Lanzano, G., Salzano, E., Magistris, F. S. de, and Fabbrocino, G. (2014). "Seismic vulnerability of gas and liquid buried pipelines." J. Loss Prev. Process Ind, 28 (Apr):

Legg, M. R., Nozick, L. K., and Davidson, R. A. (2010). "Optimizing the selection of hazard-consistent probabilistic scenarios for long-term regional hurricane loss estimation." Structural Safety, 32(1), 90–100.

Manzour, H., Davidson, R. A., Horspool, N., and Nozick, L. K. (2016). "Seismic Hazard and Loss Analysis for Spatially Distributed Infrastructure in Christchurch, New Zealand." Earthquake Spectra, Earthquake Engineering Research Institute, 32(2), 697–712.

Martins, V., Louis-Charles, H., Nigg, J., Kendra, J., and Sisco, S. (2018). "Household disaster preparedness in New York City before Superstorm Sandy: findings and recommendations." Journal of Homeland Security and Emergency Management, 15(4): 201. https://doi.org/10.1515/jhsem-2017-0002

Maurer, B. W., Green, R. A., Cubrinovski, M., and Bradley, B. A. (2014). "Evaluation of the liquefaction potential index for assessing liquefaction hazard in christchurch, New Zealand." Journal of Geotechnical and Geoenvironmental Engineering, American Society of Civil Engineers (ASCE), 140(7), 04014032.

Mayfield, R. T., Kramer, S. L., and Huang, Y. M. (2010). "Simplified approximation procedure for performance-based evaluation of liquefaction potential." Journal of Geotechnical and Geoenvironmental Engineering, 136(1), 140–150.

Miles, A. (2015). “Obtaining predictions from models fit to multiply imputed data.” Sociol Methods Res, 45(1).

Miller, M., and Baker, J. (2015). “Ground-motion intensity and damage map selection for probabilistic infrastructure network risk assessment using optimization.” Earthquake Engineering and Structural Dynamics, John Wiley and Sons Ltd, 44(7), 1139–1156.

Mongold, E., Davidson, R., Trivedi, J., DeYoung, S., Wachtendorf, T., and Anyidoho, P. (2020). “Hurricane evacuation beliefs and behaviour of inland vs. coastal populations.” Environmental Hazards, 20:4, 363–381. https://doi.org/10.1080/17477891.2020.1829531

Moreno, J., and Shaw, D. (2019). “Community resilience to power outages after disaster: A case study of Chile earthquake and tsunami.” Int. J. Disaster Risk Reduct, 34, 448–45. https://doi.org/10.1016/j.ijdrr.2018.12.016

NEHRP Consultants Joint Venture. (2014). Earthquake-Resilient Lifelines: NEHRP Research, Development and Implementation Roadmap. Redwood City, CA.

NIBS and FEMA. (2003). Multihazard Loss Estimation Methodology, Earthquake Model, HAZUS MH Technical Manual, Federal Emergency Management Agency. Washington D.C.

O’Rourke, T. D., M, Jeon, S.-S., Toprak, S., Cubrinovski, M., Hughes, M., Sjoerd Van Ballegooy,), and Bouziou, D. (2014). “Earthquake Response of Underground Pipeline Networks in Christchurch, NZ.” journals.sagepub.com, Earthquake Engineering Research Institute, 30(1), 183–204.

O'Rourke, T., Jeon, S., Toprak, S., Cubrinovski, M., Hughes, M., van Ballegooy, S., and Bouziou, D. (2014). "Earthquake Response of Underground Pipeline Networks in Christchurch, NZ." Earthquake Spectra, 30(1), 183–204.

Omidvar, B., and Kivi, H. K. (2016). "Multihazard failure probability analysis of gas pipelines for earthquake shaking, ground failure and fire following earthquake." Natural Hazards, Springer Netherlands, 82(1), 703–720.

Osberghaus, D., and Abeling, T. (2022). "Heat vulnerability and adaptation of low-income households in Germany." Global Environmental Change, 72(0959–3780), 102446. https://doi.org/10.1016/j.gloenvcha.2021.102446

Petersen, M. D., Dawson, T. E., Chen, R., Cao, T., Wills, C. J., Schwartz, D. P., and Frankel, A. D. (2011). "Fault displacement hazard for strike-slip faults." Bulletin of the Seismological Society of America, 101(2), 805–825.

Petersen, M. D., Dawson, T. E., Chen, R., Cao, T., Wills, C. J., Schwartz, D. P., and Frankel, A. D. (2014). "Fault Displacement Hazard for Strike-Slip Faults." Bull. Seismol. Soc. Am., 101 (2): 8(March 2011).

Powers, P. (2015). "GitHub - usgs/nshm-cous-2014: NSHM: Conterminous U.S. 2014." <https://github.com/usgs/nshm-cous-2014> (Jun. 1, 2018).

Salman, A. M., and Li, Y. (2018). "A probabilistic framework for multihazard risk mitigation for electric power transmission systems subjected to seismic and hurricane hazards." Structure and Infrastructure Engineering, Taylor and Francis Ltd., 14(11), 1499–1519.

Sattar, S., Ryan, K., Arendt, L., Bonowitz, D., Comerio, M., Davis, C., Deierlein, G., and Johnson, K. (2021). Recommended Options for Improving the Built Environment for Post-Earthquake Reoccupancy and Functional Recovery Time.

Special Publication (NIST SP), National Institute of Standards and Technology, Gaithersburg, MD.

SCG (Southern California Gas Company). (2003). Liquefaction susceptibility maps.

Seed, H. B., and Idriss, I. M. (1971). “Simplified procedure for evaluating soil liquefaction potential.” ASCE J Soil Mech Found Div, 97(SM9), 1249–1273.

Stewart, J., Seed, R., and Bray, J. (1996). “Incidents of ground failure from the 1994 Northridge.” Bulletin of the Seismological Society of America, 86 (1B), S300–S318.

Stock, A. (2020). “Understanding engagement as a prerequisite to the protective action decision-making process: an application of life course theory.” Master Thesis, Department of Civil and Environmental Engineering, Univeristy of Delaware.

Tabandeh, A., Gardoni, P., and Murphy, C. (2018). “A reliability- based capability approach.” Risk Analysis, 38(2):, 410–424. https://doi.org/10.1111/risa.12843

Tabandeh, A., Gardoni, P., Murphy, C., and Myers, N. (2019). “Societal risk and resilience analysis: Dynamic Bayesian network formulation of a capability approach.” ASCE-ASME Journal of Risk and Uncertainty in Engineering Systems, Part A: Civil Engineering, 5(1), 04018046. https://doi.org/10.1061/AJRUA6.0000996

Texas Department of State Health Services (DSHS). (2021). February 2021 Winter Storm-Related Deaths – Texas.

Toprak, S., Nacaroglu, E., Koc, A., Van Ballegooy, S., Jacka, M., Torvelainen, E., and O'Rourke, T. (2017). "Pipeline damage predictions in liquefaction zones using LSN." 16th World Conference on Earthquake Engineering, Santiago, Chile.

US Census Bureau. (2019). "ACS demographic and housing estimates. American Community Survey."<https://data.census.gov/cedsci/table?q=UnitedStates&table=DP05&tid=ACSDP1Y2017.DP05&g=0100000US&lastDisplayedRow=29&vintage=2017&layer=state&cid=DP05_0001E> (Accessed Nov. 1, 2019).

van Buuren, S. (2012). Flexible imputation of missing data. Interdisciplinary statistics series. Chapman and Hall, Boca Raton.

van Buuren, S., and Groothuis-Oudshoorn, K. (2011). "mice: multivariate imputation by chained equations in R." J Stat Softw, 45(3), 1–67.

Vaziri, P., Davidson, R., Apivatanagul, P., and Nozick, L. (2012). "Identification of optimization-based probabilistic earthquake scenarios for regional loss estimation." Journal of Earthquake Engineering, 16(2), 296–315.

Watson, K. P., Buttorff, G., Cross, R., Granato, J., Jones, M. P., Pinto, P. M., Sipole, S., and Vallejo, A. (2021). The Winter Storm of 2021.

White, I., Royston, P., and Wood, A. (2011). "Multiple imputation using chained equations: issues and guidance for practice." Stat Med, 30(4), 377–399.

Wills, C., and Clahan., K. (2006). "Developing a map of geologically defined site-condition categories for California." Bull. Seismol. Soc. Am., 96 (4): 1483-1501.

Wolf, J., Adger, W. N., Lorenzoni, I., Abrahamson, V., and Raine, R. (2010). "Social capital, individual responses to heat waves and climate change adaptation: An

empirical study of two UK cities." Global Environ. Change, 20, 44–52. https://doi.org/10.1016/j.gloenvcha.2009.09.004

Yang, Y., Tatano, H., Huang, Q., Liu, H., Yoshizawa, G., and Wang, K. (2021). "Evaluating the societal impact of disaster-driven infrastructure disruptions: A water analysis perspective." International Journal of Disaster Risk Reduction, 52:101988. https://doi.org/10.1016/j.ijdrr.2020.101988

Youd, T. L., Hansen, C. M., and Bartlett, S. F. (2002). "Revised multilinear regression equations for prediction of lateral spread displacement." Journal of Geotechnical and Geoenvironmental Engineering, 128(12), 1007–1017.

Zhang, F. (2019). In the Dark : How Much Do Power Sector Distortions Cost South Asia? World Bank, Washington, DC. https://openknowledge.worldbank.org/handle/10986/30923

Zhu, J., Baise, L. G., and Thompson, E. M. (2017). "An updated geospatial liquefaction model for global application." Bulletin of the Seismological Society of America, 107(3), 1365–1385.

Zolfaghari, M. R., and Peyghaleh, E. (2016). "Development of optimization-based probabilistic earthquake scenarios for the city of Tehran." Computers and Geosciences, 86, 129–145.

Appendix A

CITI CERTIFICATES

Completion Date 04-Jul-2022
Expiration Date 03-Jul-2026
Record ID 49950940

This is to certify that:

Nafiseh Soleimani

Has completed the following CITI Program course:

Not valid for renewal of certification through CME.

Responsible Conduct of Research
(Curriculum Group)
Responsible Conduct of Research (RCR)
(Course Learner Group)
1 - RCR
(Stage)

Under requirements set by:

University of Delaware

CITI
Collaborative Institutional Training Initiative

Verify at www.citiprogram.org/verify/?w09cb09ce-61b1-44d3-a8c5-806b2f82eac3-49950940

CITI PROGRAM

Completion Date 08-Jul-2021
Expiration Date 07-Jul-2024
Record ID 38454341

This is to certify that:

Nafiseh Soleimani

Has completed the following CITI Program course:

Not valid for renewal of certification through CME.

Course In The Protection Human Subjects
(Curriculum Group)
Human Subjects Protections - Social-Behavioral-Educational Focus - All UD Researchers/Faculty/Staff
(Course Learner Group)
1 - Basic Course
(Stage)

Under requirements set by:

University of Delaware

CITI
Collaborative Institutional Training Initiative

Verify at www.citiprogram.org/verify/?wed703c5e-2bbb-4e2e-8dd0-638788aef153-38454341

Appendix B

IRB LETTER

Institutional Review Board
210H Hullihen Hall
Newark, DE 19716
Phone: 302-831-2137
Fax: 302-831-2828

DATE:	July 27, 2021
TO:	James Kendra, PhD
FROM:	University of Delaware IRB
STUDY TITLE:	[1420175-4] Collaborative Research: CRISP Type 2: Defining and Optimizing Societal Objectives for the Earthquake Risk Management of Critical Infrastructure
SUBMISSION TYPE:	Amendment/Modification
ACTION:	DETERMINATION OF EXEMPT STATUS
EFFECTIVE DATE:	July 27, 2021
REVIEW CATEGORY:	Exemption category # *(2)*

Thank you for your Amendment/Modification submission to the University of Delaware Institutional Review Board (UD IRB). According to the pertinent regulations, the UD IRB has determined this project is EXEMPT from most federal policy requirements for the protection of human subjects. The privacy of subjects and the confidentiality of participants must be safeguarded as prescribed in the reviewed protocol form.

This exempt determination is valid for the research study as described by the documents in this submission. Proposed revisions to previously approved procedures and documents that may affect this exempt determination must be reviewed and approved by this office prior to initiation. The UD amendment form must be used to request the review of changes that may substantially change the study design or data collected.

Unanticipated problems and serious adverse events involving risk to participants must be reported to this office in a timely fashion according with the UD requirements for reportable events.

A copy of this correspondence will be kept on file by our office. If you have any questions, please contact the UD IRB Office at (302) 831-2137 or via email at hsrb-research@udel.edu. Please include the study title and reference number in all correspondence with this office.

Appendix C

COPYRIGHT PERMISSION FROM AMERICAN SOCIETY OF CIVIL ENGINEERS

CCC | Marketplace™

Order Number: 1235834
Order Date: 15 Jun 2022

Payment Information

Nafiseh Soleimani
nafisehs@udel.edu
Payment method: Invoice

Billing Address:
Miss Nafiseh Soleimani
University of Delaware
20C Duke street
Newark, DE 19711
United States

+1 (302) 763-2878
nafisehs@udel.edu

Customer Location:
Miss Nafiseh Soleimani
University of Delaware
20C Duke street
Newark, DE 19711
United States

Order Details

1. Journal of Infrastructure Systems

Billing Status: Open

Order License ID	1235834-1	Type of use	Republish in a thesis/dissertation
Order detail status	Completed	Publisher	American Society of Civil Engineers
ISSN	1943-555X	Portion	Page

0.00 USD
Republication Permission

LICENSED CONTENT

Publication Title	Journal of Infrastructure Systems	Country	United States of America
Author/Editor	American Society of Civil Engineers	Rightsholder	American Society of Civil Engineers
Date	01/01/1995	Publication Type	e-Journal
Language	English	URL	http://ojps.aip.org/iso/

REQUEST DETAILS

Portion Type	Page	Rights Requested	Main product
Page range(s)	1-14	Distribution	United States
Total number of pages	14	Translation	Original language of publication
Format (select all that apply)	Electronic	Copies for the disabled?	No
Who will republish the content?	Academic institution		

Duration of Use	Life of current edition	Minor editing privileges?	No
Lifetime Unit Quantity	Up to 499	Incidental promotional use?	No
		Currency	USD

NEW WORK DETAILS

Title	Multihazard Scenarios for Regional Seismic Risk Assessment of Spatially Distributed Infrastructure	Institution name	University of Delaware
		Expected presentation date	2022-07-12
Instructor name	Nafiseh Soleimani		

ADDITIONAL DETAILS

The requesting person / organization to appear on the license	Nafiseh Soleimani

REUSE CONTENT DETAILS

Title, description or numeric reference of the portion(s)	Multihazard Scenarios for Regional Seismic Risk Assessment of Spatially Distributed Infrastructure	Title of the article/chapter the portion is from	N/A
		Author of portion(s)	American Society of Civil Engineers
Editor of portion(s)	N/A	Issue, if republishing an article from a serial	1
Volume of serial or monograph	27		
Page or page range of portion	1-14	Publication date of portion	2021-01-13

Total Items: 1

Subtotal: 0.00 USD

Order Total: 0.00 USD